# Stony Brook University

# Optimization and Verification of a Novel Trileaflet Polymeric Prosthetic Heart Valve

A Dissertation Presented

by

**Thomas Edward Claiborne, III**

to

The Graduate School

in Partial Fulfillment of the

Requirements

for the Degree of

**Doctor of Philosophy**

in

**Biomedical Engineering**

Stony Brook University

**August 2012**

**Stony Brook University**

The Graduate School

**Thomas Edward Claiborne, III**

We, the dissertation committee for the above candidate for the

Doctor of Philosophy degree, hereby recommend

acceptance of this dissertation.

**Danny Bluestein, Ph.D.**
**Professor, Dept. of Biomedical Engineering**

**Stefan Judex, Ph.D.**
**Professor, Dept. of Biomedical Engineering**

**Barry Lieber, Ph.D.**
**Professor, Dept. of Biomedical Engineering**
**Professor, Dept. of Neurological Surgery**
**Director, Cerebrovascular Research Center**

**Dr. Todd Rosengart, M.D.**
**Professor and Chair, Dept. of Surgery**
**Chief, Div. of Cardiothoracic Surgery**
**Co-Director, Heart Institute**

This dissertation is accepted by the Graduate School

Charles Taber
Interim Dean of the Graduate School

Abstract of the Dissertation

**Optimization and Verification of a Novel Trileaflet Polymeric Prosthetic Heart Valve**

by

**Thomas Edward Claiborne, III**

**Doctor of Philosophy**

in

**Biomedical Engineering**

Stony Brook University

**2012**

Valvular heart disease remains a significant public health issue with Calcific Aortic Valve Disease (CAVD) its most life threatening form. Current treatment for CAVD involves open-heart surgical replacement of the diseased aortic valve (AV) with either a tissue (THV) or mechanical (MHV) prosthesis, with THVs being mostly nonthrombogenic but vulnerable to structural valve deterioration (SVD) and MHVs being highly durable but thrombogenic, thus requiring lifelong anticoagulant therapy. Alternatively, recently approved transcatheter aortic valve replacement (TAVR) is now available for inoperable patients with severe aortic stenosis. TAVR currently utilizes balloon- or self-expandable THVs. Polymeric valves (PHV) promise to avoid SVD and anticoagulants by using new biostable polymers and mimicking the native AV form and function. PHVs may be better suited for TAVR, where the valve experiences potentially damaging loads during crimping and deployment, and in devices such the Total Artificial Heart, which currently utilizes MHVs. We present the development of a novel PHV using a new thermoset polyolefin, xSIBS, and the completion of one optimization cycle using our Device Thrombogenicity Emulation (DTE) methodology, the goal of which is to reduce or eliminate the need for anticoagulants by employing a combination of numerical and experimental methods to optimize device designs, including finite element analysis, fluid-structure interaction, two-phase computational fluid dynamics (CFD), computer aided design, in vitro human platelet activation state (PAS) measurements, and hydrodynamics verification testing. Key features of the PHV were altered to optimized hemodynamics, and computer numerical control machined compression molding was used to create precision valve prototypes. The optimized PHV showed reduced stress concentrations in the leaflets under diastolic pressure loads, CFD produced favorable Thrombogenic Footprints, with stress loading waveforms extracted from regions of interest and emulated in our Hemodynamic Shearing Device showing significantly lower PAS in the optimized PHV. Prototype hydrodynamics were comparable to a gold-standard THV. This work has moved PHVs closer to clinical viability.

## Dedication Page

This work is dedicated to my two wonderful daughters, Madeleine and Meredith, whom are the loves of my life, and whom have sacrificed time with their father for his education.

## Table of Contents

## LIST OF FIGURES

## LIST OF TABLES

**Acknowledgments**

This work was funded by the National Institutes of Health (NIH) National Institute of Biomedical Imaging and Bioengineering (NIBIB) Quantum Grant Program (DB).

The following people were integral to this work: from the Stony Brook University (SBU) Dept. of Biomedical Engineering (BME) Prof. Stefan Judex, Ph.D. and his post-doc Shikha Gupta, Ph.D.; Prof. Barry Lieber, Ph.D., and his students Ronak Dholakia, M.S. and Joe Santore, M.S. (also appointed to the Dept. of Neurological Surgery); from The Biofluids Lab, former members Gaurav Girdhar, Ph.D., Michalis Xenos, Ph.D. and Dinesh Peter, M.S., current members, students Wei-Che (Philip) Chiu, B.S. and Chao Gao, B.S., post-docs Jawaad Sheriff, Ph.D., Yared Alemu, Ph.D., Joao Soares, Ph.D.; and external collaborators from Innovia LLC, Miami, FL, Len Pinchuk, Ph.D. and Yasushi Kato, Ph.D., from the Helmholtz Institute of Applied Medical Engineering in Aachen, Germany, Prof. Ulrich Steinseifer, Ph.D. and Maximilian Kutting Dipl.-Ing., and from the Sarver Heart Center at the University of Arizona in Tucson, AZ, Dr. Marvin J. Slepian, M.D.

I would also like to acknowledge and thank Richard T. Schoephoerster, Ph.D., Dean of the College of Engineering at the University of Texas at El Paso, El Paso, TX, who was my Master's Thesis Advisor at Florida International University (FIU), Miami, FL and who encouraged me to pursue a doctorate and recommended me to Prof. Bluestein. I would also like to thank James E. Moore, Jr., Ph.D., Professor of Biomedical Engineering at Texas A&M University, College Station, TX, and formerly FIU, for his support and mentorship, and Anthony J. McGoron, Ph.D., Assoc. Prof. of Biomedical Engineering at FIU, for his support and mentorship.

I would like to thank all of the Faculty and Staff at the SBU and FIU Depts. of BME, especially Anne-Marie Dusatko, Assistant to Chair and Graduate Program Coordinator at SBU-BME. I would also like to thank the Faculty and Staff of the FIU Dept. of Mechanical Engineering.

I would like to thank Sean Boykevisch, Ph.D. of the SBU Office of Technology Licensing and Industrial Relations for his help with our intellectual property concerns.

Thanks as well to my former colleagues, Siobhain Gallocher-Lowe, Ph.D. and Qiang "Tony" Wang, Ph.D. from FIU.

Thanks to Dr. Todd Rosengart, M.D. for participating on my dissertation committee.

Special thanks to my advisor, Prof. Danny Bluestein, Ph.D., who made this work possible and whose belief in me and support has allowed me to earn a doctorate and to create significant advances in our field of study.

## Vita, Publications and/or Fields of Study

## EDUCATION

**Ph.D. Biomedical Engineering, 2012**

SUNY Stony Brook University, Stony Brook, NY

**Dissertation Title:** "Optimization and Verification of a Novel Trileaflet Polymeric Prosthetic Heart Valve"

**Advisor:** Danny Bluestein, Ph.D.

**M.S. Biomedical Engineering, 2008**

Florida International University, Miami, FL

**Thesis Title:** "Development and Evaluation of a Catheter Deliverable Artificial Aortic Heart Valve Prosthesis and Delivery System"

**Advisor:** Richard T. Schoephoerster, Ph.D.

**B.S. Mechanical Engineering, 2002**

*Minor in Biomedical Engineering*

Florida International University, Miami, FL

## MILITARY SERVICE

**1991-1996** Enlisted United States Army Medical Department

## LISCENSURE

Florida Department of Business and Professional Regulation

Engineering Intern License # 1100008389

## INTELLECTUAL PROPERTY

- USPTO Application #20110295361 Thomas E. Claiborne, Siobhain Gallocher, Richard T. Schoephoerster, "Catheter Deliverable Artificial Multi-Leaflet Heart Valve Prosthesis and Intravascular Delivery System for a Catheter Deliverable Heart Valve Prosthesis" Filed February 25, 2009.
- USPTO Provisional Application #61/546,832 Thomas E. Claiborne, Marvin Slepian, Yasushi Kato, Leonard Pinchuk, Danny Bluestein, "Polymeric prosthetic heart valve designed for optimized durability and hemodynamics" Filed October 13, 2011.

## BUSINESS VENTURES

- **Sunshine Sitters LLC**, Miami, FL: Founder and Manager 2007-2008: A babysitter screening and referral service connecting eligible college students with parents for temporary child care in the Miami area

- **PolyNova**, Stony Brook, NY: Co-Founder and Chief Operations Officer, 2012-: A start-up biotech company developing polymeric prosthetic heart valves and related technology for the treatment of heart valve disease.

## TEACHING EXPERIENCE

**2010: Senior Design Advisor**, SUNY Stony Brook University

BME 441 Senior Design Project in Biomedical Engineering

**2009: Teaching Assistant**, SUNY Stony Brook University

BME 305 Biofluids

**2008: Teaching Assistant**, SUNY Stony Brook University

BME 212 Biomedical Engineering Research Fundamentals

**2007: Teaching Assistant**, Florida International University

Cardiovascular Biomechanics Lab

## PROFESSIONAL EXPERIENCE

**2008-Present: Research Assistant**, Biomedical Engineering, Biofluids Lab, SUNY Stony Brook University, Stony Brook, NY

Under my advisor, Prof. Danny Bluestein, Ph.D., I am working on the optimization and verification of a novel polymeric trileaflet prosthetic heart valve using numerical and experimental methods developed in the Biofluids Lab at Stony Brook University. This includes finite element analysis to perform fluid-structure interaction simulations, two-phase computational fluid dynamics to calculate platelet stress accumulation, and human platelet activation quantification via the measurement of thrombin generation in response to fluid shear stress. Additional *in vitro* tests include hydrodynamics and accelerated durability analysis of valve prototypes. This work will produce novel intellectual property and multiple refereed publications.

**2007-2008: Research Assistant**, Biomedical Engineering, Florida International University (FIU), Miami, FL

Under my advisor, now Dean Richard T. Schoephoerster, Ph.D. of the College of Engineering at The University of Texas at El Paso, and formerly Wallace H. Coulter Chair and Professor of Biomedical Engineering at FIU, I developed and evaluated a novel transcatheter heart valve prosthesis, a complementary peripheral artery delivery system, and method for *in vitro* testing of these devices. This work resulted in one refereed publication and novel intellectual property.

**2003-2007: Quality Analyst**, Hill-Rom, Charleston, SC

I performed post-market quality analysis of the rental fleet of medical beds (FDA Class I & II medical devices) via customer complaint processing. I participated in quality system

audits and ensured compliance with FDA and ISO standards. I also helped develop a method of increasing complaint processing speed and efficiency.

**2002-2003: Mechanical Engineer,** CR Bard, Moncks Corner, SC

I assisted the plant engineer in the design and installation of manufacturing equipment for latex based medical devices, e.g. urinary catheters and wound drains.

**Summer 2002: Intern**, Medtronic Vascular, Sunrise, FL

I worked on the development and bench-top testing of a novel feature for abdominal aortic stent grafts to mitigate *in vivo* graft migration.

**Summer 2001: Intern**, Scion Cardiovascular, Miami, FL

I worked on the competitive analysis of a novel vascular ligation clip.

**Spring 2000: Undergraduate Research Assistant**, Cellular Biomechanics Lab, Florida International University, Miami, FL

Under the supervision of Prof. James E. Moore, Jr., Ph.D., I assisted graduate students and post-doctoral fellows in the manufacture of silicone rubber blood vessel analogs for the study of the combined effects of blood vessel stretch and fluid shear stress on the growth on endothelial cells.

**1996-2000: Certified Surgical Technologist**, Mt. Sinai Medical Center, Miami Beach, FL

I primarily assisted surgeons in cardio-thoracic surgery at a high throughput medical center.

**1991-1996: 91D Operating Room Specialist**, United States Army Medical Department

I directly aided surgeons in a variety of surgical procedures including cardio-thoracic surgery both domestically and abroad. Decorated with honorable discharge.

## HONORS & AWARDS

- Pi Tau Sigma Mechanical Engineering Honor Society Member (Undergraduate)
- Dean's List Summer 2002 Term at FIU (Undergraduate)
- Best Poster Presentation, BME Research Day 2010, Department of Biomedical Engineering, Stony Brook University
- Certificate of Achievement from the State University of New York University Faculty Senate for Participation in the Research that Matters Exposition March 8, 2011 Albany, NY
- Stony Brook University Provost's Graduate Student Lecture Series Presenter Spring 2012 (Competitive Invitation)
- ASME Summer Bioengineering Conference 2012 Ph.D. Student Paper Competition 3rd Place $100 Prize
- Stony Brook University Graduate Student Organization Distinguished Travel Award $1400

## PROFESSIONAL ACTIVITIES

- **Current Member** of the American Society of Mechanical Engineers (ASME) Bioengineering Division
- **Current Member** of the Biomedical Engineering Society (BMES)
- **Current Member** of the American Heart Association (AHA)
- **Founder and 1st President** of the BMES Student Chapter at Florida International University 2000-2002
- ***Ad hoc* Reviewer** for "Medical and Biological Engineering and Computing" and the "Journal of Mechanics in Medicine and Biology"

## RESEARCH SKILLS

**Experimental**

- Human blood platelet activation quantification via chromogenic assay
- Phlebotomy (human blood collection and safe handling)
- Vivitro Labs Left Heart Simulator Prosthetic Heart Valve Hydrodynamics Testing
- Vivitro Labs Hi-Cycle Accelerated Wear Tester for Prosthetic Heart Valves
- Plastic/Rubber Mold and Medical Device Design
- Material Mechanics Testing
- Statistical Experimental Design
- *In vitro* Medical Device Testing

**Numerical**

- ADINA Finite Element Analysis: Fluid-Structure Interaction
- ANSYS Fluent /Gambit Computational Fluid Dynamics

**Software**

- SolidWorks
- Matlab
- SPSS
- SigmaPlot
- Mimics by Materialise (CT/MRI image processing)

## REFEREED PUBLICATIONS

1. **Claiborne, T.E.**, Slepian, M.J., Hossainy, S., Bluestein, D. (**Accepted**) "Polymeric Trileaflet Prosthetic Heart Valves: Evolution and Path to Clinical Reality," Exp Rev Med Dev
2. **Claiborne, T.E.**, Xenos, M., Sheriff, J., Chiu, W.C., Soares, J., Alemu, Y., Gupta, S., Judex, S., Slepian, M.J., Bluestein, D. (**Submitted**) "Design and Optimization of a Novel Trileaflet Polymeric Prosthetic Heart Valve using the Device Thrombogenicity Emulation (DTE) Methodology" ASAIO J
3. **Claiborne, T. E.**, Girdhar, G., Gallocher-Lowe, S., Sheriff, J., Kato, Y. P., Pinchuk, L., Schoephoerster, R. T., Jesty, J., and Bluestein, D., 2011, "Thrombogenic Potential of

Innovia Polymer Valves versus Carpentier-Edwards Perimount Magna Aortic Bioprosthetic Valves," ASAIO J, 57(1), pp. 26-31.

4. Sheriff, J., Bluestein, D., Girdhar, G., Jesty, J. 2010, "High Shear Stress Sensitizes Platelets to Subsequent Low-Shear Conditions" Annals of Biomed Eng, 38(4), pp. 1442-1450. (**Acknowledgement)**
5. **Claiborne, T. E.**, Bluestein, D., and Schoephoerster, R. T., 2009, "Development and evaluation of a novel artificial catheter-deliverable prosthetic heart valve and method for in vitro testing," Int J Artif Organs, 32(5), pp. 262-271.

## PROFESSIONAL CONFERENCE PRESENTATIONS

1. **T. E. Claiborne**, J. Sheriff, D. Peter, Y. Kato, L. Pinchuk, M. Kutting, U. Steinseifer, M. Slepian, and D. Bluestein "In Vitro Evaluation of a novel Polymeric Trileaflet Prosthetic Heart Valve" BMES Annual Meeting Atlanta, GA October 24-27, 2012 (**Podium**)
2. S. George, J. Sheriff, **T. E. Claiborne**, M. J. Slepian, J. Jesty, and D. Bluestein. "Platelet "Interaction With A Novel Polymer Valve Biomaterial Under Shear Conditions" BMES Annual Meeting Atlanta, GA October 24-27, 2012 (**Poster**)
3. **Thomas E. Claiborne,** Michalis Xenos, Jawaad Sheriff, Dinesh Peter, Yared Alemu, Yasushi Kato, Leonard Pinchuk, Shmuel Einav, Jolyon Jesty, and Danny Bluestein (2012) "Development and Optimization of a Novel Polymeric Prosthetic Heart Valve using the Device Thrombogenicity Emulation (DTE) Methodology" SBC2012-80186 Proceedings of the ASME 2012 Summer Bioengineering Conference, June 20-23, Fajardo, Puerto Rico (**Ph.D. Student Paper Competition 3rd Place Winner, Podium**)
4. **Thomas E. Claiborne**, Michalis Xenos, Jawaad Sheriff, Yasushi Kato, Leonard Pinchuk, Jolyon Jesty, Shmuel Einav, Danny Bluestein (2011) "Thrombogenic Optimization of a Novel Trileaflet Polymeric Prosthetic Heart Valve" Proceedings of the Annual Meeting of the Biomedical Engineering Society Hartford, CT, October 12-15, 2011 (**Poster**)
5. Yared Alemu, Gaurav Girdhar, Michalis Xenos, **Thomas Claiborne**, Jolyon Jesty, Shmuel Einav, Marvin Slepian, Danny Bluestein (2011) "Evaluation of Syncardia Total Artificial Heart using Device Thrombogenicity Emulator" Proceedings of the ASME 2011 Summer Bioengineering Conference, June 22-25, Nemacolin Woodlands Resort, Famington, Pennsylvania, USA (**Podium)**
6. **Thomas E. Claiborne**, Michalis Xenos, Gaurav Girdhar, Yared Alemu, Jawaad Sheriff, Marvin Slepian, Leonard Pinchuk, Jolyon Jesty, Shmuel Einav, Danny Bluestein (2011) "Dynamic numerical and experimental evaluation of polymer prosthetic heart valves." Proceedings of the ASME 2011 Summer Bioengineering Conference, June 22-25, Nemacolin Woodlands Resort, Famington, Pennsylvania, USA (**Poster**)
7. **Thomas Claiborne**, Michalis Xenos, Yared Alemu, Jawaad Sheriff, Leonard Pinchuk, Marvin Slepian, Stefan Judex, Shmuel Einav, Jolyon Jesty, Danny Bluestein (2011) "Trileaflet Polymeric Valves and their uses for Transcatheter Delivery and in the Total Artificial Heart." Research that Matters: An Exposition of Graduate Research in SUNY and CUNY, March 8, New York State Legislative Office Building, 1st floor, Empire State Plaza, Albany, NY (**Poster**)
8. **Thomas E. Claiborne**, Guarav Girdhar, Jawaad Sheriff, Jolyon Jesty, Marvin J. Slepian, Leonard Pinchuk, Danny Bluestein (2010) "In Vitro Platelet Activity in Cardiovascular Medical Devices." Proceedings of the ASME 2010 Summer Bioengineering Conference, June 16-19, Grande Beach Resort, Naples Florida, USA **(Podium)**

9. Girdhar, G., **Claiborne, T.**, Sheriff, J., Slepian, M., Einav, S., Jesty, J., Bluestein, D. (2009) "Platelet Activity Measurement in CardioWest Total Artificial Heart and Ventricular Assist Device." BMES Annual Fall Meeting, Pittsburgh, PA, October 7-10, 2009. **(Poster)**
10. **Thomas E. Claiborne** and Richard T. Schoephoerster. (2008) "Development and Evaluation of a Catheter Deliverable Artificial Aortic Heart Valve Prosthesis and Delivery System" 24th Southern Biomedical Engineering Conference (SBEC), El Paso, TX, April 18th – 20th, 2008 **(Podium)**

## RESEARCH FUNDING APPLICATIONS

- American Heart Association Founders Affiliate FDA Spring 2011 Predoctoral Fellowship App# 11PRE8000026; Project Title: Dynamic numerical and experimental characterization of polymer transcatheter valve prosthesis. Score 2.19; Percentile Rank 33.64%; Status: Unfunded.

## INTRODUCTION AND SPECIFIC AIMS

Valvular heart disease (VHD) remains a significant public health issue affecting 1-2% of Americans, which is likely increasing as the 'baby boomer' population reaches retirement age [1,2]. An estimated 2-4% of people over the age of 65 suffer from aortic stenosis (AS) as a result of calcific aortic valve disease (CAVD) with an estimated mortality rate of 25-54% [1]. Current treatment is primarily provided at the end-stages of the disease via open-heart surgical replacement of the diseased valve with either mechanical or tissue prosthetic heart valves [1]. Mechanical heart valves (MHV) are highly durable but thrombogenic, therefore they are implanted more frequently in younger healthier patients and lifelong anticoagulant (warfarin[1]) therapy is required to achieve an INR[2] of 2.0-3.5 depending on the patient's risk factors [3,4]. Conversely, tissue heart valves (THV) are prone to structural valve deterioration (SVD) and have a lower risk of thrombosis, therefore THV recipients are typically older and less tolerant of anticoagulation and only require 75-100 mg of aspirin[3] per day [3]. This method of treatment of VHD has remained largely unchanged for the last 30 years until the recent FDA-approval of transcatheter aortic valve replacement (TAVR), in which the prosthesis is implanted via peripheral artery catheterization without the need for opening the chest or the heart [5]. Polymeric heart valves (PHV) promise to avoid SVD and anticoagulants, and have been designed to mimic the native aortic valve (AV) in form and function. PHVs have been under development since 1960, but persistent *in vivo* thrombosis and degradation have hampered progress. Advances in polymer science and our understanding of the dynamics of heart valves is finally moving PHVs closer to reality [6]. New technology, such as TAVR and the Total Artificial Heart (TAH) [7], represent devices where PHVs may be superior. TAVR is indicated for inoperable patients with severe AS. The current TAVR devices utilize xenograft tissue valves primarily in order to quickly navigate regulatory pathways, but crimping and catheter deployment is likely to damage the tissue [8,9]. In that application, a more durable material may be a better choice. The current model of the TAH utilizes monoleaflet MHVs. Replacing MHVs with trileaflet polymer PHVs may reduce the thrombogenic potential of the TAH as well as acoustic disturbances.

One such promising polymer is the 'super-biostable' polyolefin[4] poly(Styrene-*block*-IsoButylene-*block*-Styrene) or SIBS in commercial development by Innovia LLC, Miami, FL [10]. It is a thermoplastic elastomer that has no reactive pendant groups rendering it hydrolytically, enzymatically, oxidatively stable. It has been commercialized in Boston Scientific's Taxus paclitaxel eluting coronary stent [10]. It has also been investigated as a potential heart valve material where the final design was a composite material comprised of a reinforcing Dacron mesh and a cast SIBS coating [11,12]. However, the design failed in animal trials due to the viscoelastic creep[5] properties of the thermoplastic formulation [13]. But we did learn from other studies that SIBS itself is hemocompatible and will likely produce a PHV with a

[1] Warfarin is an anticoagulant drug that inhibits vitamin K dependent synthesis of biologically active forms of key clotting factors.
[2] International Normalized Ratio (INR) is a measure of tissue factor clotting time calculated by the ratio of prothrombin time test value to normal raised to the power of the International Sensitivity Index (ISI); normal range is 0.8-1.2.
[3] Aspirin is a cyclooxgenase inhibitor that reduces platelet activation and aggregation.
[4] Polyolefins are synthetic hydrocarbon thermoplastics derived from petroleum. Olefin means "oil-like."
[5] See Polymer Valve History below.

low risk of thrombosis [14,15,16,17]. Innovia has produced a novel thermoset polyolefin (xSIBS) that may eliminate the deleterious viscoelastic creep properties of the thermoplastic SIBS formulation. The **goal of this work** was to optimize and verify the design of a novel PHV design based on xSIBS and to validate the Device Thrombogenicity Emulation (DTE, explained below) methodology of thrombogenic optimization in trileaflet valves [18,19]. This has been accomplished via the following **specific aims**:

**Specific Aim 1: Determine the mechanical properties of xSIBS via uniaxial tensile testing for Finite Element Analysis (FEA)**

Samples of xSIBS were prepared in the lab and their stress vs. strain behavior was measured in a uniaxial tensile testing device. This data was used in the numerical material model of the valve in finite element modeling (FEM).

**Specific Aim 2: Design an optimized PHV and its compression mold**

Computer aided design (CAD) software was used to design a novel PHV and its compression mold by analyzing the failure modes of the prior Innovia composite SIBS-Dacron PHV and the native AV structure.

**Specific Aim 3: Apply the DTE method to evaluate a novel optimized PHV**

Structural FEA was performed to determine the stress distribution in the valve design and feed geometries into two-phase computational fluid dynamics (CFD), where platelet stress accumulation was evaluated. Selected platelet trajectories were emulated in the Hemodynamic Shearing Device (HSD). Comparison of Thrombogenic Footprints (TF) and freshly isolated human platelet activation measured via our modified prothrombinase assay was made to evaluate the thrombogenicity new PHV design. Fluid-structure interaction (FSI) studies were performed to further analyze predicted hemodynamics.

**Specific Aim 4: Fabricate the optimized PHV mold and valve prototypes**

Computer numerical controlled (CNC, 5-axis) machining was used to fabricate the valve mold from aluminum alloy. Raw xSIBS was compressed and heated to 260°C for 30 minutes in the mold to create a precision molded PHV.

**Specific Aim 5: Measure and compare optimized valve prototype hydrodynamics**

Valve prototype hydrodynamics including; transvalvular pressure gradient, regurgitant flow fraction, energy loss, and effective valve area, were measured in the Vivitro Left Heart Simulator (LHS) following FDA guidance.

**Specific Aim 6: Measure and compare valve prototype bulk platelet activation**

Valve prototype bulk flow human platelet activation was measured via our modified prothrombinase assay and flow cytometry in a small volume (200 ml) pulsatile left ventricular assist device (LVAD) under physiologic flow conditions.

## BACKGROUND AND SIGNIFICANCE

### Valvular Heart Disease (VHD)

The heart valves are passive structures that direct the flow of blood through the heart (Figure 1). There are four valves, two atrial and two ventricular, categorized as exit valves. During the outward stroke (systole), blood is ejected from the heart by the ventricles, and during the filling phase (diastole) the atria contract to aid in filling the ventricles. The focus of this work is the replacement of a diseased aortic valve (AV), which resides at the base of the aortic root and directs blood flow out of the left ventricle (LV) into the arterial circulation. It also serves to direct blood flow to the coronary arteries during diastole, which supply oxygenated blood to the heart (myocardium) itself.

The AV has two basic failure modes, **stenosis** and **insufficiency**. Aortic stenosis (AS) is a narrowing of the valve opening, which restricts the flow of blood out of the LV, and aortic insufficiency (AI) (regurgitation) is caused by a leaking valve that fails to close properly during diastole. Stenosis is typically caused by a congenital defect (bileaflet or quadrileaflet valve), calcification, commissural fusion, or fibrosis; any of which can also cause insufficiency. Insufficiency alone is typically caused by rheumatic heart disease or aortic root dilatation. The typical markers for diagnosing AV malfunction are shown in Table 1. In both cases the workload ($W$) on the heart increases and may lead to heart failure. Stenosis causes an increase in pressure gradient ($\Delta P$) and an increase in "afterload" (increased ventricular wall tension), and insufficiency causes an increase in stroke volume ($SV$). Cardiac work is calculated as (1).

$$W = \Delta P \times SV \tag{1}$$

The ejection fraction ($EF$) of the heart is calculated as (2),

$$EF\% = \left( SV \big/ EDV \right) \times 100 \tag{2}$$

where $EDV$ is the end diastolic volume. A healthy value is 55%, but as the heart becomes weakened by the increased workload the $EF$ drops. A combination of decreasing $SV$ and increasing $EDV$ caused by AV disease leads to heart failure. Stenosis can cause hypertrophy of the ventricle making it less compliant- leading to decreased coronary flow and ischemia, and regurgitation can stretch the ventricle beyond its elastic limits (Frank-Starling mechanism and Law of LaPlace) and reduce its contractility (inotropy). Both scenarios have the effect of reducing $EF$. The remodeling of the heart due to AS occurs over many years and is mostly asymptomatic until the final stages of the disease. The classic symptoms of AS are angina[6], syncope[7], and heart failure ($EF < 50\%$) [20]. In many cases, heart failure induced by a AS can be arrested or reversed by valve replacement [21].

The **calcific aortic valve disease** (CAVD) process has similarities to atherosclerosis (lipid deposition, inflammation, and calcification) but it is distinctly different. The AV was considered to an extension of arterial tissue and CAVD a passive effect of wear and tear until relatively

[6] Angina is chest pain associated with decreased coronary blood flow and unmet myocardial oxygen demand.
[7] Syncope is transient postural loss of consciousness or fainting due to decreased cardiac output and reduced cranial blood flow.

recently. Now we know that the AV is a distinct organ with its own unique physiology, and that CAVD is an active disease process that may be arrested or reversed with novel drug therapies, however statins[8] have had no significant effect on CAVD in recent clinical trials, highlighting the difference between CAVD and atherosclerosis [22]. For example, in CAVD, AV fibroblasts (valve interstitial cells-VICs) undergo a phenotype change to become osteoblasts that begin to form lamellar bone in the valve rather than the diseased valve simply passively accumulating calcium deposits. The large accumulation of foam cells[9] seen in atherosclerosis is absent as well [23]. There may be a genetic predisposition for CAVD, but the primary risk factor is age >50 years [20]. Additionally, CAVD may produce blood flow patterns that may lead to bleeding in the gastrointestinal tract (Heyde syndrome) through several mechanisms including the formation of arteriovenous malformations and the presence of acquired von Willebrand factor syndrome[10] resulting from exposure of blood to elevated shear stress across the stenotic valve [20,24].

| Defect | Indicator | Mild | Moderate | Severe |
|---|---|---|---|---|
| **AS** | Jet Velocity (m/s) | <3 | 3-4 | >4 |
| | Mean Pressure Gradient (mmHg) | <25 | 25-40 | >40 |
| | Valve Area ($cm^2$) | >1.5 | 1.0-1.5 | <1.0 |
| **AI** | Regurgitant Volume (ml/beat) | <30 | 30-59 | ≥60 |
| | Regurgitant Fraction (%) | <30 | 30-49 | ≥50 |
| | Regurgitant Orifice Area ($cm^2$) | <0.10 | 0.10-0.29 | ≥0.30 |
| **Qualitative Score** | | +1 | +2 | +3 to +4 |

**Table 1: American College of Cardiology-American Heart Association VHD classifications.**

[8] Statins are a class of drugs used to lower LDL or "bad" cholesterol by inhibiting enzymes in the liver involved in cholesterol production.

[9] Foam cells are macrophages (white blood cells) that have ingested large amounts of lipids forming fatty streaks in arteries.

[10] von Willebrand factor (vWF) is a coagulation protein that binds platelets to one another and to the site of a blood vessel injury. vWF syndrome may be caused by shear stress induced proteolysis.

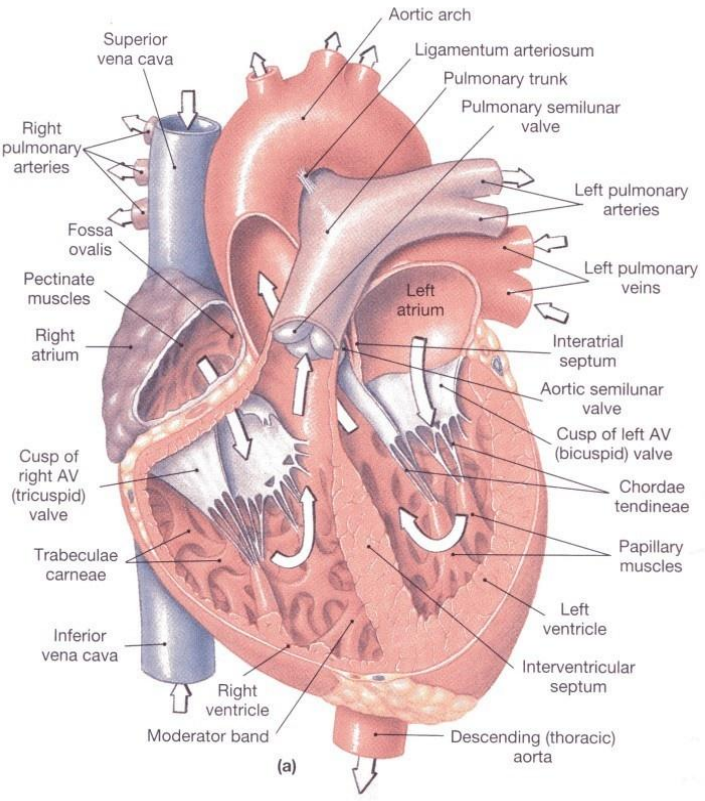


**Figure 1: Anatomy of the human heart (adapted from open source www).**

## Coagulation and Hemocompatibility

As PHVs are fabricated from biomaterials that may activate certain components of the coagulation cascade, leading to both contact- and flow-induced platelet activation, it is essential to test the thrombogenicity of both the material and the hemodynamics resulting from the valve's structural and functional components. This concept is illustrated via Virchow's triad of coagulation: blood-flow-surface. In prosthetic devices, this becomes a major design and optimization consideration. The blood coagulation process is very complex requiring many steps and elements for the formation of a clot (thrombus). There are **two pathways for the initiation of coagulation**; contact and tissue (Figure 2). Contact (**intrinsic**) is a calcium independent pathway that is initiated by coagulation factor XII activated by adherence to a negatively charged surface, which may be an implanted medical device. In the healthy person the intrinsic pathway is clinically insignificant. Hemostasis in vascular injury is maintained via the tissue factor (III) mediated pathway (**extrinsic**). This process is calcium dependent and involves different factors from the intrinsic pathway. The **common pathway,** mediated by factor X, is where the two former pathways converge and thrombi can begin to form. Coagulation involves the conversion of soluble fibrinogen to insoluble fibrin which forms a polymer network and the basis for a thrombus. **Platelets** are key to the clotting process because they are the first to arrive at the vascular injury site and adhere to the exposed collagen (via vWF) forming a platelet plug while forming sites for the conversion of prothrombin to thrombin via activated factor X (Xa), which catalyzes the formation of fibrin. Platelets are highly sensitive to mechanical forces as well. Pathological flow disturbances and elevated shear stresses created by diseased valves or

implanted medical devices can activate them and cause the formation of free flowing emboli, which could lodge downstream causing ischemia and thrombotic stroke [21,25,26].

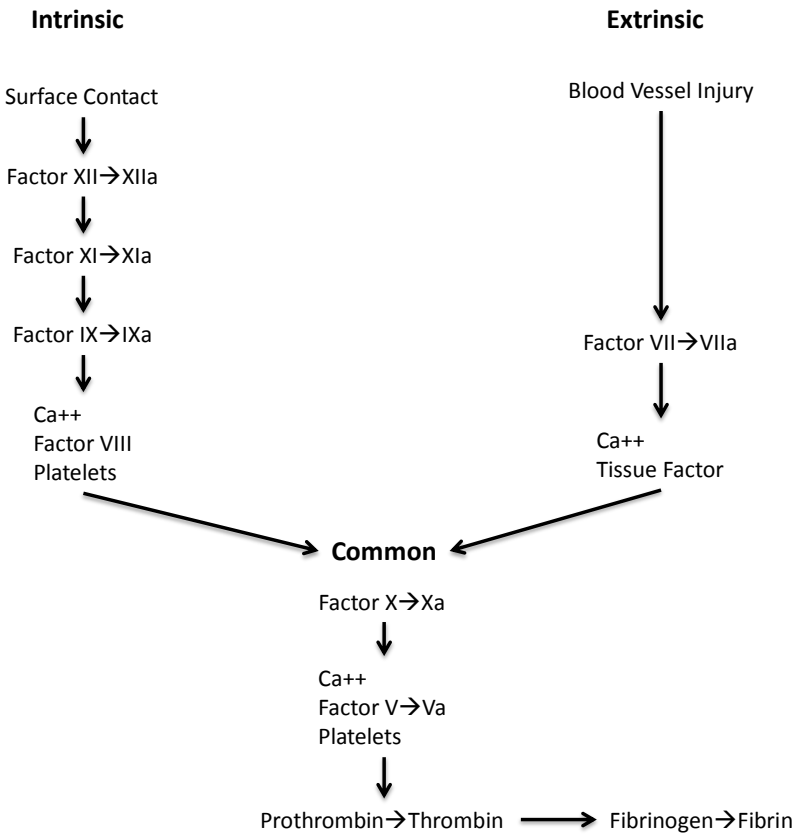


**Figure 2: Coagulation factor interactions[25].**

In the initial phase of the **intrinsic pathway**, contact factors adsorb to negatively charged surfaces (Factors XII, XI, plasmaprekallikrein-PPK, and high-molecular weight kininogen-HMWK). *In vitro*, the initial event is the adsorption of factor XII (Hageman factor) to a negatively charged surface where it is activated – XIIa. Factor XIIa converts PPK to plasmakallikrein (PK), and then the activation loops to create more of each protein thus amplifying the original signal. Then PK cleaves HMWK and releases the vasoactive proinflammatory peptide bradykinin. Factor XIIa also activates factor XI – XIa. HMWK serves to bind factor XI and PPK to the surface. Calcium comes into play in the middle phase of the intrinsic coagulation cascade by facilitating the activation of factor IX – IXa by factor XIa and the activation of factor VIII – VIIIa. Calcium facilitates the formation of the tenase complex, IXa + VIIIa, on phospholipid surfaces to activate factor X, which is the first step of the common coagulation pathway. An enzyme such as thrombin is required for factor VIII to exert cofactor functionality [25,27]. Factor XIIa may also trigger formation of fibrin via its substrate factor XI. The major regulator of the contact system proteins factor XII and PK in plasma is C1-esterase inhibitor (C1Inh). C1Inh is a member of the serpin family, which inhibits serine proteases by irreversible binding into the enzymatic pocket. However, the physiological activator of factor XII *in vivo* remains unknown. Interestingly, a deficiency in factor XII leads to

decreased thrombosis in the vasculature and increased activated partial thromboplastin time (aPTT) but not to a higher risk for bleeding from injury, which makes factor XII an attractive target for new anticoagulant drugs [28,29,30]. Until recently, it was thought that that thrombin-mediated feedback activation of factor XI on the activated platelet surface was preferred over contact activation by factor XIIa [31]. Since that manuscript was retracted, new studies indicate that factor XII mediated contact activation is elicited by activated platelets contributing to clot formation, thus **platelet activation triggers factor XII-mediated contact activation** on the surface and in the vicinity of activated platelets [32].

The **common pathway** of coagulation is mediated by factor Xa and its interaction with activated platelets and factor Va (mostly secreted from the activated platelets). The process occurs on the surface of the activated platelets and platelet aggregates which express anionic phospholipids, and is mediated by $Ca^{++}$. Factor Xa generates the prothrombinase complex which converts prothrombin into thrombin. The generated thrombin in turn feeds back to reactivate platelets, and catalyzes the soluble fibrinogen from the blood plasma into insoluble fibrin, which enmeshes RBCs and platelets to form the physical bulk of an effective thrombus (blood clot) necessary for hemostasis. Besides prior activation of the platelets, the availability of coagulation factors and efficacy of the prothrombinase reactions in the common pathway is additionally goverened by flow-mediated transport processes. The modified prothrombinase **Platelet Activation State (PAS) assay** is based on blocking the thrombin positive feedback [33]. This facilitates establishing direct correspondence between the agonist (e.g., flow induced stresses leading to platelet activation) and the procoagulant activity of the platelets (expressed in terms of thrombin generation rates in the assay).

**Biomaterial hemocompatibility** depends on surface characteristics, including hydrophilicity (less adsorption), hydrophobicity (more adsorption), and charge, influencing protein adsorption during the initial response to material-blood contact. Adsorbed proteins can affect platelet and leukocyte adhesion, and modulate the coagulation response. The most important proteins that promote cell adhesion on biomaterials include fibrinogen, von Willebrand factor, collagen, and vitronectin, with fibrinogen being the most abundant in plasma and the best studied in the context of hemocompatibility. The amount, orientation, and conformation of a particular adsorbed protein significantly influence hemocompatibility. However, when identical quantities of fibrinogen are adsorbed to the surface of biomaterials with differing wettability, varying amounts of fibrin formation can be observed. New information suggests that protein-surface interactions play a significant role in hemocompatibility. It has been proposed that the adsorption of coagulation factor XII to negatively charged surfaces, such as connective tissues and a number of biomaterials, leads to subtle conformational changes in the enzymes that provoke auto-activation. A new theory states that it is not the presence of negative charges but differences in protein displacement of competing proteins, partly described as an adsorption–dilution effect, that is responsible for the different degrees of contact activation on hydrophobic versus hydrophilic materials. However, the **activation of platelets** on biomaterials is surface initiated and primarily depends on the composition of the adsorbed protein layer. [34]

It may be a surprise, but there is no consensus on how to measure blood compatibility or what constitutes a hemocompatible material. From Ratner 2007, “So, why after 60 years of serious study of blood compatibility and development of blood compatible surfaces do we not have truly blood compatible surfaces? Here are some hypotheses: (1) The task is impossible. (2) We do not

understand the biology behind blood compatibility. (3) We do not understand how to test for or evaluate blood compatibility. (4) Certain materials of natural origin seem to show better blood compatibility but we do not know how to exploit this concept. (5) We do have better blood compatible materials but the regulatory and economic climate prevent adoption in clinical practice." [35] We have International Organization for Standardization ISO 10993-4 (2002) for guidance or suggestions on how to proceed, whereas the FDA has no such draft guidance, but instead has a laboratory exploring methods for hemocompatibility testing standards.

**Heart Valve Design and Optimization**

A thorough analysis of the human aortic valve was performed by Thubrikar *et al.* [36]. The native AV has a complex hemispherical (semilunar) geometry with three leaflets each composed of distinct tissue layers including (from the aortic surface to the ventricular surface): the lamina fibrosa - a ridged collagen rich layer, the lamina spongiosa - a disorganized connective tissue, and the lamina ventricularis – a thin elastin-rich layer. This tissue organization allows the AV to open and close under high loads virtually without failure, approximately 1.5 billion times in a lifetime (Figure 3). The technology to create a flexible artificial structure with such durability does not yet exist. However, we may be able to achieve more than 10 years of use (about 400 million cycles). Since the valve bears the greatest load during diastole, indistensible collagen fibers are arranged in the circumferential direction to provide strength while the elastic protein elastin is arranged in the radial direction to facilitate full valve closure (Figure 3). Early iterations of the Innovia polymer valve attempted to mimic this unique architecture, but the design failed [12]. Therefore, close approximation of the natural leaflet may not be necessary.

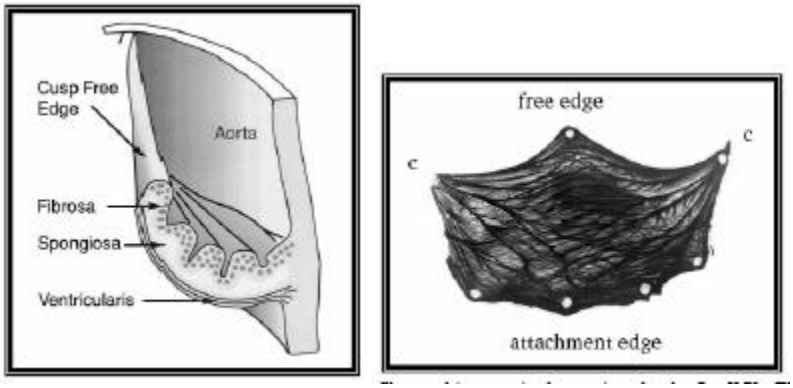


**Figure 3: Tissue structure of the native aortic valve, tissue organization schematic left and collagen fiber orientation right (Adapted from Gallocher 2007).**

Important design parameters for prosthetic valves include effective orifice area, jet velocity, pressure gradient, regurgitation, thrombogenic potential, and acoustic disturbances. Other design parameters include stent strut curvature, leaflet coaptation height, commissure gap, leaflet thickness, rounding hard edges, built-in regurgitant flow or "wash out", and collapsing cylinder vs. hemispherical leaflet geometries (Figure 4). For trileaflet PHVs, a major design parameter is optimization of the **leaflet thickness**. Flexible thinner leaflets have better hemodynamic performance (lower transvalvular pressure and weaker central flow jet inducing lower fluid shear stresses, etc.) but they may compromise durability. Once the valve has been designed it can be verified by determining whether or not it meets the design inputs. **This work has focused on**

**two key parameters:** (1) leaflet thickness (tapering) and (2) leaflet material. Future work will investigate the optimization of other aforementioned relevant parameters.

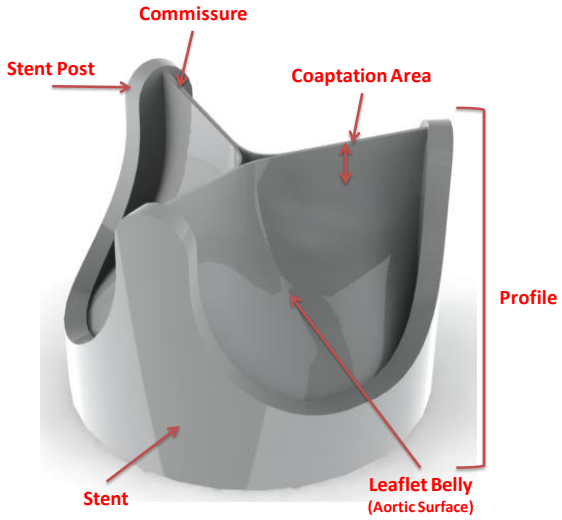


**Figure 4: Design features of polymer valves.**

The design of a prosthetic heart valve depends upon its intended use, and a summary of medical device development is shown in Figure 5. Although emulating the precise architecture of the native AV is not necessary, and various geometrical configurations can achieve AV functional design goals (e.g., as in MHV- typically a bileaflet design with the leaflets opening and closing in the opposite direction of the native AV leaflets), PHVs lend themselves more readily to mimic the native AV trileaflet structure and geometry, thus benefiting from the improved hemodynamics that such an architecture offers. General design considerations for successful prosthetic AV performance can be aided by the Draft Guidance for Industry and FDA Heart Valves--Investigational Device Exemption (IDE) and Premarket Approval (PMA) Applications document and ISO 5840:2005 Cardiovascular Implants-Cardiac Valve Prostheses standards [37,38]. The valve must survive in a highly dynamic and corrosive environment for several years. The FDA guidelines indicate the minimum durability requirement for flexible valves to be 200 million cycles, simulating about 5 years of use, with a backpressure of 125 mmHg. Valves must have a non-pathological pressure gradient during forward flow so as to not "over work" the left ventricle, and must not allow pathological regurgitant flow to prevent ventricular volume loading and overfilling, which is dependent upon the cardiac output.

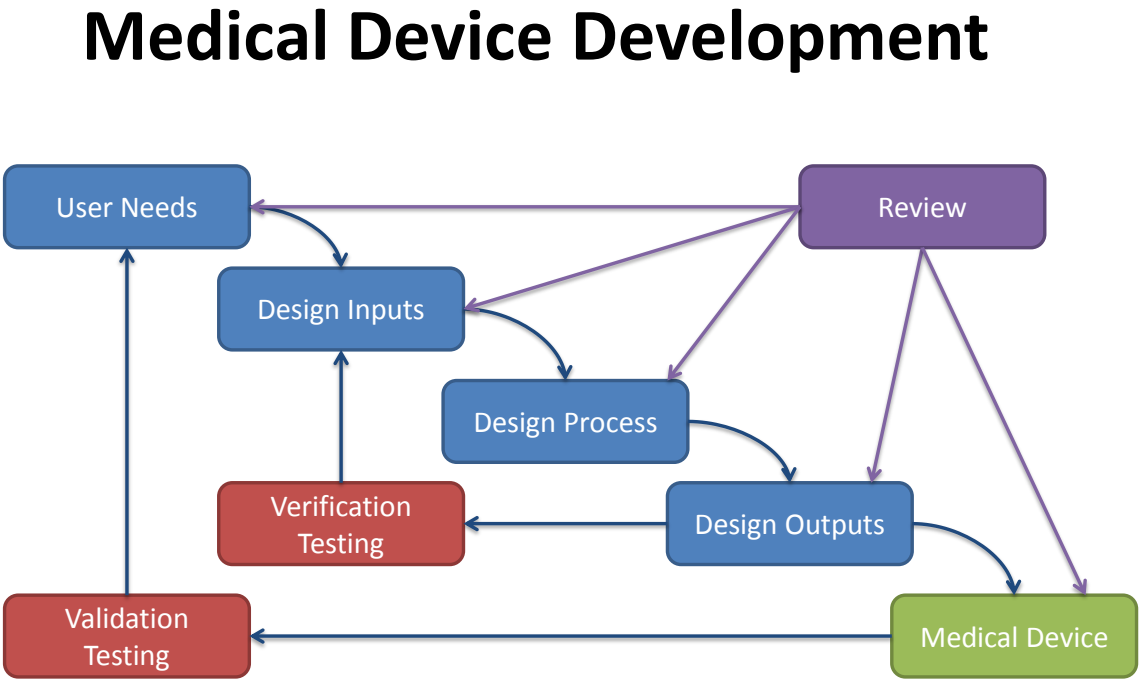


**Figure 5: Design process schematic with focus on design verification (adapted from FDA 21 CFR 820.30).**

Generally, the FDA requires that pre-clinical testing includes: material property testing, biological safety, hydrodynamic performance, structural performance, device durability, component fatigue assessments, and device specific testing. Biocompatibility testing according to ISO-10993, Biological Evaluation of Medical Devices Part-1: Evaluation and Testing, for blood-contacting, long-term implanted devices must be conducted (as discussed above). Additional recommended tests included, component fatigue testing (600 million cycles), corrosion testing for exposed metals, failure mode analysis, magnetic resonance safety, and shelf life. Pre-clinical animal trials may be conducted following FDA 21 CFR 58, Good Laboratory Practice (GLP). *In vivo* hemodynamics should be assessed along with complete blood chemistry including serum calcium and phosphorus. Necropsy and histology should be performed on explanted valves.

**Motivation**

The first prosthetic heart valve was introduced by Hufnagel and initially implanted in a patient in 1952 [39]. It was comprised of a methyl methacrylate tube with an encaged polyethylene ball, and was implanted in the thoracic aorta to treat AI. Hufnagel proved the feasibility of heart valve replacement and ignited interest in this treatment. The subsequent invention of the heart-lung machine by Gibbon initiated open-heart surgery in 1953 [40], leading to the further development of MHVs. Subsequently, MHVs evolved to become increasingly durable, though remaining thrombogenic, due to biomaterial and design issues, mandating lifelong anticoagulant therapy [41]. The anti-coagulation requirement necessarily has limited the utility of this therapy in patients with bleeding diatheses. Cadaveric aortic valves (homografts) were developed as implants, which [42] preceded the advent of prosthetic xenograft THVs, the first being the

glutaraldehyde-fixed Hancock stented porcine valve in 1969 [43], followed by the Carpentier-Edwards bovine pericardial valve in 1976 [44]. These THV alternatives to MHVs eliminated the need for anticoagulant therapy for most patients, however they introduced the problem of structural valve deterioration (SVD) due to the non-vital nature of the valvular tissue. Fixed tissue valves are composed of nonviable cells, unable to maintain calcium homeostasis and other acellular denatured material, favoring calcium crystallization and nucleation, with resultant calcium nodule formation [45]. Since THVs improve the quality of life of thousands of people, their stewards have made incremental progress in trying to minimize their shortcomings. Nevertheless, many clinicians now believe that these devices "replace one disease with another," [46] and their imperfections leave room for improvement, which leads to the idea of a flexible trileaflet PHV.

Past PHVs have been hampered by limited *in vivo* durability and thrombosis. It has proven to be exceedingly challenging to create a flexible polymeric material that can withstand the rigors required of an AV prosthesis. Over time, many designs, primarily comprised of polyurethanes (PU), have been tested and failed for various reasons, including material degradation, thrombosis, and calcification [47,48,49]. An **ideal PHV** would provide a permanently functioning valve that mimics the native valve in form and function, that is easy to implant, and that produces no adverse effects, e.g. thrombosis, calcification, degradation, tissue in-growth, stenosis, and regurgitation. Children and adolescents would benefit from prostheses that could grow with them, but that is decades from reality and is more in the area of tissue engineering. In the future pharmaceutical therapies may be developed to arrest or reverse CAVD. Until then, polymeric valves may be a safer, cheaper, more durable, and more widely applicable choice than the tissue valves currently available.

**Polymer Valve History**

Earliest descriptions of flexible polymeric heart valves appeared in 1958 [50],[51]. Braunwald[11] *et al.* described the first human implantation of a bileaflet polyurethane (PU) valve to replace the mitral valve in 1960 [52] (Figure 6). Despite this early effort, utilization of polymeric heart valves initially did not materialize due to the success of the Starr-Edwards valve and later prosthetic valves and subsequent invention of safe and effective mitral valve open surgical and minimally invasive repair techniques [53]. PHVs have long been researched, but a lack of suitable materials has prevented their realization (Table 2). Polyurethane valves were thought to be promising and have been thoroughly evaluated over the last 20 years, but the development of polyurethanes with sufficient durability has been slow and is just recently producing promising formulations [54,55,56,57,58,59,60,61,62,63,64,65].

Breifly, a silastic trileaflet PHV was described by Mori *et al.* in 1973 [66], Imamura and Kaye described expanded-PTFE trileaflet PHVs in 1977 and their failure in dogs [67], Wisman *et al.* described a PU-PHV in 1982 [68], Kiraly *et al.* described a Hexsyn trileaflet PHV for use in a pulsatile left ventricular assist device (LVAD) 1982 [69], Woo *et al.* described the poor *in vitro* hydrodynamic performance of ABIOMED's valves in 1983 [70,71], Hilbert *et al.* demonstrated *in vivo* calcification of PU-PHVs in sheep in 1987 [72], Chandran *et al.* measured the *in vitro*

[11] Dr. Nina Starr Braunwald, M.D. was the first female heart surgeon in the world. She was a native New Yorker and protégé of Dr. Charles Hufnagel, M.D. at Georgetown Medical School. She designed, fabricated, and performed the first human trial of a PHV.

hydrodynamics of a PU-PHV and found them to be comparable to a pericardial THV in 1989 [64,65], Nistal *et al.* demostrated the *in vivo* failure and calcification of PTFE-PHVs in sheep in 1990 [73], a group at the University of Leeds developed a PU valve and reported good *in vitro* hydrodynamics in 1996 [74], a group at the University of Glasgow developed a PU-PHV and reported on serveral testing aspects up to *in vivo* sheep trials in 2001 that showed good results, however the valves were implanted in the mitral valve position [61], and Leo *et al.* demostrated the poor hydrodynamics of Aortech PU valves in 2005 [75]. Eventually, a key finding was that the ether groups on polyurethanes are susceptible to *in vivo* oxidization and subsequent hydrolysis, especially under flexion [10].

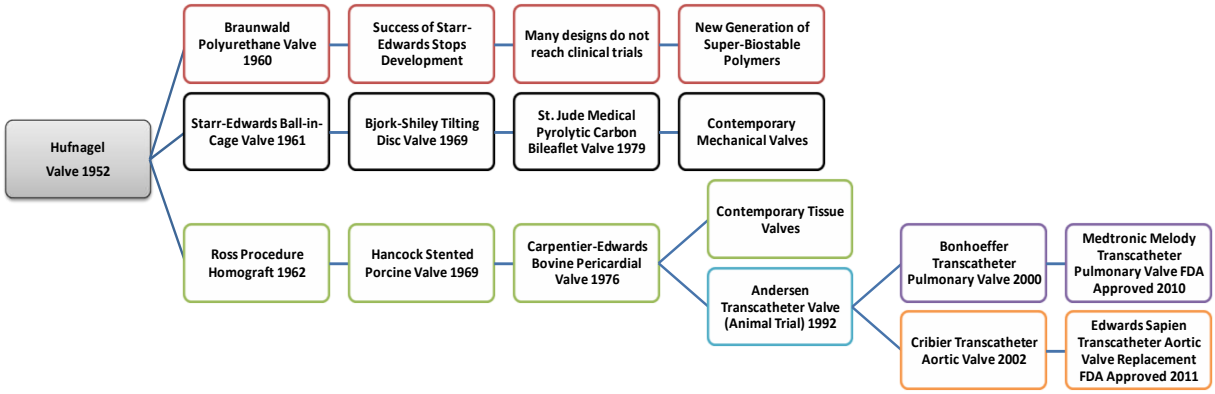


**Figure 6: Evolution of prosthetic heart valves focused on designs used in humans.**

The viscoelastic behavior of thermoplastics has limited their application in heart valves. The response can be modeled with a spring and dashpot either in series or in parallel [21]. In series the consitutive (stress) model is given by (3)

$$\sigma = K_s \varepsilon + \mu \frac{d\varepsilon}{dt} \tag{3}$$

where $K_s$ is the spring constant, $\varepsilon$ is strain, and $\mu$ is the dynamic viscosity. Creep and stress relaxation tests are used to quantify viscoelastic behavior and fatigue in plastics and rubbers [76,77,78]. Creep is the change in strain over time under a constant stress below the yield stress of the material, and stress relaxation is the change in stress over time under a constant strain. Hysteresis testing is a useful fatigue test for polymers that cyclically loads the specimen to measure the change in strain- 'dynamic creep' or energy dissipation under cyclic strain- 'dynamic stress relaxation' [79]. Generally, in a multi-block co-polymer, like SIBS, the higher the ratio of hard segments to soft segments results in reduced creep [76].

Given the steady improvement in the usable lifespan of THVs [80], the bar for regulatory approval of PHVs has been raised. As such if PHVs cannot meet or exceed the performance (safety and effectiveness) of THVs currently on the market then there is limited rationale or drive to approve their use in humans. However, a new generation of potentially more durable and bio-stable polymer formulations are being developed [81]. New nano-composite polymers may offer high durability and high biostability [82,83].

| Valve | Year Described | Pre-clinical/Clinical Experience, (Position implanted) | Reason for Dysfunction/Failure or Outcome | Reference |
|---|---|---|---|---|
| Polyurethane (PU) Bileaflet | 1960 | One human implantation resulting in death (Mitral) | Arrhythmia | [52] |
| Composite Silicone Rubber-Polyprolylene Fabric Trileaflet | 1975 | Clincal trials 1967-1973: 20 patient deaths associated with device failure (Aortic) | Degradation, fatigue failure, and thrombosis | [84,85] |
| Expanded PTFE Trileaflet | 1977 | 28 dogs 15 months, experimented with different leaflet thicknesses, (Tricuspid) | Leaflet stiffening, suture ring dehisence, strut entrapment | [67] |
| ABIOMED PU Trileaflet | 1983, 1993 | *In vitro* tests revealed stenotic turbulent flow worse than a THV | Stiff leaflets, narrow orifice | [70,71,86,87] |
| PU Trileaflet | 1987 | 17-21 week sheep studies (Mitral) | Calcification and thrombosis-stenosis and regurgitation | [72] |
| PTFE Trileaflet | 1990 | 12 sheep 8-10 weeks (Tricuspid) | Leaflet stiffening, calcification and thrombosis | [73] |
| Leeds PU Trileaflet Valve | 1996 | *In vitro* hemodynamics comparison of dip casting vs. film fabricated | Method of manufacture had significant effect on results | [74] |
| **The Advent of Biostable Polymers** | | | | |
| AorTech Methylenediphenyl Diisocyanate (MDI) Siloxane-PU Trileaflet | 2002 | 12 sheep 6-9 months (Mitral) | No evidence of degradation, thrombosis or calcification | [63] |
| Polycarbonate Urethane (PCU) Trileaflet | 2004 | 14 growing calves 20 weeks; (7 Mitral, 7 Aortic) | 2 AV animals died from pannus overgrowth causing severe AS; degradation and calcification observed to a greater degree in AVs but comparably less than in THVs | [88] |
| Innovia SIBS-Dacron Composite Trileaflet | 2010 | 6 sheep (Aortic) | Viscoelatic creep in SIBS, Dacron fatigue and calcification, no evidence of SIBS degradation | [13] |

**Table 2: Summary of PHV development focused on designs that reported *in vivo* results and other significant findings.**

## Next Generation Polymeric Materials for PHVs

Polymeric heart valves create an option for an optimized heart valve implant. Key functional targets of an optimized PHV include: allowance of hemodynamically consistent blood flow, retention of structural durability under cyclic load bearing conditions in a fluid environment, and maintenance of blood compatibility obviating the need for life-long anticoagulation [89]. Polymer surface and structural properties both play critical roles as design parameters with key variables including: backbone chemical bond stability towards degradation, thermal property such as glass transition temperature ($T_g$), melting temperature ($T_m$), heat of fusion ($\Delta H_f$), distribution of $T_g$, $T_m$, percentage crystallinity and size of crystalline and amorphous domains, and the percentage hard domain and size of the hard domain [89,90]. State of linearity of the backbone and branching of the chains are also important structural variables, for example cyclic chain extenders in polyurethanes demonstrate high $T_g$ but low tensile strength [89]. In the case of polyurethanes, backbone architecture of the soft segment is very important so as to prevent hydrolytic and oxidative degradation and reduce the potential for environmental stress cracking failure. Several new and improved polymeric materials are being investigated for use in PHVs. These material include: the first biostable polyurethane: polycarbonate-urethane (PCU) known as Bionate [88], a nano-composite polymer comprised of polyhedral oligomeric silsesquioxane (POSS) nano-particles and PCU [91], polyurethane with a poly(dimethylsiloxane) (PDMS) soft segment known as Elast-Eon$^{TM}$ by AorTech Biomaterials [92], Pellethane® 2363-80AE elastomer is a polytetramethylene glycol based polyurethane elastomer, by Lubrizol [49], the tri-block co-polymer thermoplastic polyolefin poly(styrene-*block*-isobutylene-*block*-styrene) or SIBS, held by Boston Scientific [10], and the new polyolefin thermoset elastomer xSIBS by Innovia LLC [93]. Other polymers that can potentially be used in heart valve embodiments include: fluoropolymers such as polyvinylidene difluoride (PVDF), and poly(vinylidene fluoride-co-hexafluoropropene) (PVDF-HFP); hyperbranched polyurethanes demonstrating shape memory property [94], and nano-organic clay-polyurethane composite [95]. These polymers offer improved biostability over previous generations. SIBS in particular appears to be one such 'super-biostable' polymer, showing high resilience to *in vivo* degradation.

## Transcatheter Aortic Valve Implantation (TAVR)

Although sophisticated minimally invasive surgical techniques have been developed for heart valve replacement to avoid median sternotomy [96], TAVR represents the most significant change in VHD treatment in decades and can be characterized as a potentially 'disruptive technology' [2,81,97,98,99]. TAVR serves a patient population that is considered inoperable and represents up to 33% of patients who need AV replacement [2,100]. The first transcatheter treatment for AI was described by Davies in 1965 [101]. TAVR as a new procedure was first described by Andersen *et al.* in 1992 [102] and then first performed in humans by Cribier *et al.* in 2002 [103]. Bonhoeffer *et al.* implanted the first transcatheter valve in the pulmonic position in humans in 2000 [104]. TAVR has since been FDA-approved (2011) for inoperable patients with severe AS. The procedure may be performed without extracorporeal circulatory support, and most significantly, without opening the chest or the heart by interventional cardiologists, thereby moving the procedure away from the traditional surgical realm, thus allowing rapid patient recovery, mobility and discharge, with reduced overall hospital costs. TAVR has also been explored to restore hemodynamic function in failed open-heart THVs [105,106,107,108] and in failed transcatheter valves (transcatheter-in-transcatheter) [109,110]. In the long term,

TAVR may become the new gold standard in valve replacement until tissue engineering or pharmaceutical interventions become more efficacious.

Initial transcatheter valves have been developed using xenograft valves as the essential structural component, primarily for their known *in vivo* performance and to facilitate more rapid regulatory approval in the United States. Presently, there are self- and balloon-expandable versions of transcatheter valves. Edwards Lifesciences recently gained FDA-approval (2011) to commercialize its balloon expandable Sapien® transcatheter valve for the treatment of severe AS in inoperable patients (the only FDA-approved TAVR device currently available). Medtronic is currently testing their self-expanding CoreValve® in a "U.S. Pivotal Trial", and they have an FDA-approved (2010) pulmonary transcatheter valve called Melody®. St. Jude Medical is currently developing a retrievable transcatheter valve called Portico [111]. Boston Scientific recently acquired Sadra Medical to take over development of their Lotus Valve System, which claims to be the first fully repositionable transcatheter valve. Fabrication of a transcatheter valve out of a polymeric material is likely to be a better choice than utilizing a fixed animal tissue valve, as it is more likely to tolerate the deleterious mechanical stresses that are imparted to the valve annulus and leaflets with mechanical crimping and balloon deployment [8,9]. Further, a polymeric valve lends itself easier to designs with comparatively lower profiles, which are better suited for delivery into smaller caliber arteries.

**Total Artificial Heart**

After more than 50 years of research and development, the Total Artificial Heart (TAH) (SynCardia Systems, Inc., Tuscon, AZ) is the only FDA-approved bridge-to-transplant heart replacement device available on the market [7]. Since the TAH project shifted to a 'bridge-to-transplant' treatment it has become accepted as a viable clinical therapy and its use is growing. The initial design was intended to be a destination therapy for heart failure patients in lieu of heart transplant [112,113]. However, that goal proved to be too ambitious given the current state of technology. The current model utilizes monoleaflet MHVs. Polymer PHVs may be able to increase the thromboresistance of the device and decrease the audible sounds of the device for patient comfort. Others have investigated the use of polymer PHVs in pulsatile VADs [114]. PHVs are imminently scalable and could be utilized in pulsatile pediatric VADs that currently employ MHVs [115].

**SIBS and PHV Development**

The thermoplastic elastomer SIBS, invented at the University of Akron by Kennedy *et al.* [116] and licensed and improved by Corvita Corp. (now owned by Boston Scientific) was developed to eliminate the *in vivo* degradation of PUs. SIBS has no reactive pendant groups rendering it hydrolytically, oxidatively, and enzymatically stable [10,79]. In testing to date, no evidence of *in vivo* degradation has been observed. SIBS has been commercialized as a coating material for a drug eluting coronary stent by Boston Scientific (Taxus® stent), for local contact-mediated arterial wall delivery of Paclitaxel following balloon angioplasty to prevent post-dilatation restenosis [117]. Further, it has been developed for PHV and ophthalmological uses by Innovia LLC, Miami, FL [118]. As SIBS is an elastomer with low tensile strength, it has been strengthened in the PHV leaflet design by embedding a polyester mesh (Dacron, CR Bard) [11]. The first composite SIBS-Dacron valve was fabricated via dip coating the Dacron with dissolved SIBS. This resulted in incomplete encapsulation of the Dacron and promoted platelet activation

as found in our *in vitro* flow loop studies [119]. The next design iteration was improved via casting, so as to completely encapsulate the Dacron mesh to prevent blood contact. The composite leaflet material was affixed via braided polyester sutures into a high styrene content cast SIBS stent. Human platelet adhesion studies, performed using whole blood in a parallel plate flow system have revealed low platelet adhesion, especially on phospholipid modified SIBS sheets [16]. Animal model biocompatibility testing of SIBS coated teflon sutures indicated no appreciable *in vivo* reactions [15]. We performed *in vitro* isolated human platelet activation testing of the improved cast leaflet design in comparison to a gold-standard THV in a small volume, pulsatile, flow loop using our modified prothrombinase platelet activation state (PAS) assay and flow cytometry via P-selectin [14]. Our results indicate that the platelet activation rate (PAR) in the SIBS valve measured by PAS is 5-fold lower than the THV. Additionally, *in vitro* hydrodynamics testing demonstrated a close approximation to the pressure gradient and regurgitation of the THV, with fatigue testing and finite element analysis (FEA) predicting a lifespan approximating 10 years [120]. With these positive test results, preclinical animal studies were conducted utilizing the sheep model. Animal studies revealed cracking of the SIBS coating via creep, allowing reaction with the underlying Dacron to occur, resulting in thrombosis, calcification, and tissue in-growth [13] (Figure 7). In parallel, we developed and evaluated a novel self-expandable transcatheter valve designed for AV replacement, comprised of the SIBS-Dacron composite and Nitinol wire and a complementary delivery system (Figure 8). We also formulated a method for *in vitro* testing of these devices. Our data demonstrated good hydrodynamic performance and *in situ* fixation of the final prototype [121].

In order to mitigate the failure of SIBS due to viscoelastic creep (change in strain over time under a constant stress below the yield stress), Innovia LLC (Miami, FL) has formulated the proprietary insoluble and infusible thermoset called xSIBS mentioned above, with which we are currently developing a novel PHV. The xSIBS utilizes a coupling reaction catalyzed by benzocyclobutene (BCB) that causes polymer back bones to crosslink via a Diels-Alder reaction[12]. The raw xSIBS is heated (240°C for 30 min) and compressed in the absence of oxygen to make thin films and prototypes for testing. Therefore, this work has investigated the feasibility of xSIBS as a material for use in PHVs.

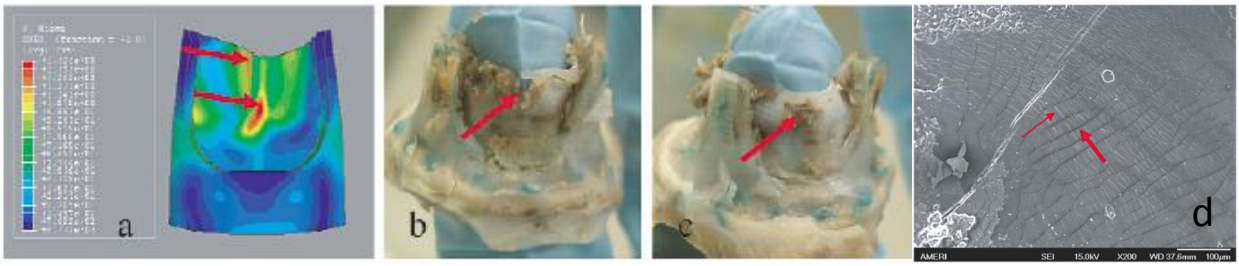


**Figure 7: The original SIBS-Dacron composite PHV design showing (a) stress concentration along its leaflets and (b through d the in vivo failure mode (Adapted from Wang et al. 2010) [13].**

[12] An Otto Diels-Kurt Alder reaction is a pericyclic (rearranging) reaction that forms a cyclohexene ring from a diene (a hydrocarbon with two carbon double bonds) and an olefin (alkene- hydrocarbons with the formula $C_nH_{2n}$) via heat. High pressure can speed up the reaction as well. Described in 1928, it has wide uses in synthetic polymers.

**Figure 8: A self-expanding SIBS-Dacron based transcatheter valve developed by our group (Adapted from Claiborne *et al.* 2009) [121].**

**Numerical Simulations**

Numerical analysis provides insight into the behavior of physical objects under expected operating conditions, but it always involves simplifications that can only approximate reality due to the limitations of mathematical models and computational resources. It involves an iterative process that can be refined towards optimization of a device (Figure 9). Numerical methods in general are used to find approximate solutions to partial differential equations (PDE). The three pillars of numerical analysis are convergence, order, and stability, each meaning whether or not the method approximates the solution, how well it approximates the solution, and the minimization of error, respectively. The two primary methods in numerical analysis are the finite element method (FEM) and the finite volume method (FVM). The former is typically used for structural analysis because it based upon the change in displacement of continuous node linked elements, and the latter is typically used for fluid analysis because it is based upon the conservation laws or flux through volumes.

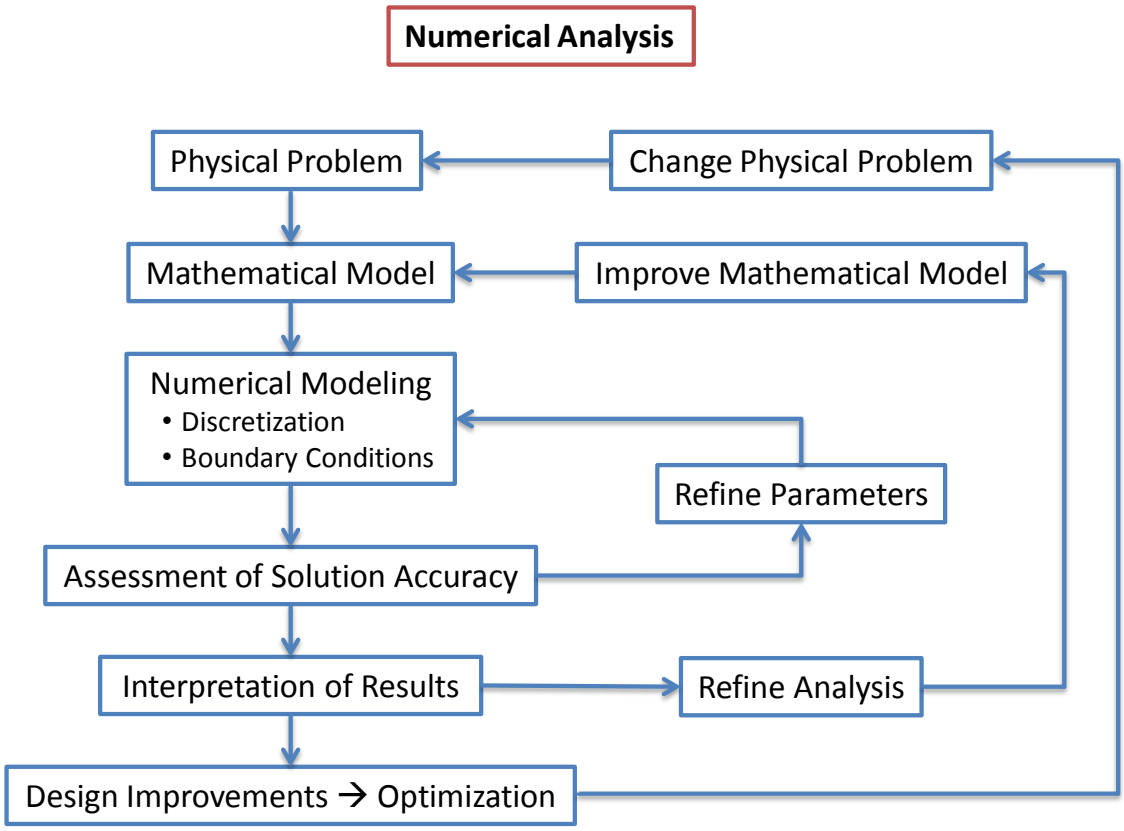


**Figure 9: Numerical analysis process [122].**

In this work two commercial numerical analysis software packages have been utilized: ADINA and Fluent (see Methods below). ADINA is based upon FEM (however the latest version has included an FVM option for fluids) and Fluent is based upon FVM. ADINA is capable of structural, fluid, and fluid-structure interaction (FSI) analysis, and Fluent is strictly capable of multi-phase fluid analysis. In **ADINA** [122], the 3-D geometries in this work have been discretized with 4-node tetrahedral elements using Delaunay meshing[13], which produces an unstructured mesh that is most suitable for complex geometries. The elements are isoparametric-displacement based and the basic assumptions are: for the coordinates (4):

$$x = \sum_{i=1}^{q} h_i x_i ; y = \sum_{i=1}^{q} h_i y_i ; z = \sum_{i=1}^{q} h_i z_i \qquad (4)$$

and for displacements (5):

[13] Boris Delaunay was a Russian mathematician who created a method to dicretize a computational domain using triangles that have a maximized minimum angle, thus eliminating the occurrence of small angles or skewed elements.

$$u = \sum_{i=1}^{q} h_i u_i ; v = \sum_{i=1}^{q} h_i v_i ; w = \sum_{i=1}^{q} h_i w_i \tag{5}$$

where $x_i,y_i,z_i$ are the nodal point coordinates, $u_i,v_i,w_i$ are the nodal point displacements, $i=1,...,q$, and $h_i(r,s,t)$ is the interpolation function (a mixed-function for Mooney-Rivlin material model) with $r,s,t$ being isoparametric coordinates. Small strain computations are considered to be $\leq 2\%$ with engineering stress-strain data as input and Cauchy stress and engineering strain as output. Engineering Strain is given by (6), engineering stress is given by (7), and Cauchy stress (true stress) is given by (8),

$$e_0 = \frac{l - l_0}{l_0} \tag{6}$$

$$\sigma = \frac{F}{A_0} \tag{7}$$

$$\tau = \frac{F}{A} = \frac{\sigma A_0}{A} \tag{8}$$

where $l$ is length, $F$ is force, $A$ is area and $0$ indicates the initial condition. From here the strain-displacement transformation matrix can be computed to evaluate the stiffness matrix. Axial stiffness is given by (9),

$$k = \frac{AE}{L} \tag{9}$$

where $E$ is the elastic modulus, $A$ is area, and $L$ is length.

**Contact between surfaces**, such as leaflet-leaflet contact in valve closure, has been modeled as well. Contact surfaces and targets are paired in ADINA with the following conditions (10):

$$g \geq 0; \lambda \geq 0; g\lambda = 0 \tag{10}$$

where $g$ is the gap between contacting surfaces, and $\lambda$ is the normal contact force. The default contact solution algorithm is the constraint function method given by (11):

$$w(g,\lambda) = \frac{g+\lambda}{2} - \sqrt{\left(\frac{g-\lambda}{2}\right)^2 + \varepsilon_N} \tag{11}$$

where $\varepsilon_N$ is a user defined parameter set to 1e-12 by default. Solutions have been found using implicit (Newmark) dynamic analysis. The implicit analysis solves the PDE at time $t$ after the solution at time $t - \Delta t$ is found, which requires the solution of a set of linear equations at each time step. This allows larger time steps to be used and is unconditionally stable.

In two-way coupled (fully coupled) **FSI analysis**, fluid forces are applied on the solid, and the solid deformation changes the fluid domain. The coupled system is always nonlinear, even if the solid domain is linear, because the fluid is always nonlinear. Convergence criteria are based on

either stress (dynamic) or displacement (kinematic) or both. The fluid nodal displacements are interpolated using the solid nodal displacements, and fluid traction at a solid node is interpolated using the stress of the fluid boundary element where the solid node is located. The dicretization of the fluid and solid meshes does not need to be identical but they need to be close to prevent errors. Currently, this fully coupled FSI is limited by insufficient fluid domain remeshing during the simulation to prevent element distortion that stops the solution process. As the fluid mesh distorts in the vicinity of the solid (especially a thin flexible structure in flow), the leading elements compress and the trailing elements stretch. These distortions should be corrected automatically before computational error (negative Jacobian[14], meaning the orientation of the tangent plane at a point has reversed) occurs every *n* timesteps. The currently available FSI software cannot yet overcome this problem.

In **Fluent**, the Navier-Stokes and Continuity equations (assuming an isothermal system) are solved numerically to describe the fluid flow [21]. Flux across a control volume's surface (*CS*) and through the control volume ($C\mathbb{V}$) is considered. These are related via the Reynolds transport theorem (12)

$$\frac{dB_{system}}{dt} = \frac{\partial}{\partial t}\int_{C\mathbb{V}} b\rho d\mathbb{V} + \int_{CS} b\rho V dA \tag{12}$$

where $B$ is the extensive property, $b$ is the amount of $B$ per unit mass ($m$), $\rho$ is density, $\mathbb{V}$ is volume, $A$ is the area of the *CS*, and $V$ is velocity. In words, the time rate of change of the extensive property (mass, momentum, or energy) is equal to the time rate of flux through a control volume plus the flux across the control surface. Conservation of Mass (Continuity Equation) is given by (13), and in discrete form (14) with velocity vector in Cartesian space (15), and "*del*" vector operator is given by (16),

$$-\int_{A_2} \rho V_2 dA + \int_{A_1} \rho V_1 dA = \frac{\partial}{\partial t}\int_{\mathbb{V}} \rho d\mathbb{V} \tag{13}$$

$$\nabla \bullet \rho \vec{V} + \frac{\partial \rho}{\partial t} = 0 \tag{14}$$

$$\vec{V} = u\,\vec{i} + v\,\vec{j} + w\,\vec{k} \tag{15}$$

$$\nabla = \vec{i}\,\frac{\partial}{\partial x} + \vec{j}\,\frac{\partial}{\partial y} + \vec{k}\,\frac{\partial}{\partial z} \tag{16}$$

where $A_1$ is the inlet surface area and $A_2$ is the outlet surface area with corresponding velocities $V_1$ and $V_2$. In words, the rate of mass in minus the rate of mass out equals time rate of change of mass in the $C\mathbb{V}$. The substantive derivative representing the time derivative of a scalar or vector quantity following the motion of the fluid is given by (17).

[14] Jacobian is the name of the determinant of a matrix comprised of the partial derivatives of a function.

$$\frac{D}{Dt} = \frac{\partial}{\partial t} + u\frac{\partial}{\partial x} + v\frac{\partial}{\partial y} + w\frac{\partial}{\partial z} \tag{17}$$

Combining (16) and (17) yields (18).

$$\frac{D}{Dt} \equiv \underbrace{\frac{\partial}{\partial t}}_{\substack{local \\ derivative}} + \underbrace{\left(\vec{V}\bullet\nabla\right)}_{\substack{convective \\ derivative}} \tag{18}$$

Using Reynolds transport theorem (12), the linear momentum of the fluid can be found (19),

$$\frac{D}{Dt}\int_{system}\vec{V}\,\rho d\mathbb{V} = \frac{\partial}{\partial t}\int_{C\mathbb{V}}\vec{V}\,\rho d\mathbb{V} + \int_{CS}\vec{V}\,\rho\vec{V}\bullet\vec{n}\,dA \tag{19}$$

with discrete form in the *x*-direction given by (20),

$$\rho\frac{Du}{Dt} = \frac{\partial\sigma_{xx}}{\partial x} + \frac{\partial\tau_{yx}}{\partial y} + \frac{\partial\tau_{zx}}{\partial z} + \rho g_x \tag{20}$$

where $g$ is gravity, $\tau$ is shear stress, $\sigma$ is normal stress, and $p$ is pressure. In words, the time rate of change of linear momentum in a system is equal to the time rate of change of linear momentum in the control volume plus the net rate of change of linear momentum through the control volume surfaces. Recognizing that normal stress in the *x*-direction is given by (21) and shear stress in the *x*-direction is given by (22) and (23), then combining (20), (21), (22), and (23) yields the Navier-Stokes equation for viscous flow in the *x*-direction (24).

$$\sigma_{xx} = -p + 2\mu\frac{\partial u}{\partial x} \tag{21}$$

$$\tau_{xy} = \tau_{yx} = \mu\left(\frac{\partial u}{\partial x} + \frac{\partial v}{\partial x}\right) \tag{22}$$

$$\tau_{zx} = \tau_{xz} = \mu\left(\frac{\partial u}{\partial z} + \frac{\partial w}{\partial x}\right) \tag{23}$$

$$\rho\frac{Du}{Dt} = \rho g_x - \frac{\partial p}{\partial x} + \mu\nabla^2\bullet\vec{u} \tag{24}$$

where $\mu$ is dynamic viscosity and $p$ is pressure. A fluid with constant viscosity where shear stress is proportional to shear rate (25), is called Newtonian.

$$\tau = \mu\dot{\gamma} \tag{25}$$

All of the numerical fluid studies performed in the this work made this assumption. Additionally, body forces (gravity) have been omitted.

In **turbulent fluid flow** simulations velocity (*V*) is decomposed into mean (over bar) and fluctuating (apostrophe) components (26), which when substituted into the Navier-Stokes equations yields the unsteady (time varying) Reynolds averaged Navier-Stokes (URANS) [ANSYS Fluent 12.0 Theory Guide]. However, this creates a closure problem (more unknowns than equations), which is addressed via the Boussinesq approximation of the Reynolds stresses (27) [123] using the two-equation Wilcox k-ω transitional flow model (29) and (30), which is best suited for aortic blood flow [124], and where turbulent viscosity is given by (28),

$$V(t) = \bar{V} + V' \tag{26}$$

$$\tau_{turb\ ij} = -\rho\overline{u_i' u_j'} \approx \mu_T \left( \frac{\partial u_i}{\partial x_j} + \frac{\partial u_j}{\partial x_i} \right) - \frac{2}{3}\left( \rho k + \mu_T \frac{\partial u_k}{\partial x_k} \right)\delta_{ij} \tag{27}$$

$$\mu_T = \alpha^* \frac{\rho k}{\omega} \tag{28}$$

where $k$ is the turbulent kinetic energy (source) (29), $\omega$ is the specific dissipation rate (sink) (30), $\alpha^*$ is the turbulent viscosity correlation coefficient that damps the turbulent viscosity, and $\delta_{ij}$ is the Kronecker delta function[15].

$$\frac{\partial}{\partial t}(\rho k) + \frac{\partial}{\partial x_i}(\rho k u_i) = \frac{\partial}{\partial x_i}\left( \Gamma_k \rho \frac{\partial k}{\partial x_j} \right) + G_k - Y_k + S_k \tag{29}$$

$$\frac{\partial}{\partial t}(\rho \omega) + \frac{\partial}{\partial x_i}(\rho \omega u_i) = \frac{\partial}{\partial x_i}\left( \Gamma_\omega \rho \frac{\partial k}{\partial x_j} \right) + G_\omega - Y_\omega + S_\omega \tag{30}$$

The effective diffusivity is given by $\Gamma$, $G$ is the energy generation term, $Y$ is the dissipation term, and $S$ is a user defined source term.

In **two-phase flow**, platelet sized particles are introduced into the flow field upstream from the device and their trajectories are predicted by calculating the particle momentum (in the *x*-direction) given by (31), and drag force given by (32) with the Reynolds number[16] (33),

$$\frac{du_p}{dt} = F_D\left(u - u_p\right) + \frac{g_x\left(\rho_p - \rho\right)}{\rho_p} + F_x \tag{31}$$

$$F_D = \frac{18\mu}{\rho_p d_p^2}\frac{C_D \mathrm{Re}}{24} \tag{32}$$

[15] The Kronecker delta function is a binary identity that has the value 1 when i=j and 0 when i≠j.

[16] The Reynolds number (Re) is derived from dimensional analysis of the Navier-Stokes equations and is the ratio of inertial forces to viscous forces. 2100 < Re < 4000 is transitional flow.

$$\mathrm{Re} = \frac{\rho d_p \left| u_p - u \right|}{\mu} \tag{33}$$

$$\sigma = \frac{1}{\sqrt{3}} \sqrt{\tau_{11}^2 + \tau_{22}^2 + \tau_{33}^2 - \tau_{11}\tau_{22} - \tau_{11}\tau_{33} - \tau_{22}\tau_{33} + \left( \tau_{12}^2 + \tau_{23}^2 + \tau_{13}^2 \right)} \tag{34}$$

where $d_p$ is the particle diameter, $C_D$ is the particle drag coefficient, $F_x$ is the inertial momentum, and $\sigma$ is the scalar particle stress. The drag force (32) governs the velocity of the particle in the flow field. The particle itself is like a probe that reports its location in the flow at any given time, which is used to calculate the scalar shear stress at that location via (34) rendered from from (27). The result is realistic behavior of the particle in flow in terms of following the flow through the device. This is more accurate than choosing random grid points at which to calculate the shear stress. Stress accumulation (SA) is given by the linear model (35),

$$SA = \int_{t_0}^{t} \sigma(t)dt \approx \sum_{i=1}^{N} \sigma_i \times \Delta t \tag{35}$$

where $\Delta t$ is the change in time.

Trileaflet PHVs have received relatively sparse attention in the literature compared to their mechanical counterparts, especially excluding tissue engineering treatises. In particular, there are few numerical models of trileaflet valves. The initial numerical models studied THVs using 2-D CFD by simulating steady turbulent flow through valves with varying degrees of stenosis [125,126]. Three-dimensional fluid-structure interaction numerical simulations of the aortic valve have been conducted by De Hart *et al.* [127] and Carmody *et al.* [128]. Carmody *et al.* used the **Immersed Boundary Method** (IBM) with the Arbitrary Lagrangian-Eulerian (ALE) approach [129] to simulate the entire cardiac cycle of the aortic valve using a left ventricle model [130] to drive flow. The IBM solves the Navier-Stokes equations on an Eulerian grid relative to Lagrangian points, but its accuracy depends upon the grid density and there is no information about what is happening at the fluid-solid interface [129]. In Lagrangian algorithms, each node of the computational mesh follows the associated material particle during motion (solid mechanics). In Eulerian algorithms, the computational mesh is fixed and the continuum moves with respect to the grid (fluid mechanics). The ALE method combines these two techniques and allows greater continuum distortions while maintaining a clear boundary between fluid and solid phases [131]. The transformation from the moving coordinate system (**x**,t) to the arbitrary moving coordinate system ($\xi$,$\tau$) is given by (36)

$$\vec{x} = \vec{\xi} + \vec{d}\left( \vec{\xi}, \tau \right) \equiv \vec{x}\left( \vec{\xi}, \tau \right) \tag{36}$$

where d is the vector describing the position and motion of the new system and time $t = \tau$ [122]. In the ALE relative velocities replace convective velocities.

De Hart *et al.* used a version of the IBM called the **Fictitious Domain Method** (FDM) to simulate the cardiac cycle of the aortic valve [132]. The FDM overcomes the complexity of adaptive fluid meshing by allowing independent discretizations of the computational domains so that the fluid mesh is not distorted by the submerged structures and remeshing and ALE methods

are not needed, however the result is a less than accurate solution. An FSI simulation of a polyurethane PHV was reported for 50 μs of forward flow using the ALE approach with ANSYS Flotran, which uses the **Sequential Weak Coupling Method** [133]. In this work we have used a fully coupled **Sharp Interface Method** (SIM) for FSI for superior realism and accuracy [134]. The SIM means that the fluid-structure interface remains two distinct meshes (solid and fluid) with a defined traceable boundary. The down side is that it is technically difficult and requires adaptive fluid remeshing every *n* timesteps to avoid mesh distortions, but it will yield the most accurate information about valve dynamics and the fluid behavior near the valve.

**Optimization of PHVs using Device Thrombogenicity Emulation (DTE) Methodology**

The DTE methodology of evaluation and optimization of the valve performance follows an iterative process (Figure 10) [18,19]. The goal of the DTE is to minimize, and ideally eliminate, the need for anticoagulants in blood contacting medical devices. This optimization methodology has been extended in trileaflet PHVs to include FEA for the structural stress minimization on the valve's leaflets.

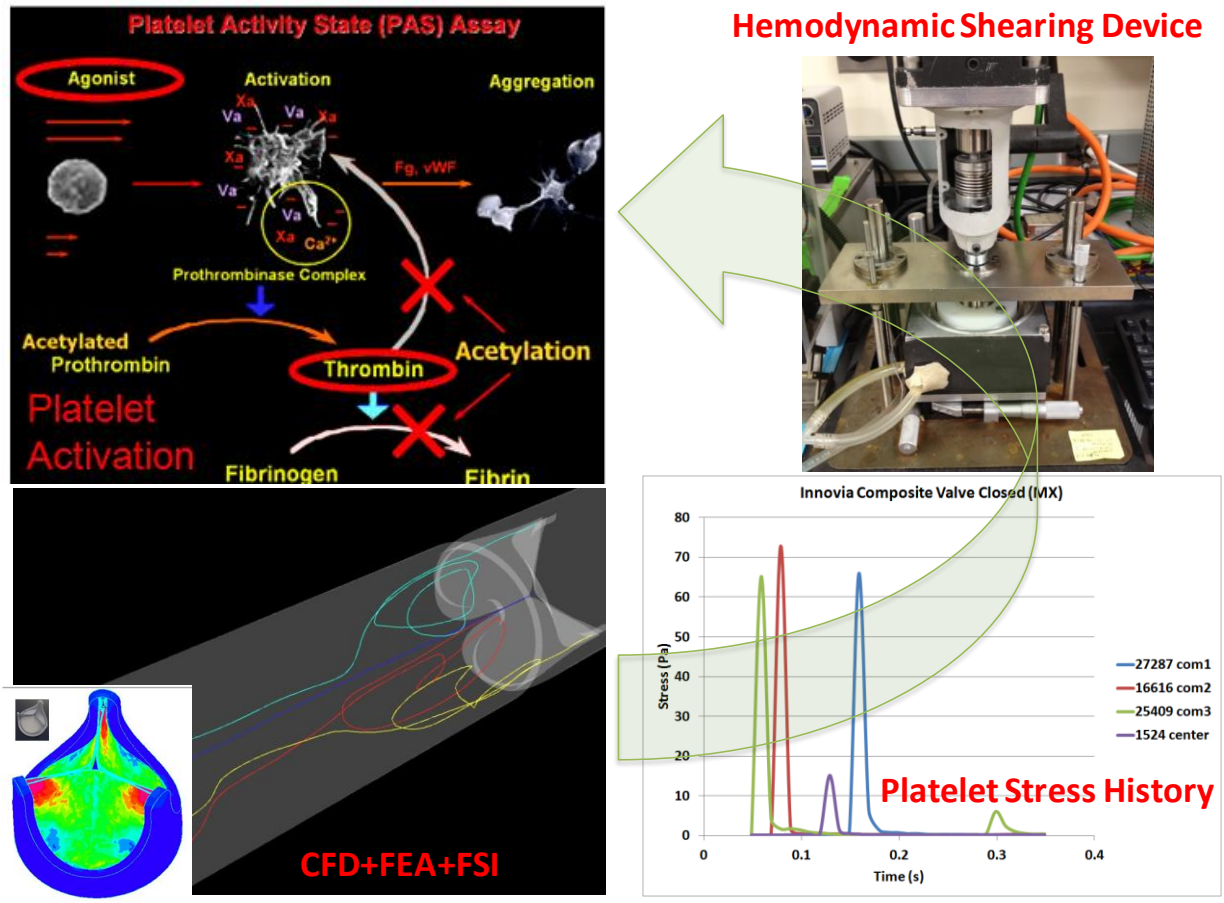


**Figure 10: Device Thrombogenicity Emulation (DTE) process involves the combination of numerical (CAD, CFD, FEA) and experimental methods (HSD-platelet activation).**

The DTE combines numerical studies with experimental platelet activation measurements in order to identify and modify undesirable design features that contribute to flow induced platelet

activation, which leads to thrombosis. We employ computer aided design (CAD), FEA, two-phase (particle and fluid) computational fluid dynamics (CFD) and Fluid Structure Interaction (FSI) simulations coupled with platelet activation measurements using our PAS assay in our large Hemodynamic Shearing Device (HSD), where stress loading waveforms extracted from geometry specific 'hot spot' regions of interest (ROI) are emulated, as previously described [135].

In order to characterize the global thrombogenicity of the device, we collapse the calculated SA information from about 50,000 platelets into a kernel smoothened Probability Density Function (PDF) of the SA to obtain SA range distribution curves that can be compared side-by-side, coined the 'Thrombogenic Footprint' of the specific device design iteration. The dominant mode of the thrombogenic footprint indicates in which SA range the majority of platelets passing through the device reside, and allows a side-by-side comparison of different designs. ROIs are identified within the flow field through the device by inspecting the velocity vector flow field at planar sections, the 3-D platelet dispersion patterns, and specific platelet trajectories. Regions of the device that create high velocity jets and shear layers are of special interest as they tend to generate the highest SA values (potential for platelet activation) and typically correlate with constricted flow regions. Platelets passing through these regions experience very high instantaneous shear stress, and the time that they spend in that region increases their stress accumulation. For trileaflet valves, the ROIs are typically the three commissures and the center near the leaflet free edge, during distinct phases of the forward flow through the open valve (systole) and regurgitant flow through the closed valve (diastole). During the iterative design optimization process, improved designs show a shift of the dominant mode toward lower SA range and a lower number of platelets residing in the higher and riskier SA range. This process can be repeated iteratively to achieve full optimization prior to prototype fabrication and testing.

The HSD human platelet studies serve as an experimental surrogate of the CFD and facilitates experimental comparison of various designs and/or devices before the optimized design prototype is fabricated and tested. Briefly, platelet experiments utilize our large HSD which is a high torque (13.3 N·m), fast response (3 ms) programmable cone-plate-couette viscometer that is capable of emulating highly dynamic platelet stress loading waveforms, reaching instantaneous shear stresses up to 900 dynes/cm$^2$. In order to select representative 'hot spot' loading waveform for HSD emulation, the stress accumulation (SA) along hundreds of platelet trajectories passing through an ROI, which is typically characterized by higher SA values, is computed and used to plot the probability density function (PDF) in the specific ROI. The most frequent SA in the subset is identified and a trajectory with the representative SA is then selected for emulation in the HSD. FEA studies feed geometries into CFD and inform us about the structural stress concentrations developed in a particular design during different phases of its duty cycle.

## SPECIFIC AIM 1: xSIBS Sheet Fabrication, Tensile Testing, and FEA Validation

### Introduction

The mechanical properties of the novel proprietary thermoset polyolefin, xSIBS (Innovia LLC, Miami, FL), are unknown. The xSIBS is a variation of the thermoplastic elastomer SIBS, which has undergone extensive testing and thoroughly characterized [10]. In order to gather data for FEA, uniaxial tensile testing was performed to obtain stress vs. strain curves. The FEA software

ADINA was validated via replication of the tensile tests and comparison of output curves to the experimental data.

## Methods

***Sheet Fabrication and Tensile Tests:*** A sheet mold was designed using computer aided design (CAD) software (SolidWorks, Dassault Systèmes SolidWorks Corp., Waltham, MA) and machined from aluminum alloy (Figure 11). The mold was coated with Teflon mold release (Super Lube Dri-Film Lubricant, Bohemia, NY) and raw xSIBS was placed in the mold, which was pressed to 3 tons and heated to 240°C for 30 min to induce cross-linking (Specac, Inc. Manual 15 ton Hydraulic Press and Atlas Series Heated Platens, Cranston, RI). Cross-linking was verified by soaking samples in toluene and observing swelling without dissolution. Uniaxial tensile tests were performed on dog-bone shaped samples (n=5) with pull rate 5 mm/min to break (Instron 3343 with 1000 N force transducer and Bluehill software, Norwood, MA). Stress vs. strain curves were created and data was input into finite element analysis (FEA). Sheets of xSIBS Lot No. 081203 (23% styrene, Innovia LLC, Miami, FL) were fabricated. Teflon sheets were sandwiched between the plates to isolate the xSIBS from air during heating to prevent oxidization.

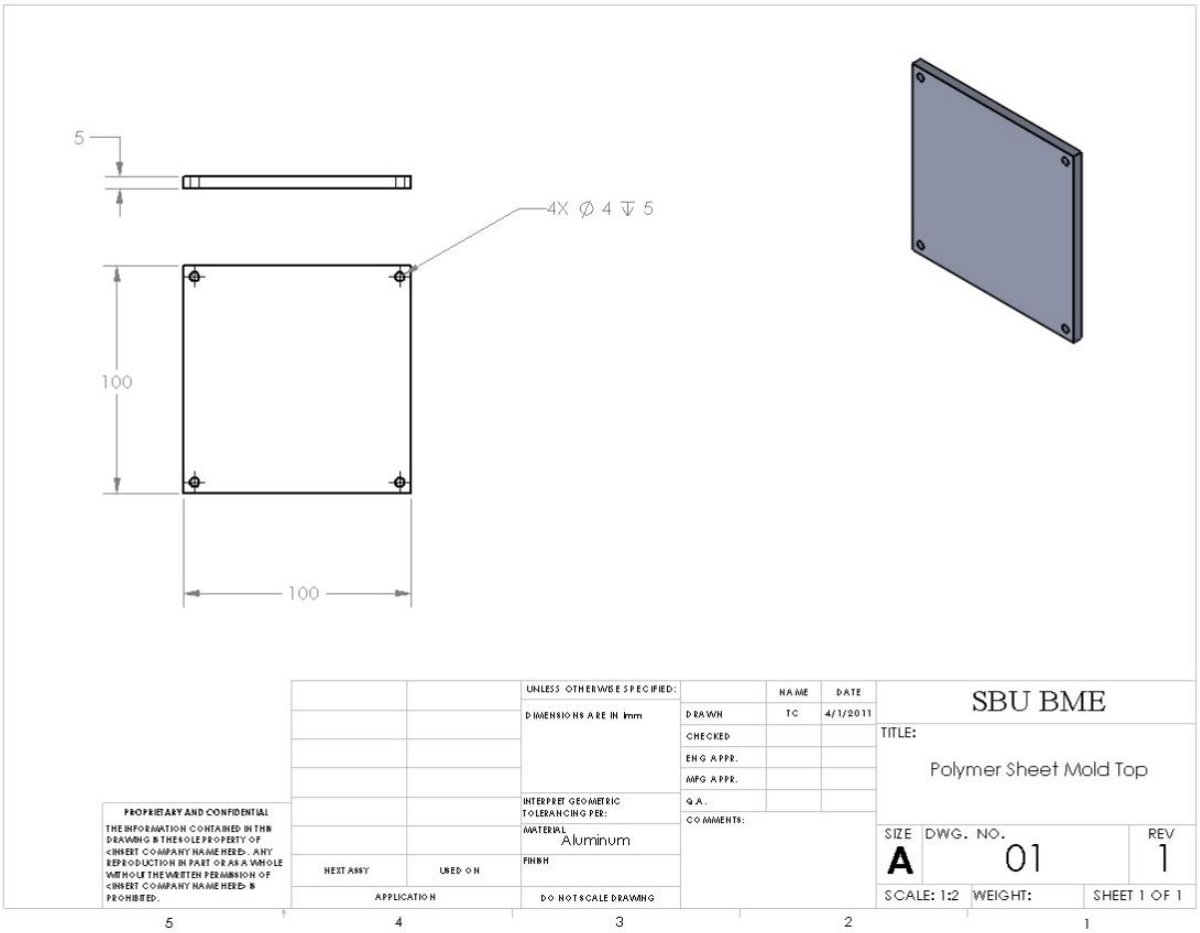


**Figure 11: Polymer sheet mold top engineering drawing.**

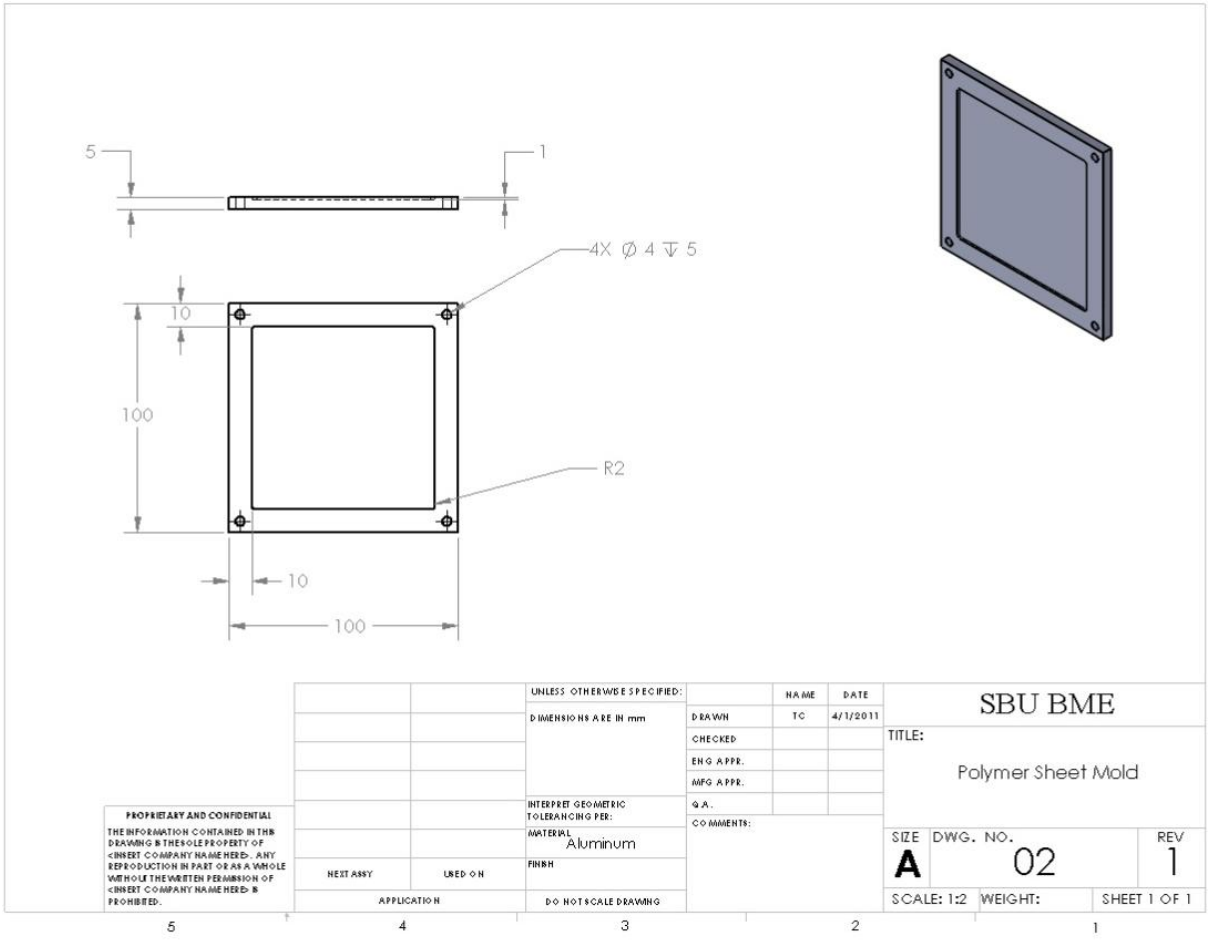


**Figure 12: Polymer sheet mold bottom engineering drawing.**

***Replication of Tensile Tests in FEA:*** Data from xSIBS sheets tensile tests were input into ADINA (ADINA R&D, Inc. Watertown, MA). The hyperelastic Mooney-Rivlin material model was used for each simulation given by the strain energy function [134] (37):

$$W_D = C_1\left(I_1 - 3\right) + C_2\left(I_2 - 3\right) + D_1\left(exp\left(D_2\left(I_1 - 3\right)\right) - 1\right) \tag{37}$$

where $C$ and $D$ are material constants and $I$ is the strain invariant or principle strain (the trace of the strain matrix). Constants $D_1$ and $D_2$ were used for the THV representing the strain stiffening phase of tissue. The elastic modulus is given by (38):

$$E = 6\left[\left(C_1 + C_2\right) + D_1 D_2\right] \tag{38}$$

Fixity was placed at the ends of the test strip, and a displacement (100% of the sample length) was prescribed for stretching the sample. The resulting stress vs. strain curve was extracted and compared to the experimental curve (Fig. 2 B&C).

## Results

***Sheet Fabrication and Tensile Tests:*** The fabricated xSIBS sheets appeared to homogeneous, flexible, and rubbery. Cross-linking was verified by soaking samples in Toluene and observing no dissolution. Instead, samples swelled in Toluene to about double their dry volume. The samples exhibited hyper-elastic responses during uniaxial tensile testing by enduring >100% stain will full elastic recovery (Fig. 2A). The mean ultimate strength was approximately 5000 kPa. The samples resisted breakage as a tear propagated across each sample during testing. The tear was not a clean break, but rather fibrous in appearance. Each specimen exhibited elastic strain beyond 100% with an average Young's elastic modulus (E) of 6 MPa. There appeared to be nonlinear anisotropic behavior in specimens pulled at orthogonal angles with slightly more linear behavior and lower break strength in the "preferred direction" (Figure 13). Strain stiffening was observed in the "cross direction" (Figure 13).

***Replication of Tensile Tests in FEA:*** The numerical FEA tensile tests in ADINA produced stress versus strain curves that matched the experimental data in strains <20% (Figure 14) . This was sufficient for our valve FEA studies.

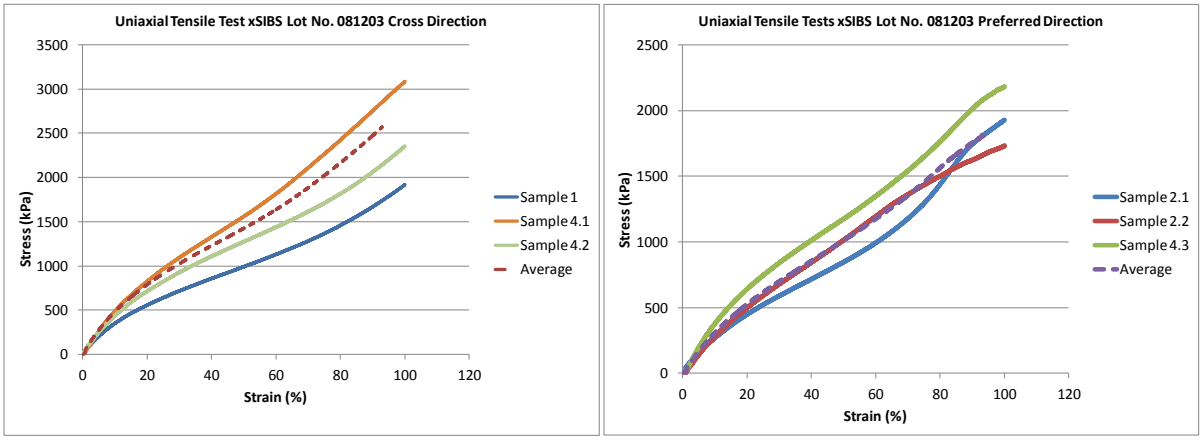


**Figure 13: xSIBS Lot No. 081203 tensile test results showing somewhat anisotropic nonlinear behavior.**

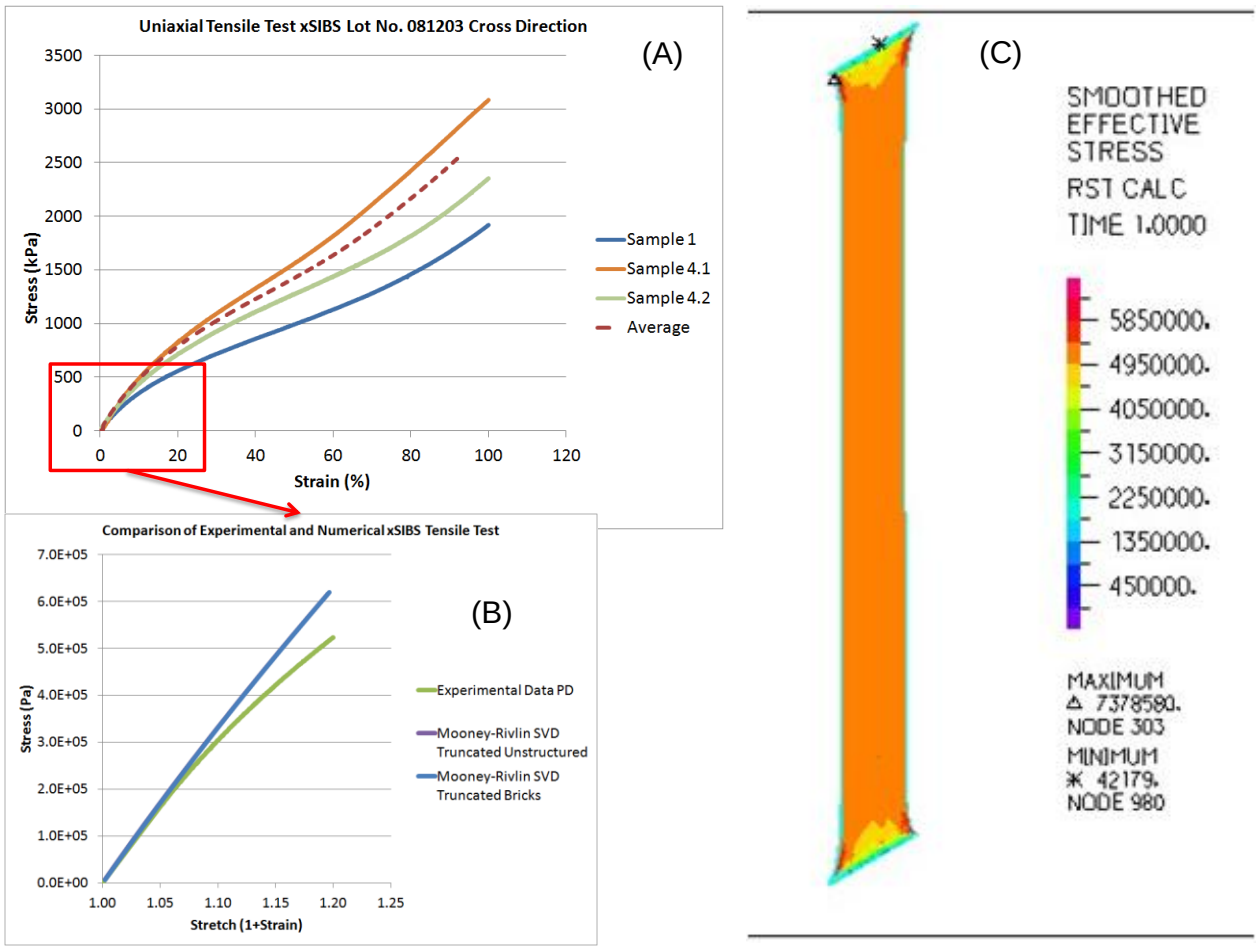


**Figure 14: FEA replication of tensile tests: (A) experimental data input into ADINA, (B) stress vs stretch curve output by ADINA using the Mooney-Rivlin hyper-elastic material model, and (C) stress map of the test sample in FEA.**

## Discussion

The new polymer xSIBS appears to have nonlinear hyper-elastic behavior under tensile loading. It exhibited a high break strength and a large elastic range. It also appears to be quite flexible and tear resistant. A more complete picture of the material mechanics will be developed in future studies including biaxial and compression testing. Ongoing studies in our lab include platelet contact activation measurements in our small HSD using the PAS assay.

## Conclusion

The new thermoset polyolefin xSIBS appears to have much improved tensile strength over the prior thermoplastic elastomer SIBS. This result suggests that fiber mesh reinforcement will not be necessary.

## SPECIFIC AIM 2: Optimized Valve and Mold Design

### Introduction

The "original" Innovia SIBS-Dacron composite valve design was the starting point for a new and improved design. The original valve was comprised of a molded high styrene SIBS formulation to create a rigid stent onto which the cast composite SIBS-Dacron leaflets were sutured with braided polyester (Ethibond by Ethicon a J&J Co.) (Figure 15). The stent was cylindrical with rounded posts, but the edges were sharp 90˚ angles. Since the leaflets were cast as a single flat sheet, they functioned as a collapsing cylinder once sutured into the stent. Several coaptation curvatures were tested [12]. The design had a nominal internal diameter of 19 mm. In order to mitigate the failures outlined above the design was altered significantly. The hypothesis being that a tapered leaflet design that resembled the native AV would produce better hemodynamics and lower stress concentrations than the original design.

**Figure 15: The "original" Innovia SIBS-Dacron composite PHV.**

### Methods

The new valve design was rendered in CAD (SolidWorks, Dassault Systèmes SolidWorks Corp., Waltham, MA). First, the cross-section of a single leaflet was sketched with 6 points of thickness changes. The free edge was set to 250 µm thick, tapering down to 180 µm, then to 200 µm, then back to 250 µm in the belly, then down to 180 µm, and finally back to 250 µm at the base attachment edge (Figure 16). The curvature was made with a spline to produce a semilunar shape. The solid was formed by sweeping the sketch about an axis. The path of the sweep was created such that a 120˚ angle was created by the leaflet free edge. The valve stent inlet internal diameter (ID) was set to 19 mm, but the outlet ID was set to 21 mm by pushing out the stent posts relative to the central axis with a deform feature. A sewing ring was added to the stent base and all edges were rounded with a 1 mm radius. The leaflet were created in a zero stress nearly closed position with a flat coaptation curvature to maximized the coaptation area.

The mold geometry was created using Gambit (ANSYS Fluent, Canonsburg, PA). The valve CAD model was converted to a parasolid file for import into Gambit. Gambit is better suited for Boolean operations than SolidWorks. The valve geometry was rendered as a volume in Gambit and then subtracted from a cylinder to create a negative space for the mold. Top, bottom and side components for the mold were created in a similar fashion. Each component was exported

as a parasolid file for further manipulation in SolidWorks. There, the outer mold block was created with fastening features, and an assembly was created to test the fit of all components (Figure 17, Figure 18, Figure 19, Figure 20, Figure 21, and Figure 22).

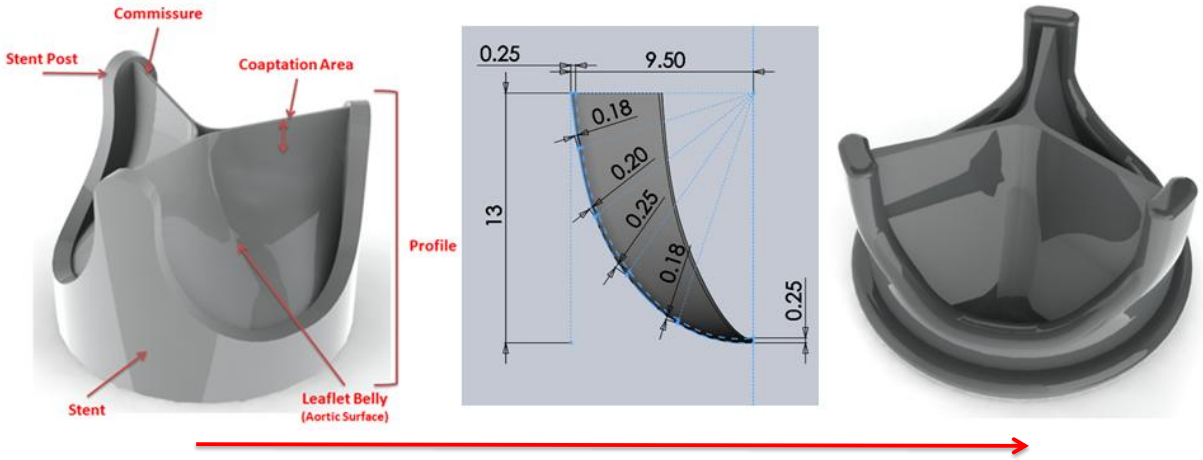


**Figure 16: Design changes made in CAD showing the original SIBS-Dacron composite design (left), the cross-sectional dimensions of the new "optimized" design (center) and the 3-D CAD rendering of the optimized PHV (right).**

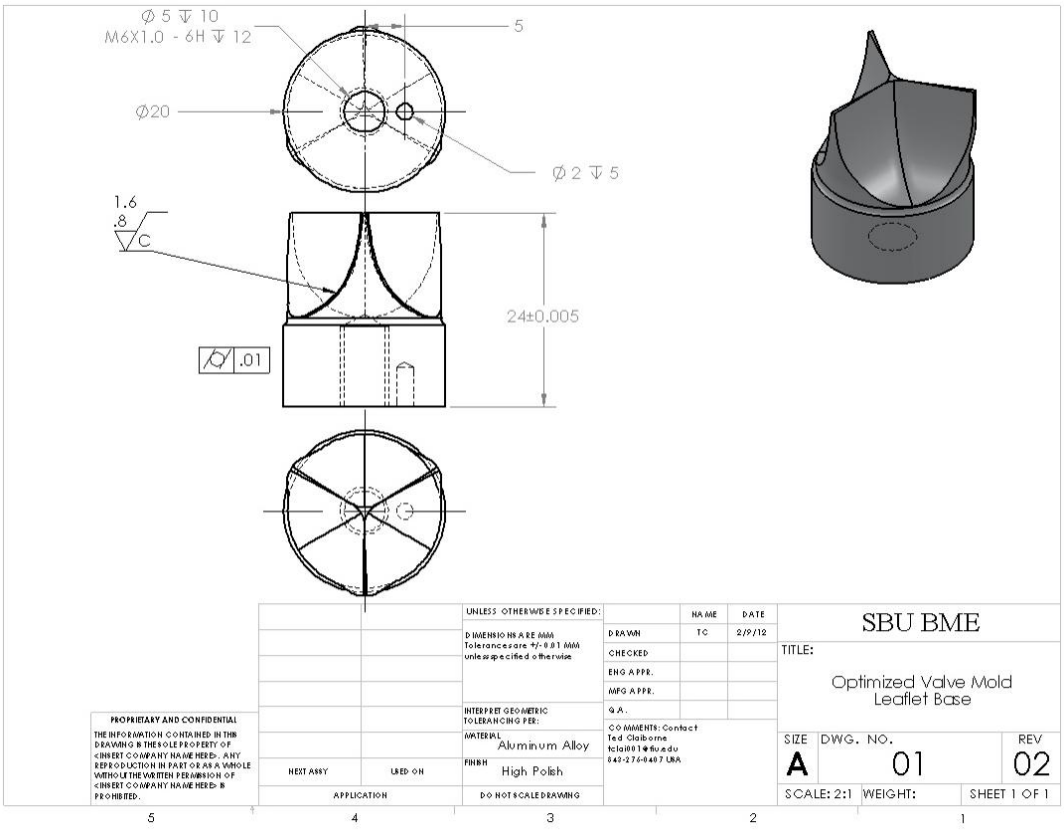


**Figure 17: Engineering drawing of the optimized valve mold leaflet base.**

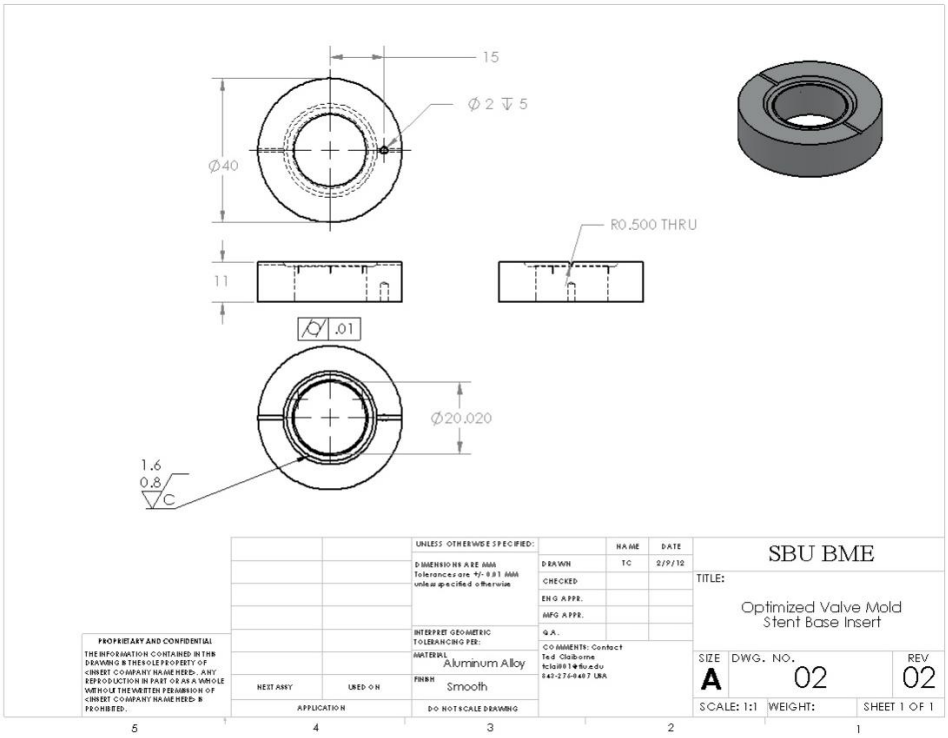


**Figure 18: Engineering drawing of the optimized valve mold stent base.**

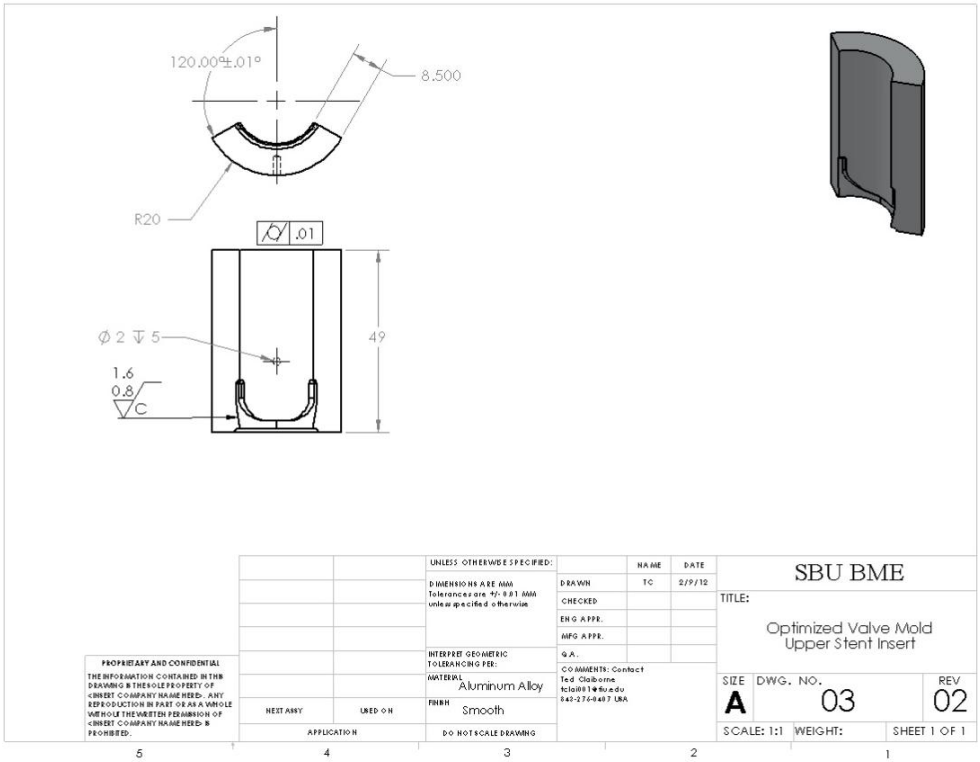


**Figure 19: Engineering drawing of the optimized valve outer stent mold.**

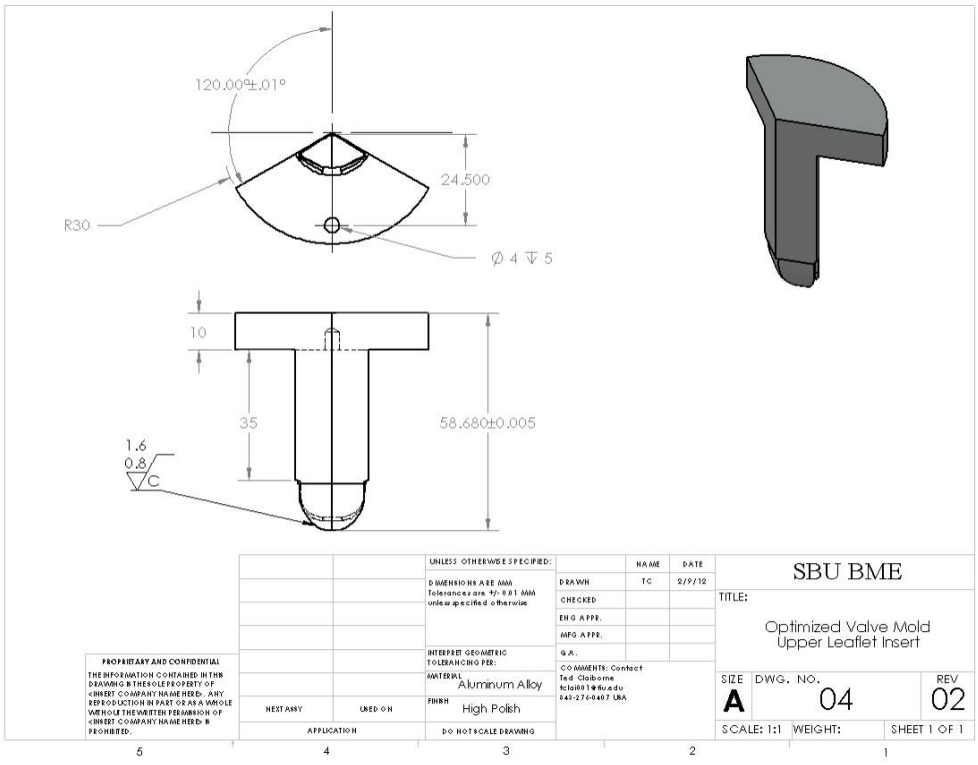


**Figure 20: Engineering drawing of the optimized valve mold leaflet top.**

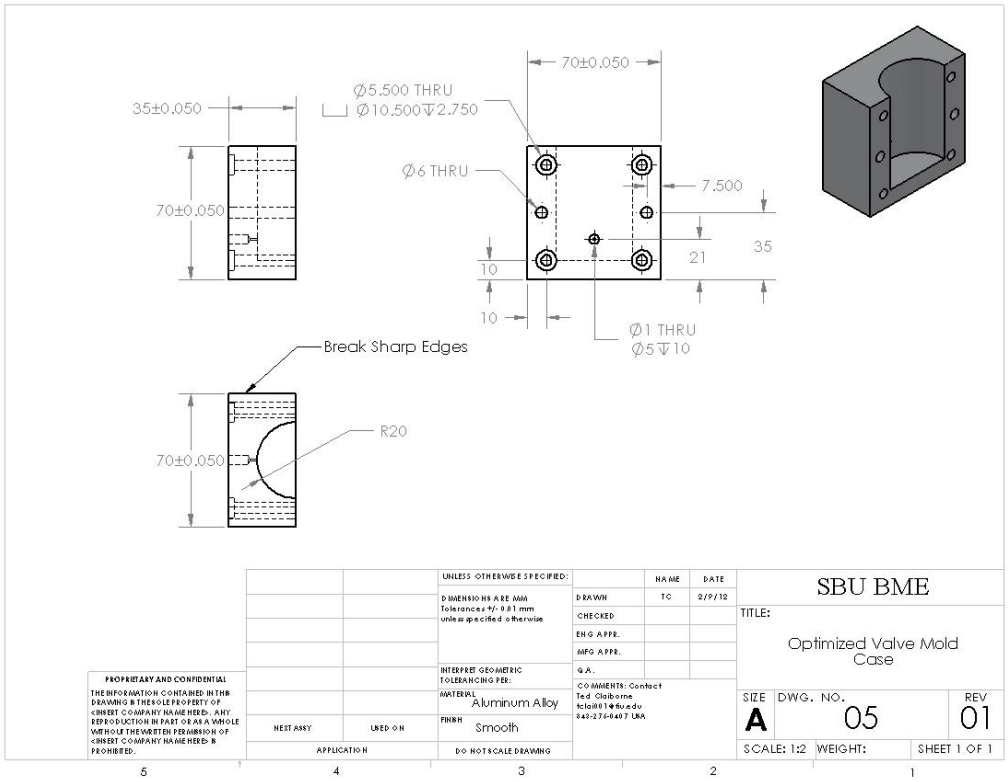


**Figure 21: Engineering drawing of the optimized valve mold case.**

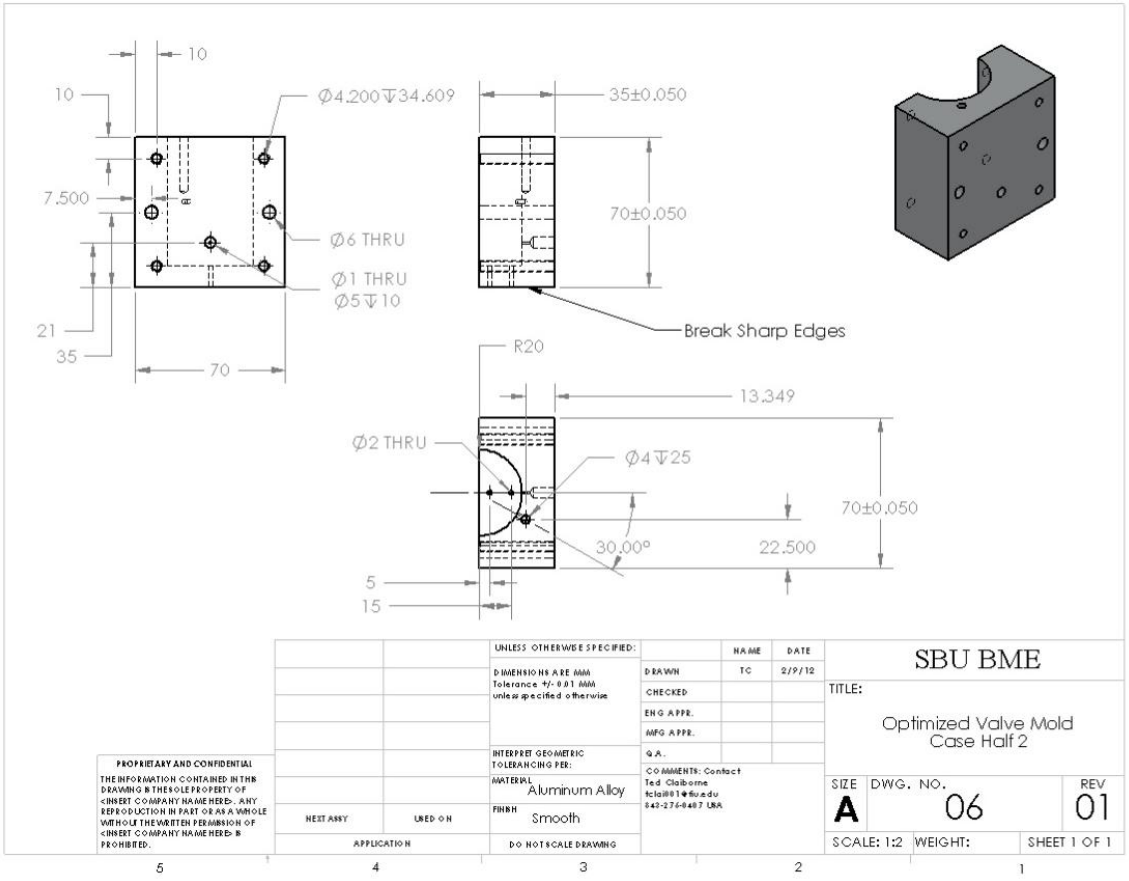


**Figure 22: Engineering drawing of the optimized valve mold leaflet base.**

## Results

The final mold design was accepted for 5-axis computer numerical controlled (CNC) machining at the Helmholtz Institute of Applied Medical Engineering in Aachen, Germany. The mold material was aluminum alloy for ease of machining and excellent thermal conductivity (Figure 34). The optimized valve design was prepared for FEA, CFD, and FSI studies.

## Discussion

The design of the optimized valve and mold was not a trivial task. The complex geometry of the valve presented several challenges in the design phase that necessitated many design iterations. SolidWorks was not capable of performing the complex Boolean operations required to create the void shape of the valve in each mold component, so Gambit was used. The communication between Gambit and SolidWorks was achieved using the parasolid file format. SolidWorks was useful in creating fastening features, assemblies, and engineering drawings. Expert CNC machinists were then able to create a precision valve mold. This is a large improvement over previous dip coating and casting methods, because precise geometries, such as the tapered leaflet thickness, can be created. The mold also facilitates the thermal cross-linking process required for xSIBS by sequestering the polymer from air to prevent oxidization an being an excellent thermal conductor. Molding also allows for more precise quality control. The constraint of CNC machining necessitated much of the mold design features. In the future electrical discharge

machining (EDM). EMD is better suited for rapidly cutting complex small shapes compared to CNC, but it is an significantly more expensive.

**Conclusion**

A novel valve and compression mold were designed, and the mold was successfully machined. This will allow for the creation of reproducible precision valve geometries.

**SPECIFIC AIM 3: DTE Evaluation of the Optimized PHV**

**Introduction**

We have developed and previously described an *in vitro* blood contacting device design, evaluation, and optimization methodology called "Device Thrombogenicity Emulation" (DTE) [18,19]. The DTE interfaces state-of-the-art numerical and experimental methods to optimize the thrombogenic performance prior to prototype fabrication and testing. The goal of this method is to reduce or eliminate the need for anticoagulants and to make the R&D cycle more efficient. In the development of novel PHVs, it is necessary to show equivalence to currently FDA-approved THVs in terms of hemodynamics and thrombogenicity. For that purpose, we have applied the DTE method to evaluate and compare the "original" SIBS-Dacron composite PHV in (Innovia, LLC, Miami, FL) (Figure 23A) to a commercially available "gold standard" THV, the Carpentier-Edwards Perimount Magna Bioprosthetic valve (Edwards Lifesciences, Irvine, CA) (Figure 23 B&C), which has shown good clinical performance [136]. Then we designed an "optimized" valve based upon the feedback from the DTE and compared the three valves (Figure 23D). The goal of this parametric study was to compare three trileaflet valve geometries and to verify our DTE method and design optimization in these devices.

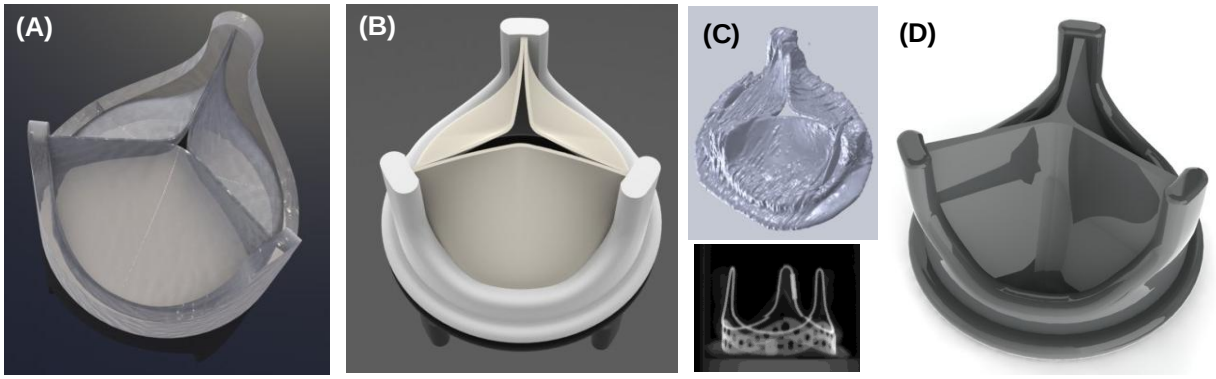


**Figure 23: CAD models of the valve compared in this study (A) the original Innovia SIBS-Dacron Composite PHV, (B) the reconstructed Cartentier-Edwards Perimount Magna Bioprosthesis or THV, (C) the THV geometry reconstructed from microCT scans, and (D) the optimized PHV design.**

## Methods

### Numerical Studies

***Optimized Valve Design and FEA:*** A novel PHV was designed SolidWorks CAD. The failure modes of the original SIBS-Dacron composite valve and the native AV geometry were considered. The radial cross-section of the leaflets were changed to a variable thickness and the shape of the leaflet was changed to hemispherical (Figure 16). Areas of expected high stress were thickened, and conversely, areas of expected lower stress were thinned. The coaptation surface was maximized by designing a flat leaflet profile. The valve stent was altered by smoothing surfaces and widening the exit orifice to a 21 mm internal diameter. Using ADINA, the optimized valve was compared to the original and tissue valves under normal diastolic pressure loading (80 mmHg) in structural FEA. Experimental tensile test data was used for the optimized valve, similar data from [12] was used for the original PHV, and constants from [137] were used for the THV. The effective stress maps from FEA were qualitatively compared (Figure 25).

***Obtaining Tissue Valve Geometry:*** Three-dimensional geometry of the tissue valve was obtained using micro-CT (μCT40, Scanco Medical, SUI). Scans were conducted at 36 micron isotropic resolution with an energy level of 70kV and 114μA (Figure 23C). A 3-D geometry was reconstructed from the micro-CT scans using Mimics (Materialise, Leuven, Belgium). The Mimics geometry file was then imported into ANSYS Gambit, where it was reconstructed in preparation for finite element analysis (FEA) solid simulations (ANSYS, Inc. Canonsburg, PA). The final geometry was created using SolidWorks (Dassault Systèmes SolidWorks Corp., Waltham, MA).

***Obtaining Valve Geometries for Computational Fluid Dynamics (CFD):*** Input parasolid files for each valve were created using Gambit for the FEA analysis in ADINA (ADINA R&D, Inc. Watertown, MA), where 3-D structural simulations under normal pressure gradient loading obtained from prior Left Heart Simulator (Vivitro Labs, Inc., Victoria, BC) studies of the Innovia valve [12] were performed. The simulations were conducted with fixed stents and free leaflets. Initially, identical isotropic linear elastic material models and mesh densities were used for each valve finite element analysis (FEA) simulation ($E$=2 MPa, $\nu$=0.40, $\rho$=1100 kg/m$^3$) in order to isolate the geometry effects. Later iterations utilized the hyperelastic model (37). The resultant fully open valve (forward flow at peak systole) and near closed valve (regurgitant flow at mid-diastole) geometries were then exported as fixed geometry parasolid files from ADINA for input into Gambit for finite volume meshing in preparation for CFD simulations.

***Fluid-Structure Interaction Studies:*** Fully coupled FSI studies were conducted in the original and optimized PHVs using ADINA. Partially open valve geometries were created using structural FEA with normal pressure loading so that upon use in FSI there would be a larger number of fluid mesh elements between the leaflet free edges in order to mitigate nonconvergence due to early mesh distortions. As such, the fluid mesh was not significantly adaptive in these case studies. Identical mesh densities (0.001 x unit length), the Mooney-Rivlin hyper-elastic material model (37) (using experimental data from xSIBS tensile tests and from [120]), and fluid density of 1050 kg/m$^3$ and viscosity of 3.5 cP, were used in each case study. Normal pressure at the inlet and outlet was used to drive flow (Figure 24). The tube walls and

valve stent were constrained to be rigid. The surfaces of the valve leaflets were selected for fluid-structure interface.

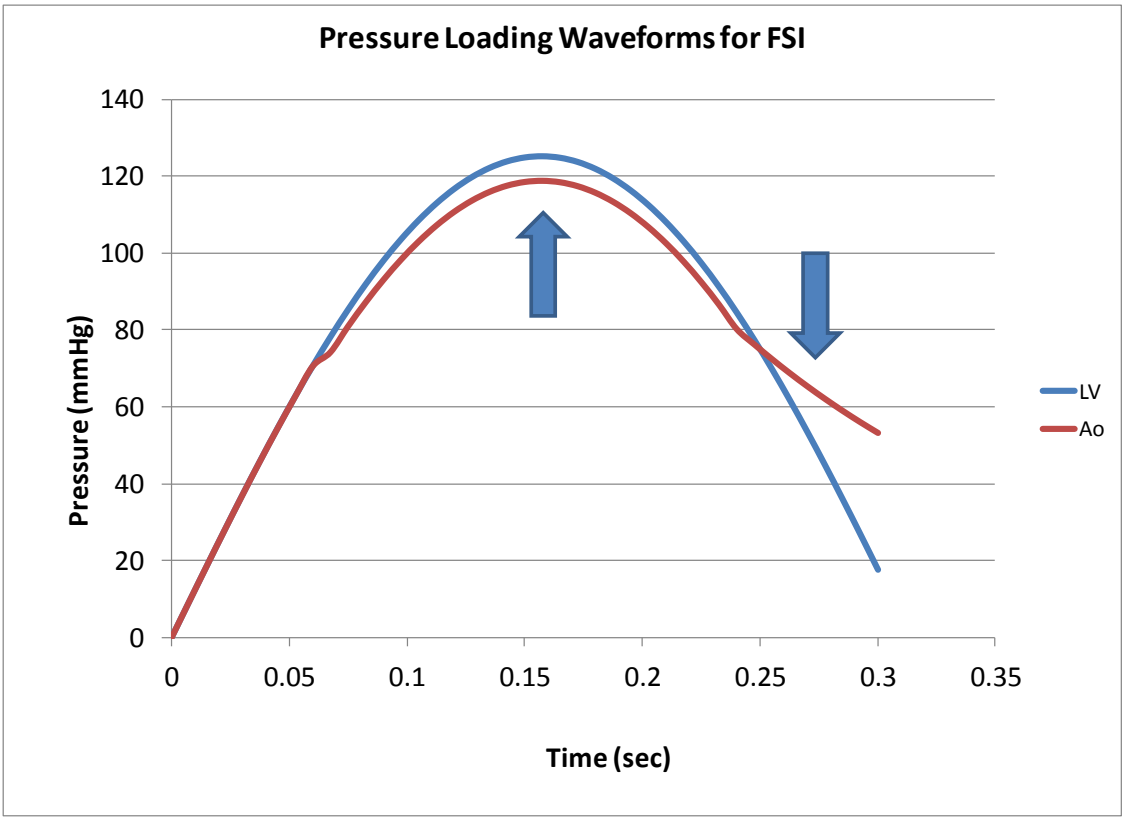


**Figure 24: Idealized FSI pressure loading waveform with arrows showing systole and diastole.**

***Two-Phase 3-D CFD:*** Each valve geometry (both opened and closed) was embedded in a rigid straight tube (length 20 cm & diameter 20 mm) and simulated using ANSYS Fluent CFD package (ANSYS Fluent, Canonsburg, PA) as two-phase (particle and fluid) CFD as previously described [18,138,139]. Briefly, the blood was simulated as two-phase Newtonian fluid with a viscosity of 3.5 cP and density 1050 kg/m$^3$, with neutrally buoyant 3 µm diameter spherical particles representing platelets. Open valve geometries were used to conduct forward Unsteady Reynolds Averaged (URANS ) turbulent flow simulations using the Wilcox k-ω turbulence model (27) with a decelerating systolic flow velocity waveform imposed on the inlet and zero pressure at the outlet [26,140]. Highly resolved progressive mesh densities consisted of 8-12×10$^6$ finite volumes small enough to resolve the Kolmogorov scale turbulent eddies (20-70 µm) [18]. For regurgitant flow in the closed valve simulations, unsteady laminar flow at constant velocity (0.05 m/s) was imposed at the inlet and zero pressure at the outlet. In both cases, the platelets were seeded into an upstream plane in the flow adjacent to the valve resulting in 4-6×10$^4$ platelets per simulation, and 350 ms of flow were simulated. The stress loading history along flow trajectories, experienced by the platelets seeded into the flow field, was computed by a summation of the combined effect of the total stress acting (34) on the platelets (a scalar representation of the various components of the stress tensor) and exposure time to obtain the Stress Accumulation (35) [18]. In post processing, spherical regions of interest (ROI), with

radius r = 1 mm, were created and queried at the three commissures (near the wall) and the center of flow, all near the leaflet free edge. In each valve the ROIs were identical. The sample of trajectories passing through the ROIs were plotted in probability density functions (PDF) of the stress accumulation (SA), and four trajectories representing the most frequently occurring SA from each SOI in each valve (12 total) were selected for emulation in our Hemodynamic Shearing Device (HSD) for *in vitro* isolated human platelet activation studies.

***Statistical Analysis:*** The quantitative "Thrombogenic Footprint" (TF), a global representation of the thrombogenic potential of a device, of each valve was obtained by collapsing information from thousands of platelet trajectories into the statistical distribution called the Probability Density Function (PDF) of the Stress Accumulation (SA) of platelet trajectories as previously described [18]. Briefly, the PDF represents a kernel smoothened continuous non-parametric probability density histogram where the discrete area under the curve correlates with the number of platelets residing at a particular SA. The major modes of the distribution characterize the TF and serve to compare the global thrombogenic potential of the three valves. A mode shift to the left, toward lower SA values, represents a device with a lower risk of thrombosis because the majority of particles reside in a low SA range, i.e., less thrombogenic. Results were compared via non-parametric one-way ANOVA with significance level $\alpha=0.05$. Bootstrapping was used to equalize population sizes.

**Experimental Studies**

***Hemodynamic Shearing Device Platelet Activation Measurements:*** Platelet trajectories from each valve were extracted from four identical SOIs, and their corresponding stress loading waveforms were programmed into our HSD as previously described [18]. The HSD is a highly dynamic cone-plate-couette viscometer capable of emulating dynamic stress loading waveforms and producing constant shear stress in the flow given by (39):

$$\tau_{cone-plate}=\tau_{couette}=\mu\frac{\omega}{\alpha}=2\mu\frac{\omega Ro^2Ri^2}{Ro^2-Ri^2}\left(\frac{1}{r^2}\right)^{r=Ri}\Rightarrow\alpha=\frac{1}{2}\left[1-\left(\frac{Ri}{Ro}\right)^2\right]\left(small\,\alpha,\frac{Ri}{Ro}=1\right) \quad (39)$$

where μ is the viscosity; ω is the angular velocity of the cone; α is the cone angle; and Ro and Ri are the inner radius of the outer ring and outer radius of the cone, respectively [141]. The cone angle $\alpha=1^\circ$, and the cone, plate and couette material is ultra-high molecular weight polyethylene (UHMWPE), which is a relatively inert material in terms of hemocompatibility. Further, we coat the UHMWPE with Sigmacote, a silicone solution in heptane that prevents blood clotting on negatively charged surfaces such as glass. The HSD is driven by a Baldor 13.3 N·m torque, 2000 rpm, 2.18 kW electric motor controlled by a Baldor Flex+Drive and Baldor WorkBench 5 software (Baldor Electric Co., Ft. Smith, AR). Briefly, human whole blood (30 ml) was obtained via antecubital venipuncture from healthy adult volunteers of both sexes who were screened for antiplatelet medications in accordance with Stony Brook University IRB. Whole blood in 10% ACD-A was separated via centrifuge (650 x g for 6 min) to obtain platelet rich plasma (PRP), which was gel filtered (Sepharose 2B, Sigma-Aldrich) to obtain purified gel filtered platelets (GFP). The GFP was diluted to a count of 20,000/μl in a Hepes modified Tyrode's platelet buffer. In order to increase the viscosity of the platelet suspension to emulate peak shear stresses, Dextran (MW 150,000 Sigma-Aldrich) was added to the platelet buffer to

achieve viscosities of 7.0 and 8.0 cP corresponding to maximum shear stress of 700 and 800 dynes/cm$^2$ for the regurgitant and forward flow experiments, respectively. A 3.0 mL sample of GFP suspension was placed into the HSD and stress waveforms were emulated for 600 repeats over 10 min. Beginning and ending time point aliquots (25 µL) were sampled from the HSD well in duplicate. The chromogenic platelet activation state (PAS) assay was performed to measure thrombin generation as previously described [33]. Results were normalized against the PAS of fully activated platelets obtained via sonication at 10 W for 10 s (Branson Sonifier 150 with microprobe, Branson, MO). Each set of 12 experiments for both forward and regurgitant flow were performed using platelets from one donor within 6 hours of obtaining GFP (n=5 sets, total 60 experiments).

***Statistical Analysis:*** The change in (Δ) PAS was calculated over the 10 min experiment. The mean ΔPAS for 5 sets was plotted in bar plots for each SOI (commissures 1-3 and the center) with standard error bars for both forward and regurgitant flow [18]. One-way ANOVA was used for statistical analysis with significance level $\alpha$=0.05 [14].

## Results

### Numerical Results

***FEA of the Optimized PHV:*** Normal diastolic pressure loading (80 mmHg) in structural FEA in all three valves showed reduced stress concentrations at the commissures, across the leaflet belly, and on the free edge and leaflet base attachments in the optimized valve compared to the original and tissue valves (Figure 25).

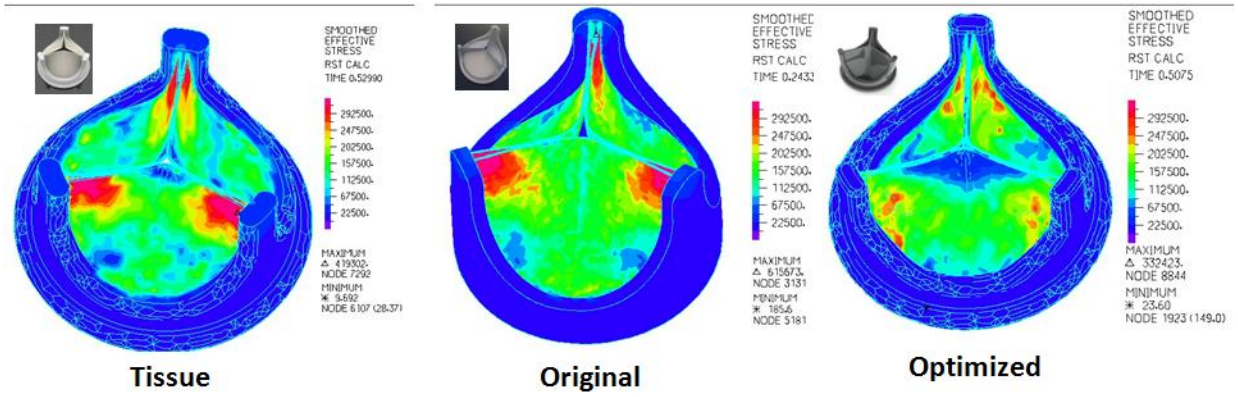


**Figure 25: Structural FEA results from normal diastolic pressure loading in the three valve designs with identical stress scales in each image. The optimized design exhibits reduced stress concentrations in the commissures, the leaflet belly attachment, and the coaptation area compared to the THV and the original PHV.**

***FSI:*** The original composite valve produced higher solid stresses and higher fluid velocities compared to the optimized xSIBS valve (Figure 26 & Figure 27).

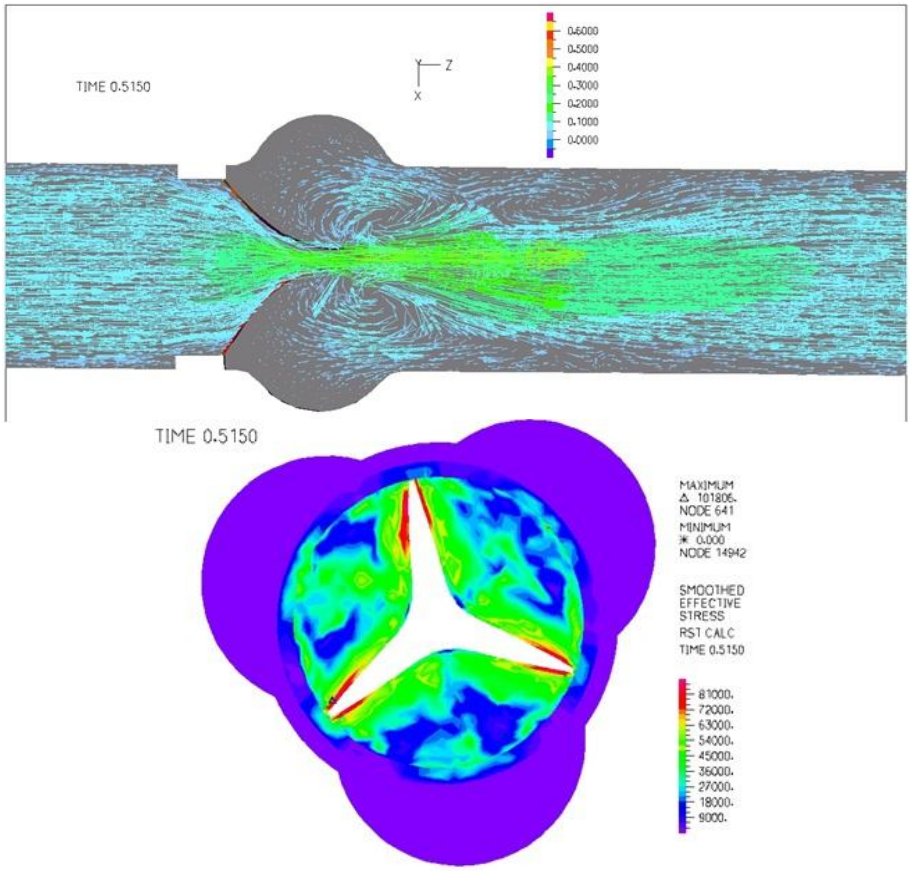


**Figure 26: FSI study of the original composite PHV, fluid phase with velocity vector field (top) and solid phase with stress map (bottom).**

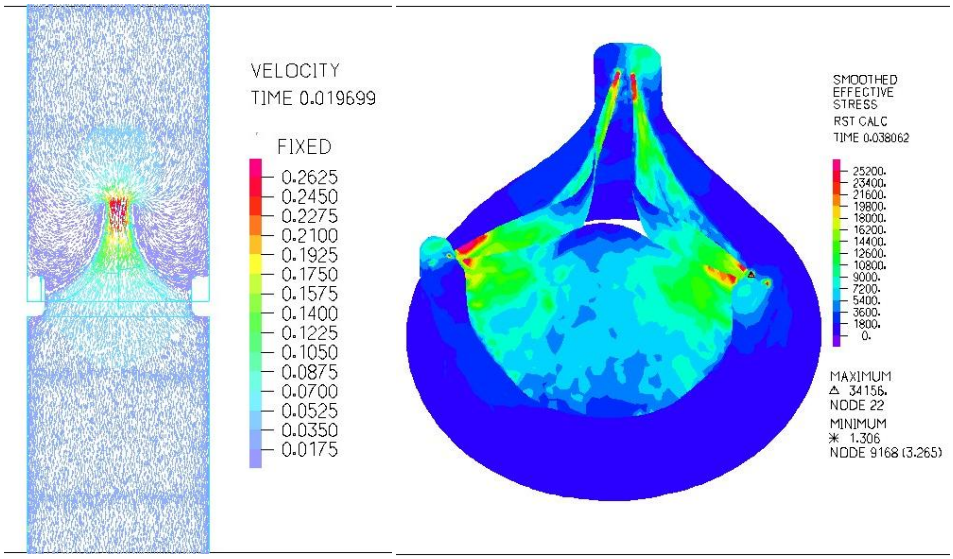


**Figure 27: FSI study of the optimized xSIBS valve, fluid phase with velocity vector field (left) and solid phase with stress map (right).**

***Two-Phase CFD:*** Important flow characteristics of the three trileaflet valve designs are presented in Table 3.

**During the systolic forward flow** (FF) phase (open valve), the flow field through the trileaflet valves is dominated by a triangular shaped central jet structure depicted via platelet dispersion colored by velocity magnitude (Figure 28). However the patterns in each valve are very different. In the tissue valve the pattern is triangular and organized, in the original valve the pattern is less triangular and more disorganized, and in the optimized valve the pattern appears to be three diverging spherical boluses. In all three valves, low velocity recirculation of platelets was observed on the aortic surface of the leaflets and near the wall, and the bulk of the platelets passed quickly through the domain in a bolus with some remaining in near wall recirculation zones. An axial planar view of the velocity vectors shows that the THV has a persistent high velocity jet emanating downstream from the leaflets free edges compared to the original and optimized PHVs (Figure 29). Comparison of the four ROI selected trajectories (emulated in the HSD) for each open valve show the straightest pathlines near the wall in the optimized valve, whereas the original and tissue valve pathlines are entrained more toward the core flow (Figure 29). Entrainment of platelets toward a core jet is not seen in the optimized valve. The TF of the open valves shows the major mode of the optimized valve has the highest and most left shifted peak indicating that the majority of the platelets experience the comparatively lowest SA of the three valves (Figure 31).

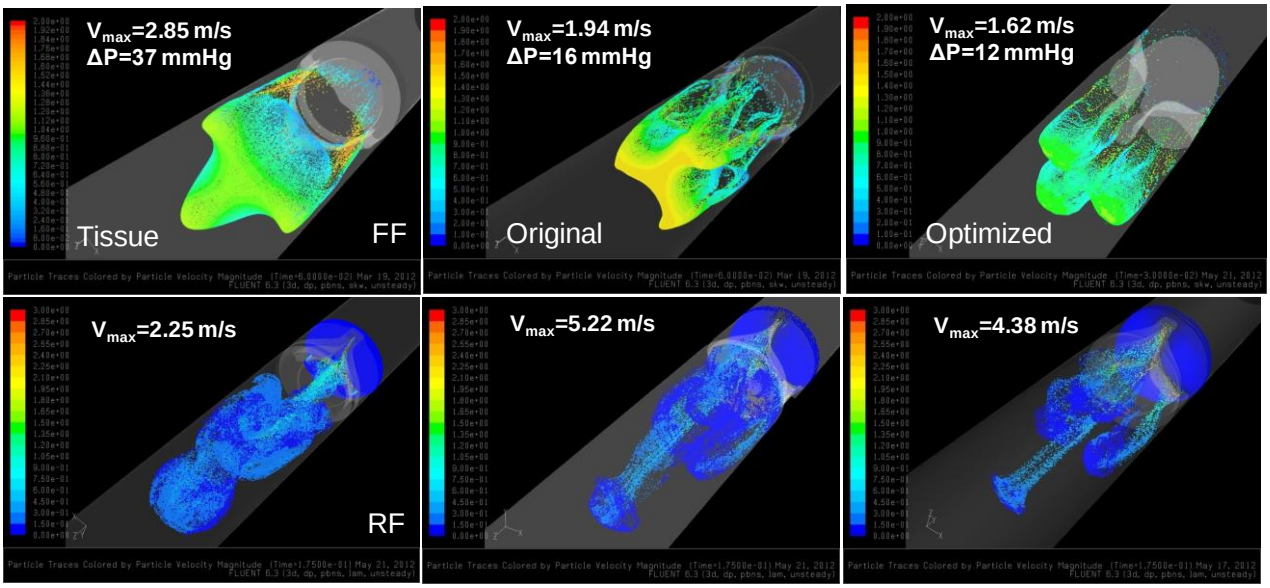


**Figure 28: Platelet dispersion patterns in forward and regurgitant flow.**

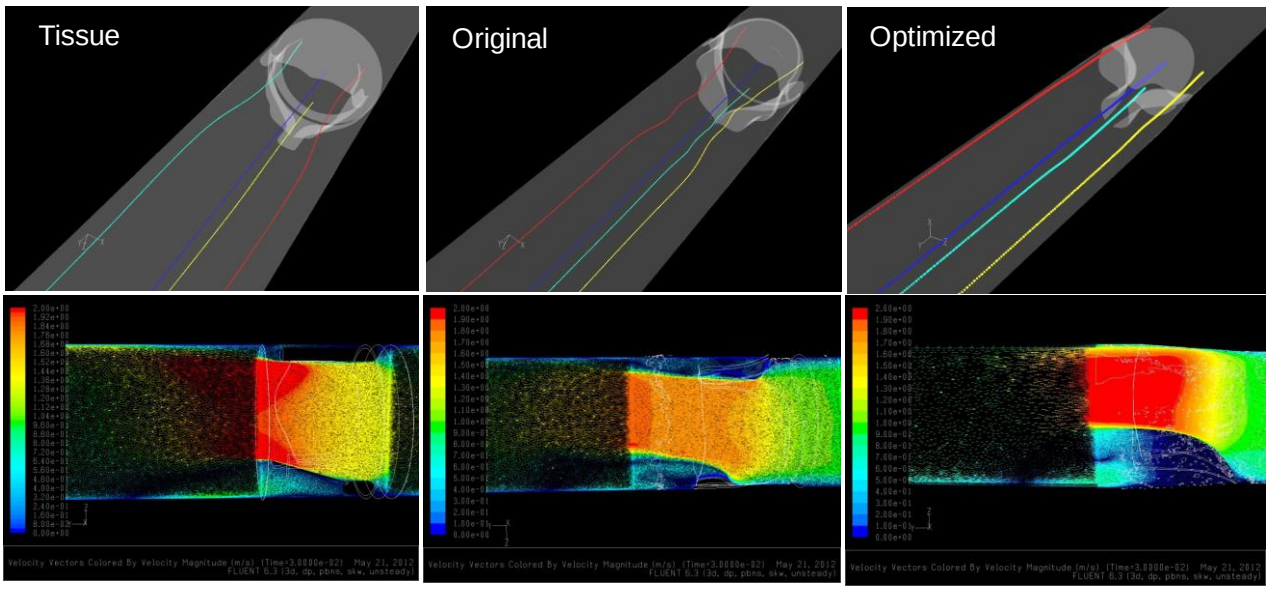


**Figure 29: Open valve platelet trajectories selected for emulation in the HSD from 4 SOIs (top), and axial planar views of the velocity vector field (bottom).**

**During the diastolic regurgitant flow** phase (closed valve) the flow field through the valves is dominated by four small jets emanating from the three commissures and the central gap as shown by platelet dispersion colored by velocity magnitude (Figure 28), however the patterns in each valve are very different. In the tissue valve the jets experience a disorganized mixing, in the original valve the jets swirls in three recirculation zones behind the valve before straightening, and in the optimized the jets are nearly straight with relatively little mixing or swirling. An axial planar view of the velocity vectors shows the difference flow patterns in each valve (Figure 30). The tissue valve has a wide medium velocity jet, the original has small high velocity jets with a recirculation jet, and the optimized has small organized jets skewed towards the wall with no recirculation. Comparison of the four ROI selected trajectories (emulated in the HSD) for each closed valve shows that the optimized valve pathlines are the straightest comparatively. The tissue valve pathlines appear comparatively more chaotic, and the original valve pathlines experience several swirls before continuing out of the domain. The TF of the closed valves shows a bimodal distribution (Figure 31). The leftmost (first) mode represents platelets trapped upstream of the closed valves and the rightmost (second) mode represents platelets that escaped through the gaps. The second mode of the optimized valve is shifted furthest to the left indicating that the majority of the particles reside in the comparatively lowest SA range. One-way ANOVA of the three valves' PDFs in both forward and regurgitant flow show significant differences between the designs ($p < 0.01$).

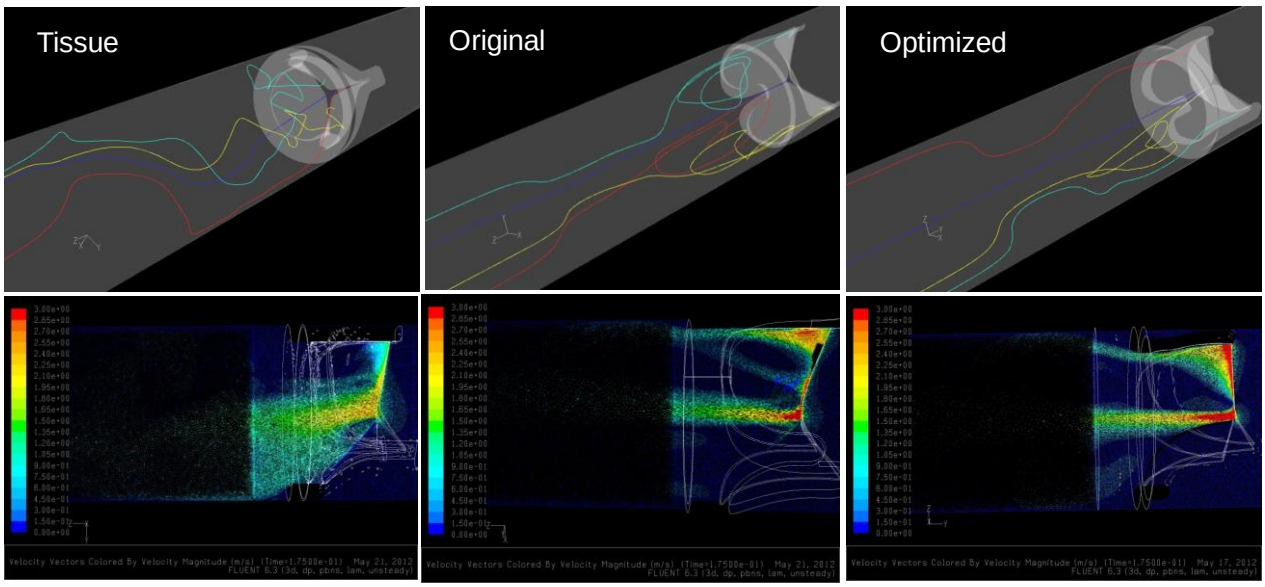


**Figure 30: Closed valve platelet trajectories selected for emulation in the HSD (top), and axial planar velocity vector fields (bottom).**

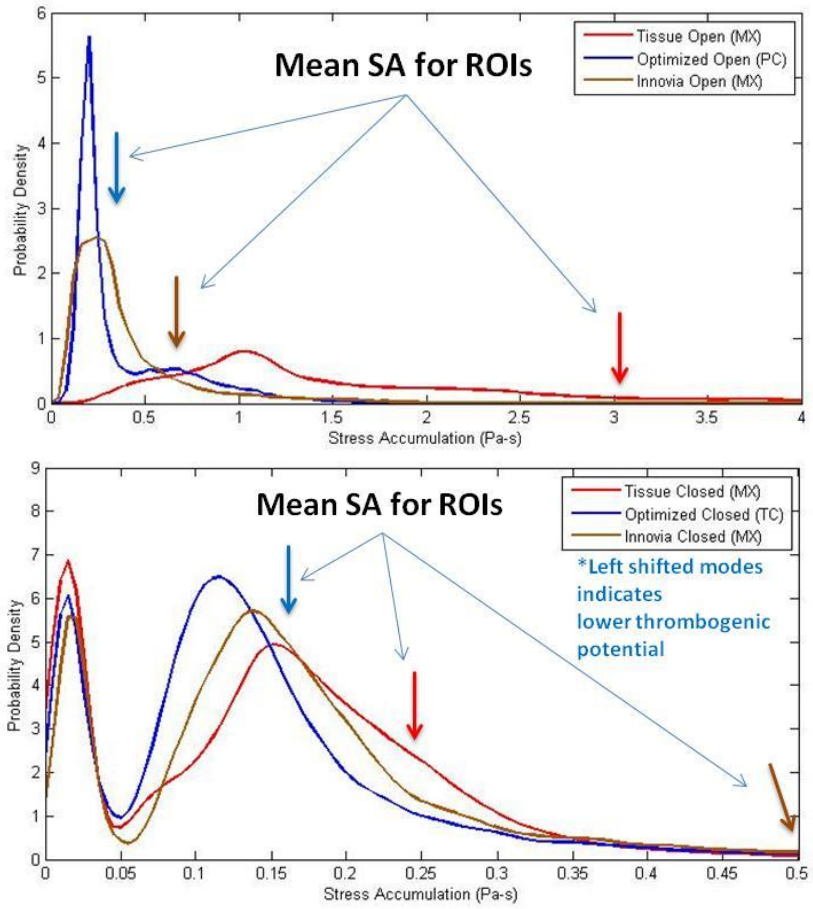


**Figure 31: Thrombogenic Footprint comparison of open and closed valve two-phase CFD using the linear stress accumulation model. See Table 4.**

| | ΔP FF (mmHg) | $u_{max}$ FF (m/s) | $u_{max}$ RF (m/s) | $SA_{mean}$ FF (dyne·s/cm$^2$) | $SA_{mean}$ RF (dyne·s/cm$^2$) | EOA FF (cm$^2$) |
|---|---|---|---|---|---|---|
| **Original** | 16 | 1.94 | 5.22 | 8.02 | 2.50 | 1.25 |
| **Tissue** | 37 | 2.85 | 2.25 | 16.35 | 1.95 | 0.83 |
| **Optimized** | 12 | 1.62 | 4.38 | 4.08 | 1.78 | 1.44 |

**Table 3: FF=forward flow; RF= regurgitant flow; ΔP= pressure gradient; u=velocity; SA= stress accumulation; EOA= effective orifice area calculated using the Hakki equation [142].**

## Experimental Results

Four selected trajectories (Figure 33) from SOIs of radius 1 mm at each of three commissures and the center in each valve were emulated in the HSD using freshly isolated human platelets and flow induced thrombin generation was measured. In all cases the commissure trajectories produced higher ΔPAS values compared to the center and the open valves produced higher ΔPAS values than the closed valves (Figure 33). In both cases, the optimized valve had by far the lowest PAS ($p<0.05$) except in the closed valve center trajectories. Across all selected trajectories in both the open and closed valve studies, the mean ΔPAS correlated with the mean SA of each trajectory (Table 4).

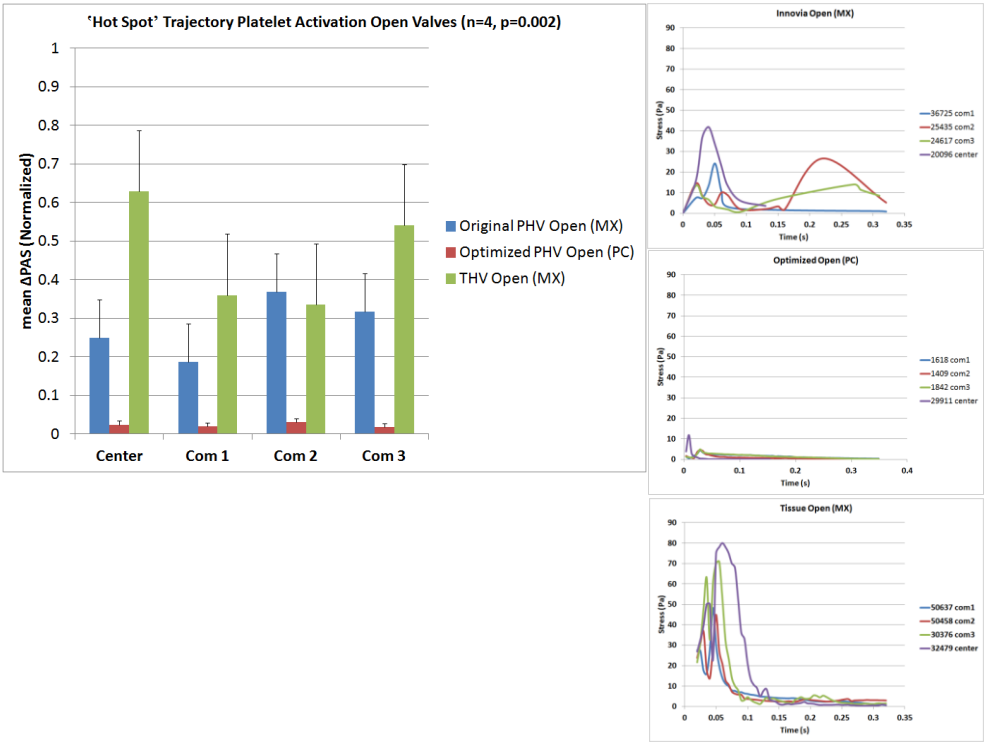


**Figure 32: HSD platelet activation results with emulated stress loading waveforms shown for the open valves (forward flow). The optimized valve had significantly lower ΔPAS in all cases ($p<0.01$).**

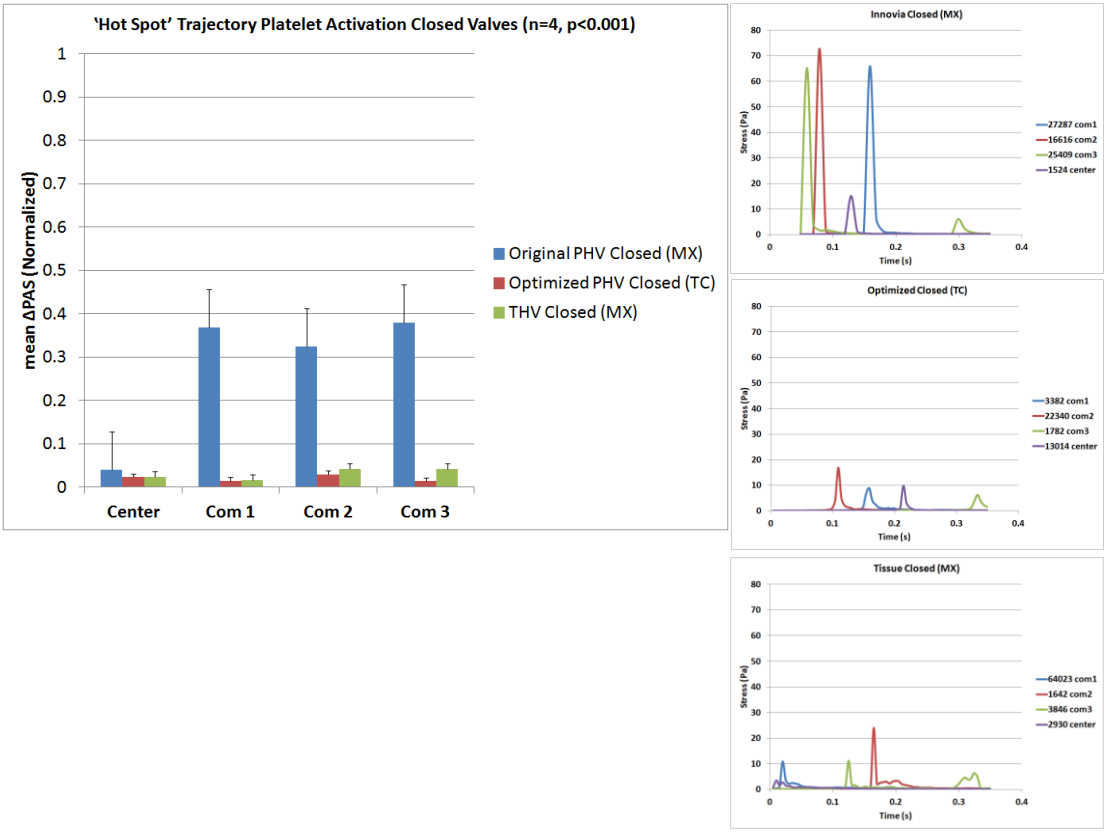


**Figure 33: HSD platelet studies with emulated waveforms for the closed valves. The optimized valve had significantly lower ΔPAS in all cases (p<0.01).**

| | Open Valves | | Closed Valves | |
|---|---|---|---|---|
| | **Mean SA (dyne·s/cm$^2$)** | **Mean ΔPAS** | **Mean SA (dyne·s/cm$^2$)** | **Mean ΔPAS** |
| **Tissue** | 33.6 | 47% | 2.5 | 3% |
| **Original** | 7.3 | 28% | 6.9 | 28% |
| **Optimized** | 3.4 | 2% | 1.6 | 2% |

**Table 4: Comparison of mean SA and ΔPAS values in both the open and closed valves for selected SOI trajectories.**

## Discussion

The previously introduced DTE method [18,19] is intended to be a blood contacting device design tool, which allows the evaluation and optimization of design parameters effecting thrombogenicity in the virtual domain prior to prototype fabrication and testing. Thus it is envisioned that the medical device research and development (R&D) cycle could be shortened and made more cost effective while producing superior products. The overarching goal of our work is to reduce or eliminate the need for anticoagulants in these devices. In this work we have verified our DTE method in trileaflet PHVs and used the method to optimize a novel PHV. We

compared three trileaflet geometries; an original composite SIBS-Dacron PHV previously developed, a novel "optimized" PHV, and the commercially available ‘gold standard’ Carpentier-Edwards Perimount Magna Bioprosthesis THV. Any PHV in development should at least meet the performance of the Magna tissue valve or a similar product to be a viable alternative. It is also important to apply the DTE method to the broadest range of blood contacting medical devices possible for verification and validation.

Finite element analysis was used to create the open and closed geometries for CFD and to evaluate the stress distributions in the three valves under a normal diastolic pressure load. The optimized valve geometry was created using information from prior SIBS-Dacron composite PHV testing and the structure of the native AV. Nonlinear hyper-elastic material models were employed utilizing experimental data to ensure accuracy of the results. The FEA structural and FSI results indicated that the new PHV design was on the path towards optimization.

Our two-phase CFD simulation method is a state-of-the-art process that captures detailed information about the flow field and the forces acting on thousands of platelet sized particles seeded into the flow. This is a departure from simply calculating the fluid forces at massless points in the flow domain. Each particle is like a probe that reports detailed information about the shear stress it is experiencing at a given time and location as it passes through the device. The end point, or the accumulated stress along its path, is calculated for each particle, and that large amount of information is collapsed in to the Probability Density Function (PDF), which we have coined the "Thrombogenic Footprint" (TF). The TF is a global predictive measure of the thrombogenicity of a device that can be used for one-to-one comparison of similar devices or altered designs of the same device. Once the TF is established we can focus in on SOIs and extract representative trajectories for emulation in our HSD.

The emulation of representative SOI trajectories in our HSD allows us to measure platelet activation caused by high shear stress trajectories and use that information to verify the CFD result and to modify the device design to reduce the occurrence platelet activating shear stress. This process can be performed iteratively to optimize the device design and increase its thromboresistance, hopefully, to the point of eliminating the need for anticoagulants. In this work we know *a priori* that tissue PHVs in clinical use do not require anticoagulants, so we are determining what kind of DTE results we will get with a device that is known to be nonthrombogenic and how a polymeric PHV in development compares.

We have found that, overall, the three trileaflet geometries produced CFD results within a reasonable range comparatively, but that globally the optimized design has an advantage in both forward and regurgitant flow. The thrombogenic footprints from both forward and regurgitant flow show that the optimized valve's major modes are shifted to the left of the original and tissue valves, respectively. In regurgitant flow, the TFs shows, via a bi-modal distribution, that a significant number of platelets are trapped upstream from the valve in a low velocity recirculation zone in all cases, but that the original valve has less trapped platelets, and the right-most mode, signifying particles that passed through the valve, shows that the optimized mode is shifted to the left of the original and the tissue valves, indicating that the bulk of the platelets that passed through the valve reside in a comparatively lower stress accumulation zone. In [14] we measured bulk platelet activation in a pulsatile left ventricular assist device in both the polymer and tissue valves and found a significantly lower platelet activation rate in the original compared to the tissue, which is also supported by our TFs from this study.

Analysis of experimental HSD platelet activation results shows that the optimized valve trajectories produced significantly lower platelet activation in all cases except the regurgitant flow central trajectories. The mean ΔPAS values correlated well with the mean SA values across all selected SOI trajectories. The HSD results support the CFD findings.

Sirois and Sun have performed a two-phase CFD evaluation of a trileaflet bovine pericardial valve geometry in order to computationally investigate hemolysis and platelet activation potential [143]. They employed a previously developed bovine pericardial valve structural model to obtain the open valve geometry. They found a transvalular pressure gradient of 6.275 mmHg, peak velocity of 1.75 m/s and peak WSS of 37.5 dynes/cm$^2$. They also found that none of the particle trajectories produced shear stress accumulation above Hellum's platelet activation threshold of 35 dyne·s/cm$^2$. In contrast, our tissue valve simulation produced higher values of these parameters likely due to the comparatively smaller valve diameter used in our study (23 vs. 19 mm respectively). Additionally, we used the Wilcox k-ω turbulence model in forward flow simulations, which is superior to the k-ε model in modeling transitional flow [124], and the number of seeded particles and our method of calculating particle stress accumulation may differ. They have also performed patient-derived transcatheter valve deployment structural modeling [144].

Dwyer *et al.* performed important but comparatively simpler CFD simulations of an idealized open transcatheter tissue valve with the purpose of comparing degrees of pathologies and drag forces on the valve. From the flow field, they found peak WSS on the leaflets of 300-500 dynes/cm$^2$ and peak velocities of 1.65 m/s. Our results produced higher values likely due to the smaller valve diameter in our study (24 vs. 19 mm respectively) [145]. Our tissue valve geometry was comparatively more realistic as well.

Limitations include the fact that numerical studies can only approximate reality, but we made significant efforts to get as close as possible by using the best models available in structural FEA and turbulent CFD, and the fact that a flexible valve leaflet may assume any number of random configurations during the cardiac cycle as noted in Thubrikar [36]. We also cannot emulate the thousands of platelet trajectories simulated in CFD in our HSD, but we made efforts to choose representative trajectories from a population of interest so that the results could be extrapolated. We may redesign the HSD in the future for higher throughput as well, but we have shown the usefulness of the HSD platelet studies in relation to the CFD studies and highlighting problematic zones in a device. Our group is currently working on a platelet activation model based upon experimental *in vitro* platelet studies that may be more accurate than the current linear model. In terms of FSI, we have reached the limits of the software in its ability to model a thin flexible structure in 3-D flow. We have consulted with industry experts and they are equally stumped by our problem. We are currently vetted newer software to tackle this complex numerical problem.

## Conclusion

We have numerically and experimentally optimized a novel PHV and compared it to a former composite PHV and a 'gold standard' tissue valve for the purpose of evaluating fluid dynamics and thrombogenicity and verifying our DTE method in these devices. We found a clear advantage to the new optimized valve, which compares favorably to a tissue valve that does not require anticoagulants. This implies that the optimized PHV is on track to be relatively

nonthrombogenic. Our DTE method was able discern the subtle differences in thrombogenicity between three similar geometries and was therefore verified for the current application.

## SPECIFIC AIM 4: Optimized PHV Prototype Fabrication

### Introduction

Previous PHVs have been fabricated using dip coating or casting techniques that create uniform thickness leaflets. They also necessitate a heterogeneous design since there needs to be a prefabricated stent onto which the leaflets are attached. Typically the stent is made from a material different from the leaflets, which complicates the design through its multi-component interactions, which can affect durability, hemodynamics, and biocompatibility to name a few. A precision molded valve comprised of a homogeneous polymer can reduce design complexity and offers greater control over features such as leaflet thickness. It also offers potentially greater quality control. For these reasons, the new xSIBS PHV has been compression molded.

### Methods

A custom designed aluminum alloy compression mold was designed and fabricated using 5-axis Computer Numerical Controlled (CNC) Machining at the Helmholtz Institute of Applied Medical Engineering in Aachen, Germany (Figure 34). The mold was lubricated with dry film PTFE and filled with raw xSIBS Lot No. 1108269 (23% styrene). The mold was compressed with 3 Tons of force between two heating platens set to 260°C for 30 min (Specac Atlas Series, Cranston, RI). The xSIBS melted at approx. 200°C and was compressed to remove air before the maximum temperature was reached to prevent oxidization. Overflow or flash was extruded through two portholes in the mold block. The platens were water cooled. Once the mold reached ambient temperature the valve was removed using ethanol as a releasing agent (Figure 35). Cross-linking was verified by submerging the prototype in Toluene and observing swelling without dissolution. Adherent xSIBS was removed from the mold using Toluene.

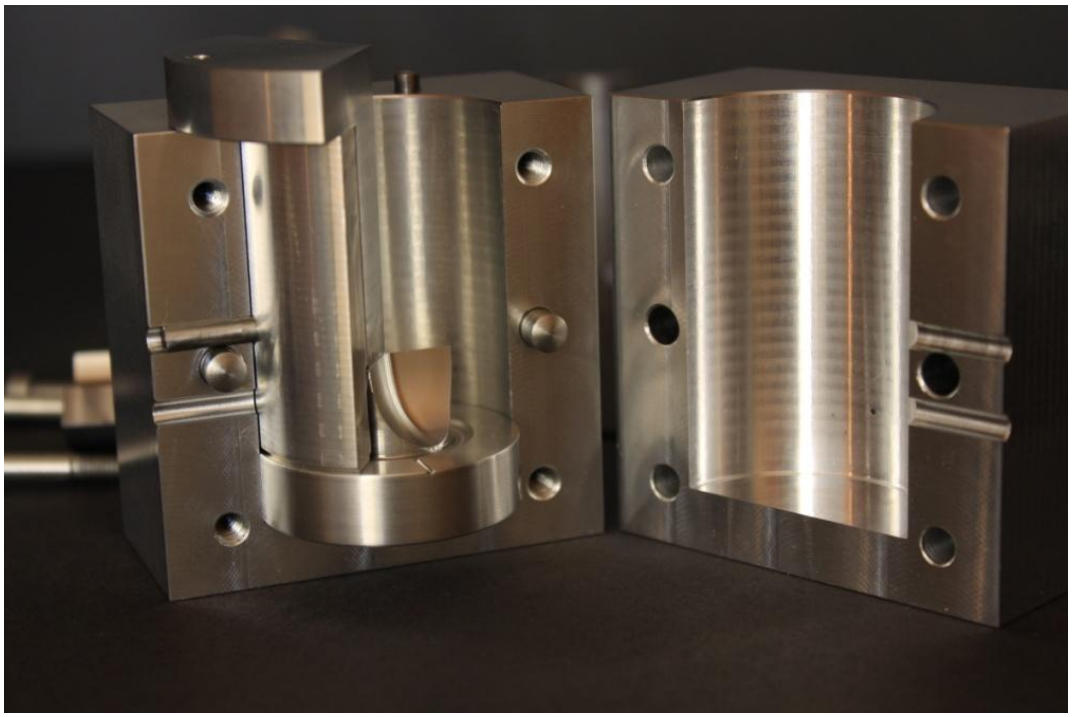

**Figure 34: Optimized valve compression mold.**

**Results**

A homogeneous xSIBS valve was successfully molded and prepared for hydrodynamic testing (Figure 35).

**Figure 35: Molded optimized xSIBS valve.**

**Discussion**

Plastic injection molding is common practice in industry that is used to make a myriad of products. The concept was applied here to the fabrication of a novel PHV using xSIBS. However, the in injection molding the plastic is heated and melted in separate cauldron and

injected under high pressure into the mold. Since xSIBS is vulnerable to oxidization in the heating process, raw xSIBS was place directly into the mold before heating and compressed to remove as much air as possible. Determining the correct combination of heating and compression to prevent oxidization was not trivial. Several trials produced failed prototypes. Eventually, the process was reduced to a reproducible one and usable prototypes were created. In the future, a process more like injection molding should be used with the incorporation of an inert gas to displace air prior to heating and compression.

### Conclusion

The compression mold design and fabricated from aluminum alloy allowed successful molding of fully cross-linked xSIBS PHVs.

## SPECIFIC AIM 5: Measurement and Comparison of Optimized PHV Prototype Hydrodynamics to a Gold-Standard THV

### Introduction

*In vitro* hydrodynamic assessment of prosthetic heart valves is a key step in the development process. The data is used to verify the design and determine whether or not it should be moved forward into preclinical animal trials. We present hydrodynamic tests of the optimized xSIBS PHV compared to a gold-standard THV, the Carpentier-Edward Perimount Magna Bioprsothesis.

### Methods

A valve holder mold was designed in CAD (SolidWorks) and machined from aluminum alloy in order to mold silicone rubber valve holders for the Vivitro Left Heart Simulator (LHS, Vivitro Labs, Inc. Victoria, BC) (Figure 36, Figure 37, Figure 38, Figure 39). The *in vitro* hydrodynamics of the optimized polymer valve prototypes (n=3) were measured and compared to a gold-standard THV, the Carpentier-Edwards Perimount Magna Bioprosthesis (n=1), both with 21 mm TAD, using the LHS following Draft Guidance for Industry and FDA Staff: Heart Valves - Investigational Device Exemption (IDE) and Premarket Approval (PMA) Applications and International Organization For Standardization (ISO), ISO 5840:2005, "Cardiovascular Implants - Cardiac Valve Prostheses."

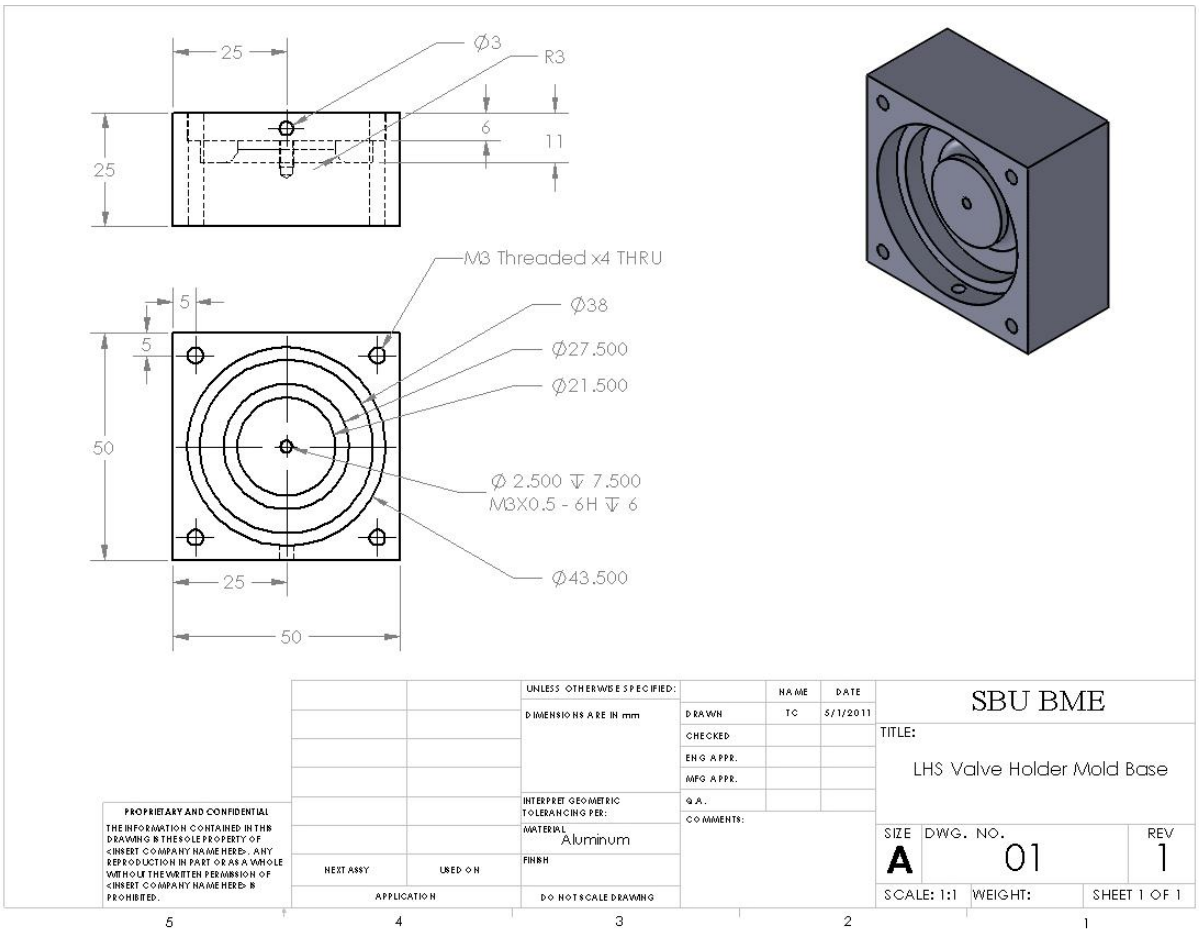


**Figure 36: LHS valve holder mold base engineering drawing.**

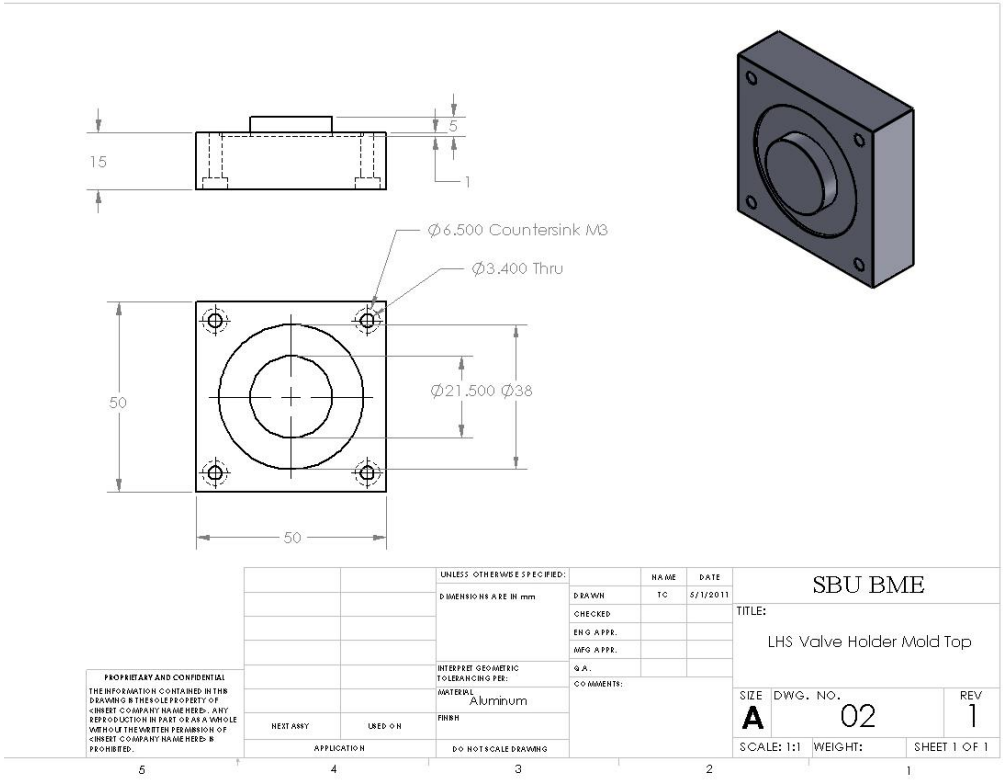


**Figure 37: LHS valve holder mold top engineering drawing.**

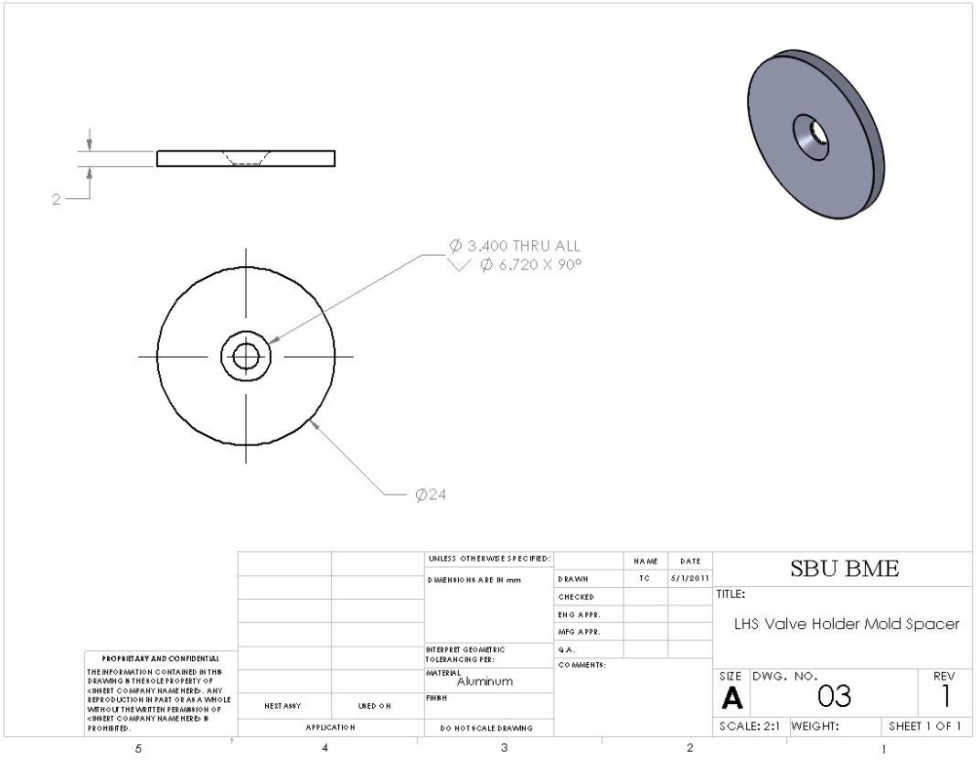


**Figure 38: LHS valve holder mold spacer engineering drawing.**

**Figure 39: LHS molded silicone rubber valve holder (left, notice suture ring groove on the inner surface) with xSIBS optimized valve (right).**

| Heart Rate (BPM) | 45 | 70 | 100 | 120 |
|---|---|---|---|---|
| CO (L/min) | 2.3 | 3.9 | 6.0 | 7.8 |
| | 3.6 | 5.6 | 8.0 | 9.6 |
| | 5.0 | 7.4 | 10.0 | 11.4 |

**Table 5: Hydrodynamics testing parameters showing heart rates (BPM) and target cardiac outputs (L/min) [121].**

Table 5 shows the hydrodynamics test protocol. A blood analog solution composed of 35% Glycerin and 65% de-ionized water was utilized. 0.9% sodium chloride was added for LHS for the electromagnetic flow meter. The resulting solution has a density of 1.133 g/ml and a viscosity of 3.2 cP, which is similar to whole blood. A 27 mm St. Jude bileaflet mechanical valve was placed in the mitral valve position during LHS testing. Pressure measured at two locations, the ventricle and the aortic outflow tract, was used to calculated the pressure gradient and to verify the Bernoulli relationship (increased velocity corresponds to decreased pressure). The LHS resistance and pump amplitude are manually adjusted to reach the test parameter goals. A mean arterial pressure (MAP) (40) of 100 mmHg is maintained throughout the testing.

$$MAP = \frac{p_{systolic} + 2p_{diastolic}}{3} \tag{40}$$

The LHS is comprised of a linear actuated piston superpump with DC motor (SP3891), a superpump head (SPH5891B) a viscoelastic impedance adapter (VIA7991), a power amplifier (SPA3891), a signal filter (AP9991), an analog input/output module (22008), and a square wave

electromagnetic flow meter (Carolina Medical). Hydraulic pressure transducers (Vivitro 3017) and blood flow probe (Carolina Medical EP688) are used to measure pressure and flow. Vivitest v3.5.02 software is used to acquire and process the test data. Vivitest uses equation (41) to calculate the effective orifice area (EOA):

$$EOA \equiv \frac{Q_{RMS}}{51.6\sqrt{\Delta p / \rho}} \tag{41}$$

where $\Delta p$ is the pressure gradient across the valve, $\rho$ is the fluid density, and $Q_{RMS}$ (root mean square volumetric flow rate) is given by (42)

$$Q_{RMS} = \sqrt{\frac{\int_{t1}^{t2} Q(t)^2 dt}{t_2 - t_1}} \tag{42}$$

where $t$ is time. The regurgitant fraction ($RF$) is calculated by (43)

$$RF\% = \frac{CV + LV}{FV} \times 100 \tag{43}$$

where $CV$ is the closing volume, $LV$ is the leakage volume and $FV$ is the forward volume. The total energy loss across the valve is calculated by (44)

$$Energy_{total} = FE + CE + LE \tag{44}$$

where $FE$ is the forward energy, $CE$ is the closing energy, and $LE$ is the leakage energy, with energy ($E$) given by (45)

$$E = 0.1333 \int_{Fn}^{Fn+1} \Delta p Q(t) dt \tag{45}$$

where $Fn$ to $Fn+1$ is the range of a phase of the cardiac cycle corresponding to $FE$, $CE$, or $LE$, and 0.1333 is an energy unit conversion from mmHg*ml to mj. For comparison, max. velocity can be estimated as (46)

$$V_{\max} = \frac{Q_{\max}}{EOA_{\max}} \tag{46}.$$

**Results**

The molded valve holders held the valves in place securely throughout testing. Hydrodynamics were tested over a range of heart rates and cardiac outputs. A summary of key hydrodynamic parameters are shown in Table 6. Figure 40 shows the representative curve plot from Vivitest depicting an xSIBS valve test. The Bernoulli relationship held in the valve testing, increased velocity is proportional to increased pressure gradient, with the tissue valve having a slightly lower pressure gradient than the xSIBS valve (Figure 41). The regurgitant fraction was much

lower in the optimized xSIBS valve compared to the tissue with the regurgitation decreasing with increasing cardiac output (Figure 42). The transvalvular energy loss converges in the two valve at about 5 L/min then diverges with the xSIBS valve having a slightly higher loss compared to the tissue valve (Figure 43). The tissue valve exhibited a larger effective orifice area compared to the xSIBS valve (Figure 44).

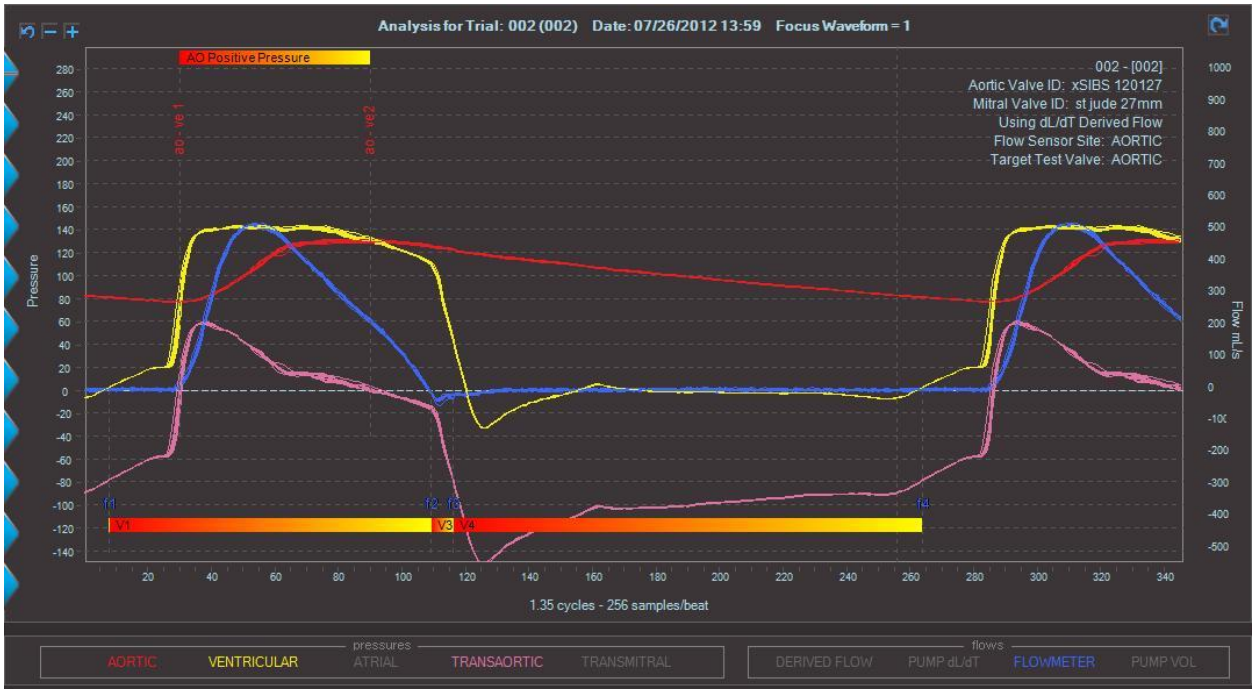


**Figure 40: Representative graphical output from Vivitest; xSIBS valve test data shown.**

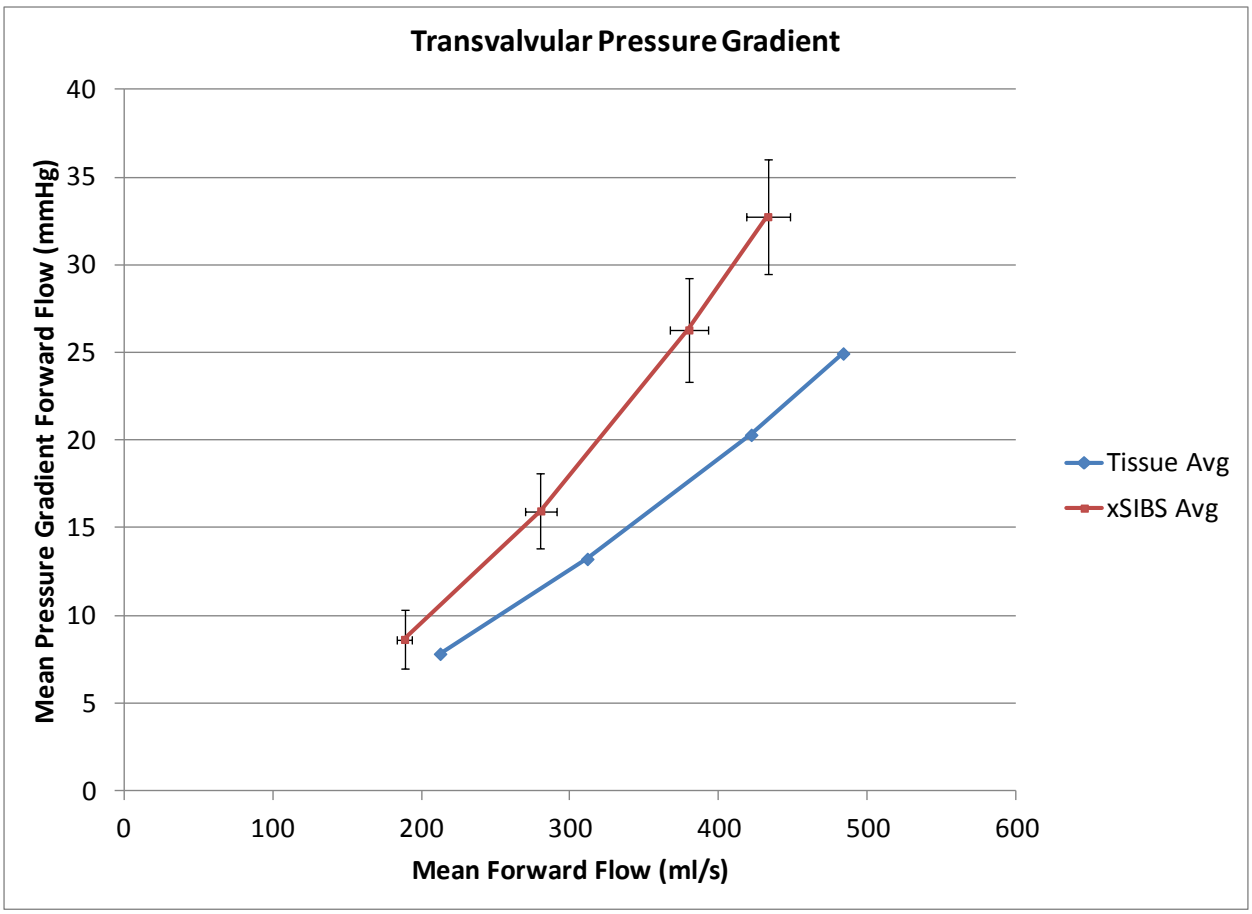


**Figure 41: Hydrodynamics test showing the Bernoulli relationship. The optimized PHV has a slightly higher pressure gradient in forward flow likely due to the material being stiffer than tissue.**

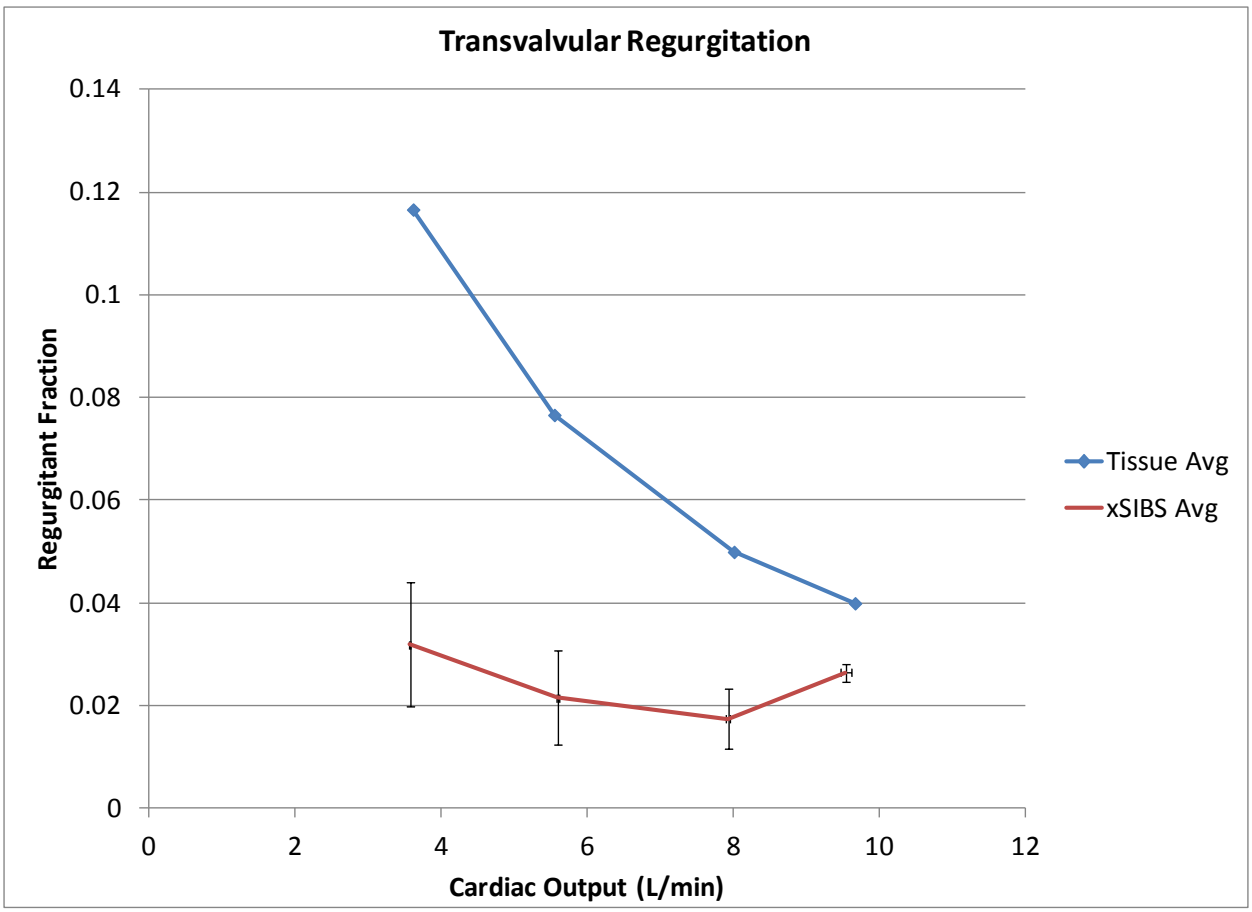


**Figure 42: Hydrodynamic results showing the advantage to the xSIBS PHV in closing dynamics and regurgitation likely due to the increased coaptation area.**

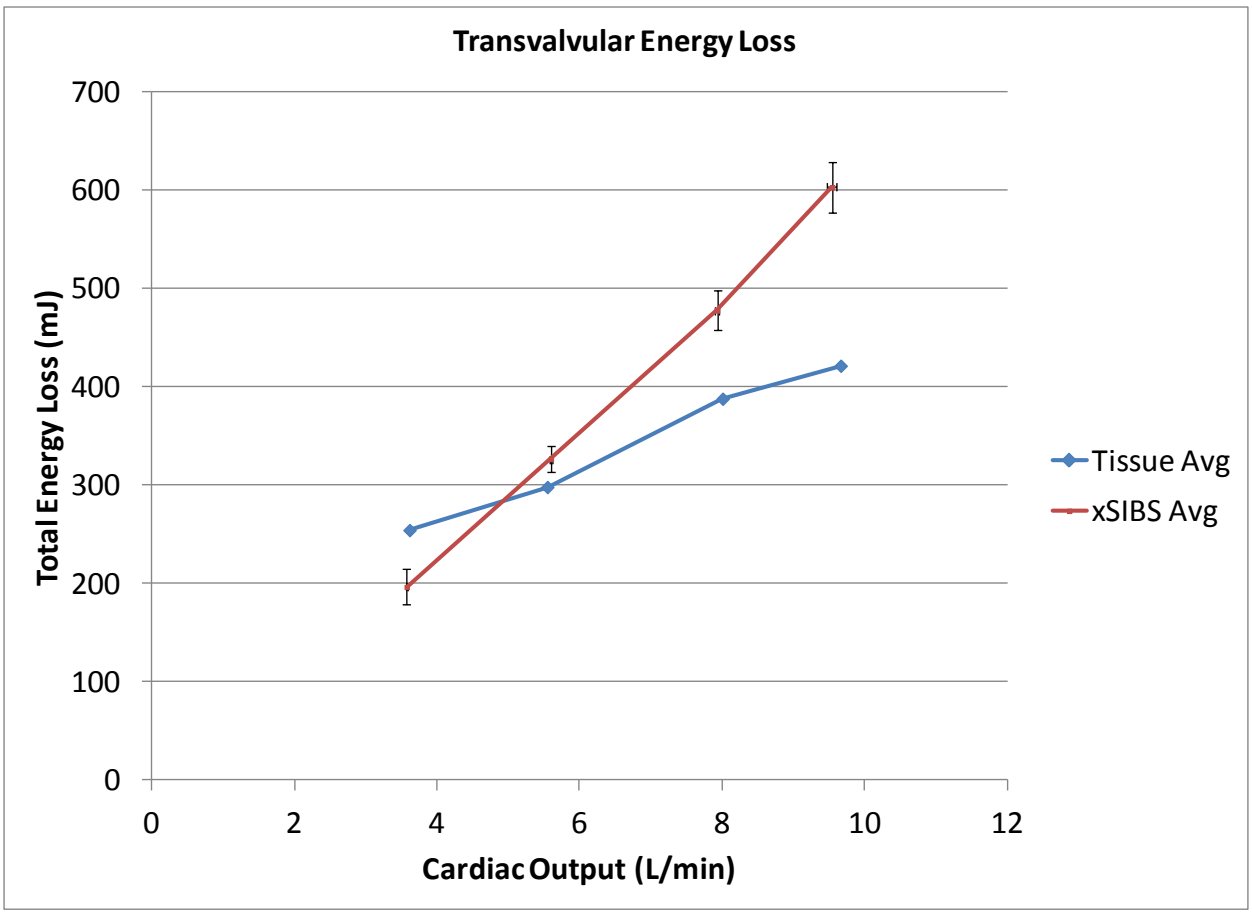


**Figure 43: Transvalvular energy loss comparison of the xSIBS PHV to the tissue valve; equivalent to the work performed by the heart to pump blood through the valve.**

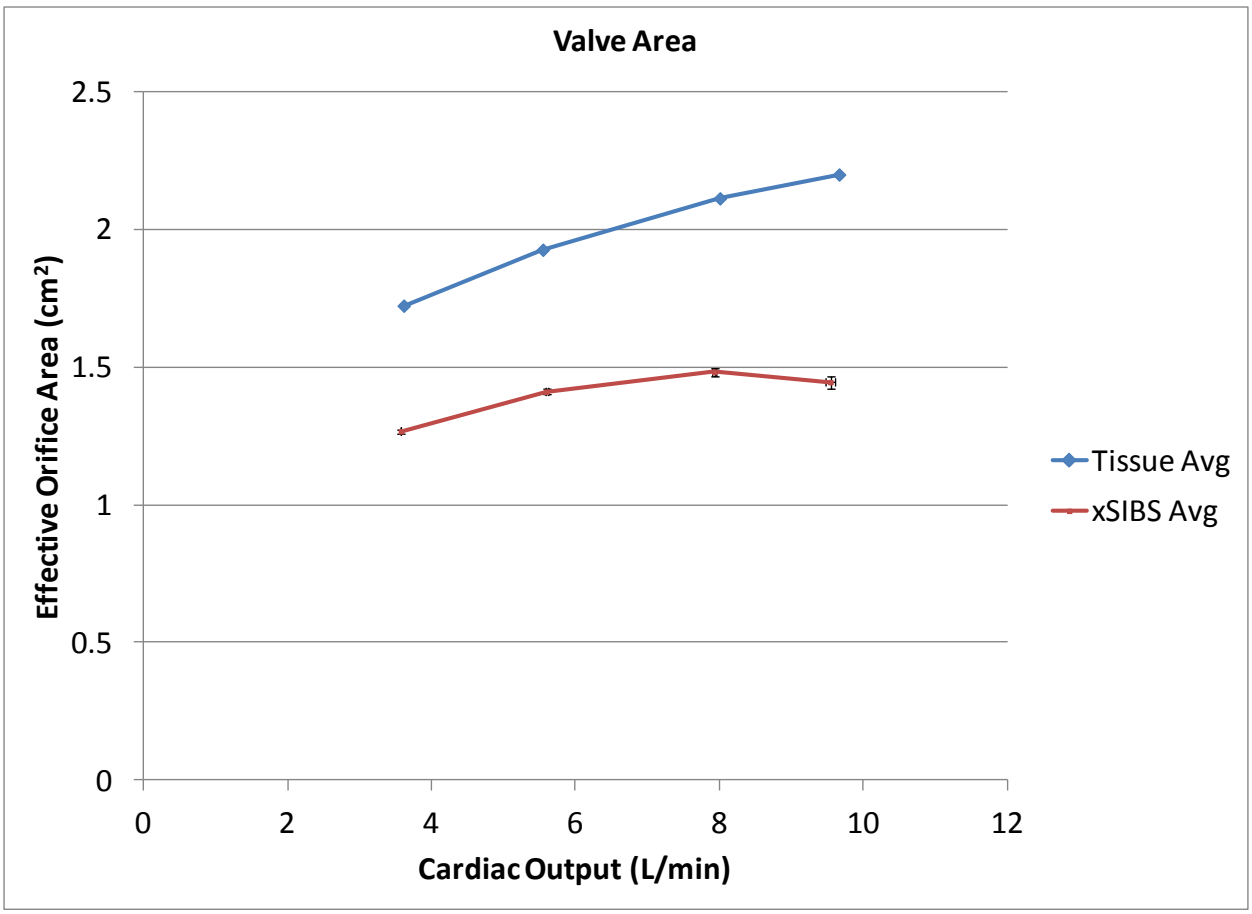


**Figure 44: Effective orifice area as a function of cardiac output in the xSIBS versus tissue valves.**

| | mean ΔP (mmHg) | mean RF% | Max. Velocity @ rest (m/s) | EOA @ rest ($cm^2$) |
|---|---|---|---|---|
| **Tissue (n=1)** | 16.57 | 7.08 | 2.96 | 1.95 |
| **Optimized (n=3)** | 20.91 | 2.43 | 3.42 | 1.47 |

**Table 6: Hydrodynamic data comparing the functionality of the tissue versus the optimized xSIBS valve prototypes at resting physiological conditions (HR= 70 bpm and CO= 5.6 L/min).**

## Discussion

Hydrodynamic assessment of prototype prosthetic heart valves is an essential part of the verification process in development. Until these tests are conducted, we only have numerical data, which is quite reliable but does not accurately reflect "real world" conditions. These *in vitro* hydrodynamics tests give a clear indication of whether or not the valve design is viable. Here we have compared the new optimized molded xSIBS valve to a gold-standard THV. The results are favorable and show that the performance of the PHV is close to the THV. The pressure gradient during forward flow is slightly higher in the PHV compared to the THV likely because the xSIBS leaflet are stiffer than the glutaraldehyde fixed bovine pericardium. Additionally the THV had a larger EOA, which led to a comparatively lower max. velocity and pressure gradient as well. The PHV exhibits much lower regurgitation than the THV likely due to the flat leaflet profile and increased coaptation area. In comparison, the THV has an angled leaflet profile with a smaller coaptation area. The 23% styrene xSIBS may be too stiff or the leaflets may be too thick or both compared to the THV. The 21 mm TAD also produces less than ideal hydrodynamics at physiologic flow conditions since it is the smallest possible adult aortic valve size. A larger TAD prototype may fare better. The results of the xSIBS valve compared to the composite SIBS-Dacron PHV show a reduced mean pressure gradient and a larger EOA in the optimized valve. The regurgitation results differ likely due to the altered calculation techniques. (Regurgitation was manually calculated in the Vivitro device at Florida International University, whereas pressure gradient is directly measured in both systems.) These results are encouraging and indicate that the current optimized PHV design is on the path toward full optimization.

## Conclusion

*In vitro* hydrodynamics testing revealed the favorable performance of the optimized molded xSIBS PHV in comparison to a gold-standard THV. This encourages further development and testing of the xSIBS valve.

## SPECIFIC AIM 6: Bulk Flow Platelet Activation in the "Original" SIBS-Dacron Composite PHV vs. Carpentier-Edwards Perimount Magna Bioprosthesis [14]

## Introduction

The aim of this study was to assess the flow induced thrombogenic potential of the prior cast Innovia composite PHV design compared to a clinically relevant and FDA-approved THV Activation of platelets, the principal thrombogenic elements in blood, is required for both the initiation and propagation of clot formation,[146] and is responsible for thrombotic complications associated with MCS devices [147].

We have compared the *in vitro* thrombogenic potential of the original cast Innovia composite SIBS-Dacron PHV to the FDA-approved and commercially available Carpentier-Edwards Perimount Magna Bioprosthetic valve, a ‘gold standard’ THV [14].

## Methods

This *in vitro* study was performed using a Berlin pulsatile LVAD (Figure 45) filled with 200 mL of a modified Tyrode’s platelet buffer solution containing 3 mM $CaCl_2$ and Sepharose gel filtered

platelets (GFP) at a count of 20,000/μL. The test was run for 30 minutes with 50 μL aliquots sampled from the system via syringe every 10 minutes. Negative controls consisted of running the LVAD without valves *in situ*. The stroke rate was set to 90 bpm, the stroke volume set to 65 mL, and the systole/diastole ratio was 0.375, which produced a flow rate of 5.85 L/min. The near real-time platelet activation state was quantified using the previously described modified prothrombinase Platelet Activation State (PAS) assay [33] and has been utilized by us in a number of studies in various prosthetic heart valves [119,148,149]. Each time point sample was analyzed in duplicate. All PAS values were then normalized against the activity of fully activated platelets via sonication at 10 W for 10 sec from the same batch [33]. Experiments were run in pairs using platelets from a single donor per pair ($n$=6 pairs). Flow cytometric measurements were performed using CD62P or P-selectin as previously described [150]. Platelet surface expression of P-selectin was determined using phycoerythrein-labeled antibody against P-selectin. Platelet activation was quantified as the ratio of gated positive platelets to total platelets, expressed as a percentage and normalized to maximum platelet activation for each platelet batch by 100 μM TRAP (Thrombin Receptor Activator Peptide, Sigma, St. Louis, MO). Gate settings remained unchanged for each pair of valves investigated. Fluorescence intensity was determined for 25,000 events.

The *in vitro* hydrodynamic performance of both previous and new designs of the Innovia polymer valve, and the Edwards tissue valve were assessed using a Vivitro Left Heart Simulator (LHS) (Vivitro Labs, Inc., Victoria, BC) at Florida International University, Miami, FL in accordance with FDA Replacement Heart Valves Draft Guidance V.5.0 as previously described [11,151]. Tests were run at 45, 70, 100, and 120 bpm over a range of 2.3 to 11.4 L/min (Table 5).

A custom Matlab program was used to calculate the output data as follows: the regurgitant volume fraction was measured as a function of cardiac output and the pressure gradient during forward flow was measured as a function of forward flow rate. The average values of the 6 tests were plotted per time point. For the PAS and P-selectin results, linear trend lines were fitted using the least squares method; the slopes of which were the platelet activation rate (PAR) values. The log (47) of each pair of valves was compared to zero using SigmaPlot software v.11.0 to calculate Student's t-test.

$$\log\left(PAR_{TISSUE} \Big/ PAR_{POLYMER}\right) \tag{47}$$

The PAR for each valve was similarly compared to the PAR of the negative control. Significance level $\alpha$=0.05 was utilized. Data is shown with standard error bars. Hydrodynamic data points correlating to 45, 70, 100, and 120 bpm were plotted and consisted of the average of three flow rate data entries per bpm category. Standard deviation is shown for each parameter, *e.g.* mean pressure gradient. The clinical ACC scale was used for comparison [3].

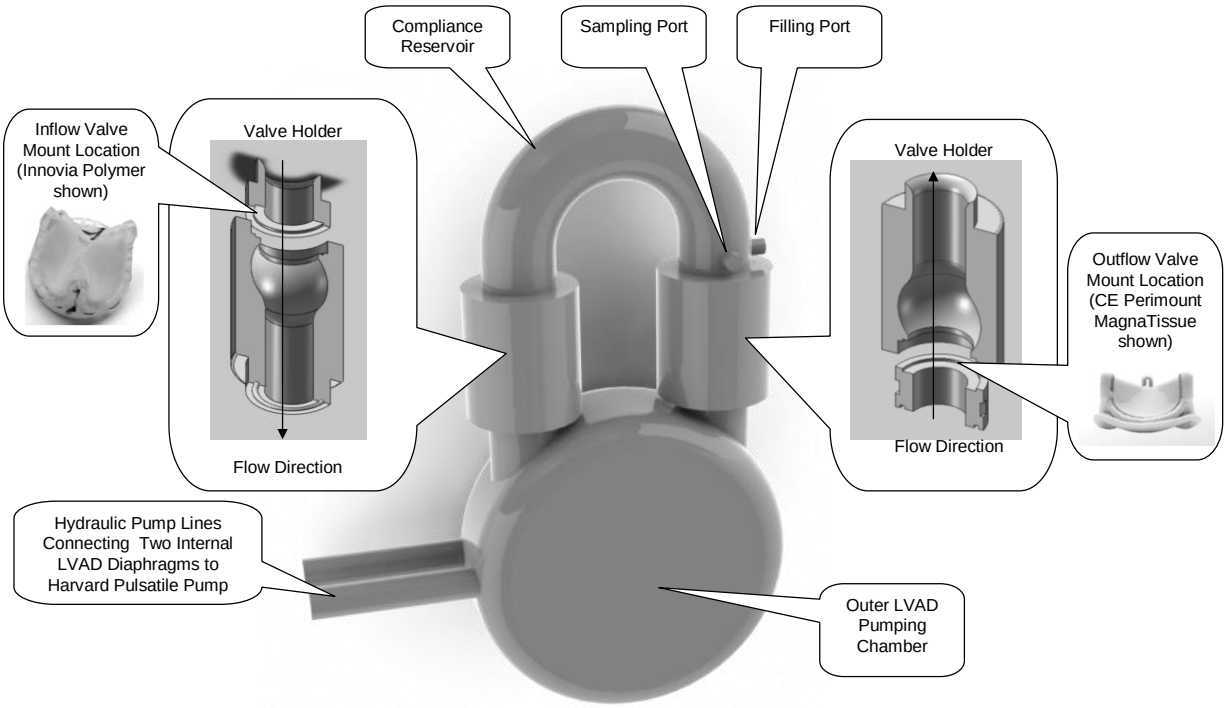


**Figure 45: Schematic of LVAD flow loop with universal valve holders and compliance tubing.**

## Results

PAS: The Edwards tissue valve PAR was 5-fold higher than the Innovia polymer valve (Figure 46, $n$=6, $p$=0.005). Negative control tests ($n$=6) conducted with the LVAD operated without the valves *in situ* had significantly lower PAR value (0.000027 $min^{-1}$) than the PARs generated with the Innovia polymer and Edwards tissue valves mounted in the LVAD ($p$<0.05 respectively).

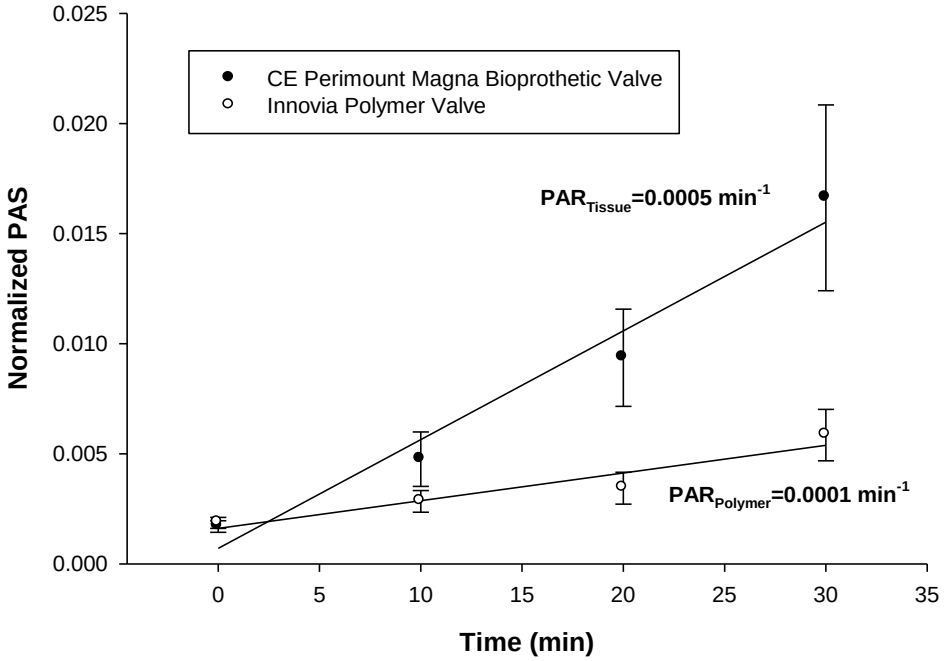


**Figure 46: PAS results comparing polymer vs. tissue.**

P-Selectin: The Edwards tissue valve PAR was 4-fold higher than the Innovia polymer valve (Figure 47, $n$=6, $p$=0.007).

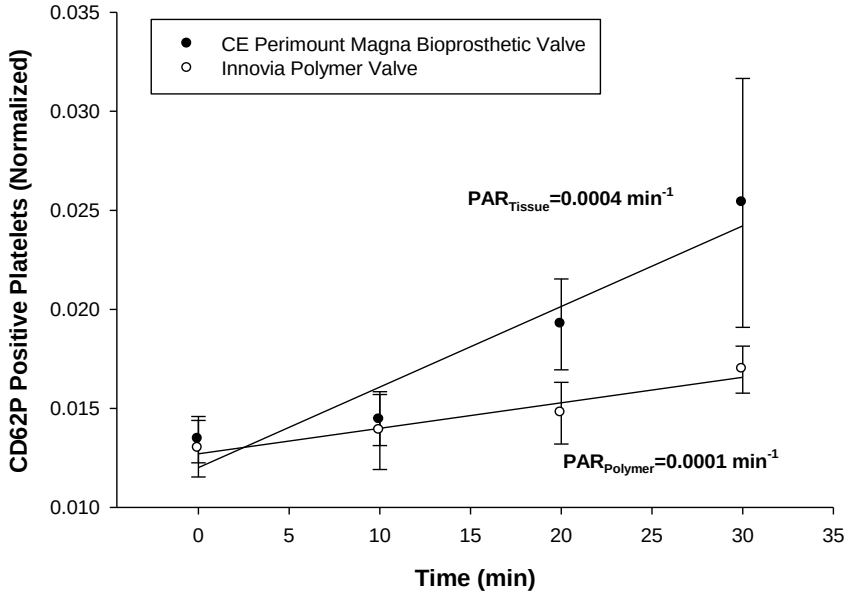


**Figure 47: P-selectin results comparing polymer vs. tissue.**

Hydrodynamics: The valve *in vitro* hydrodynamic tests results are shown in Table 7 and Figure 48. The most recent cast Innovia composite PHV design produced results clinically similar to the Edwards tissue valve, indicating normal physiologic regurgitation volume fraction as a function of the cardiac output and non-pathological pressure gradients, normally associated with mild stenosis. In comparison, the former dip coated Innovia design produced moderate stenosis conditions and higher regurgitation. The effective orifice area (EOA) was calculated via the Gorlin equation (41) from ISO 5840:2005, which requires the minimum EOA for a PHV with a tissue annulus diameter (TAD) of 19 mm to be at least 0.70 $cm^2$ ($\rho$ is the blood analog density (1.057 $g/cm^3$). All valves exceed the ISO-EOA requirements.

| **Valve Type** | **Mean Pressure Gradient (mmHg)** | **Mean Regurgitant Fraction (%)** | **EOA ($cm^2$)** |
|---|---|---|---|
| Dip Coated Innovia Composite | 42.85 +/- 9.52 | 7.35 +/- 2.90 | 0.80 |
| Cast Innovia Composite | 25.73 +/- 8.12 | 1.01 +/- 0.65 | 1.09 |
| CE Magna Tissue | 17.91 +/- 4.81 | 0.41 +/-0.30 | 1.28 |

**Table 7: Hydrodynamic results comparing the polymer and tissue valves (n=1 each).**

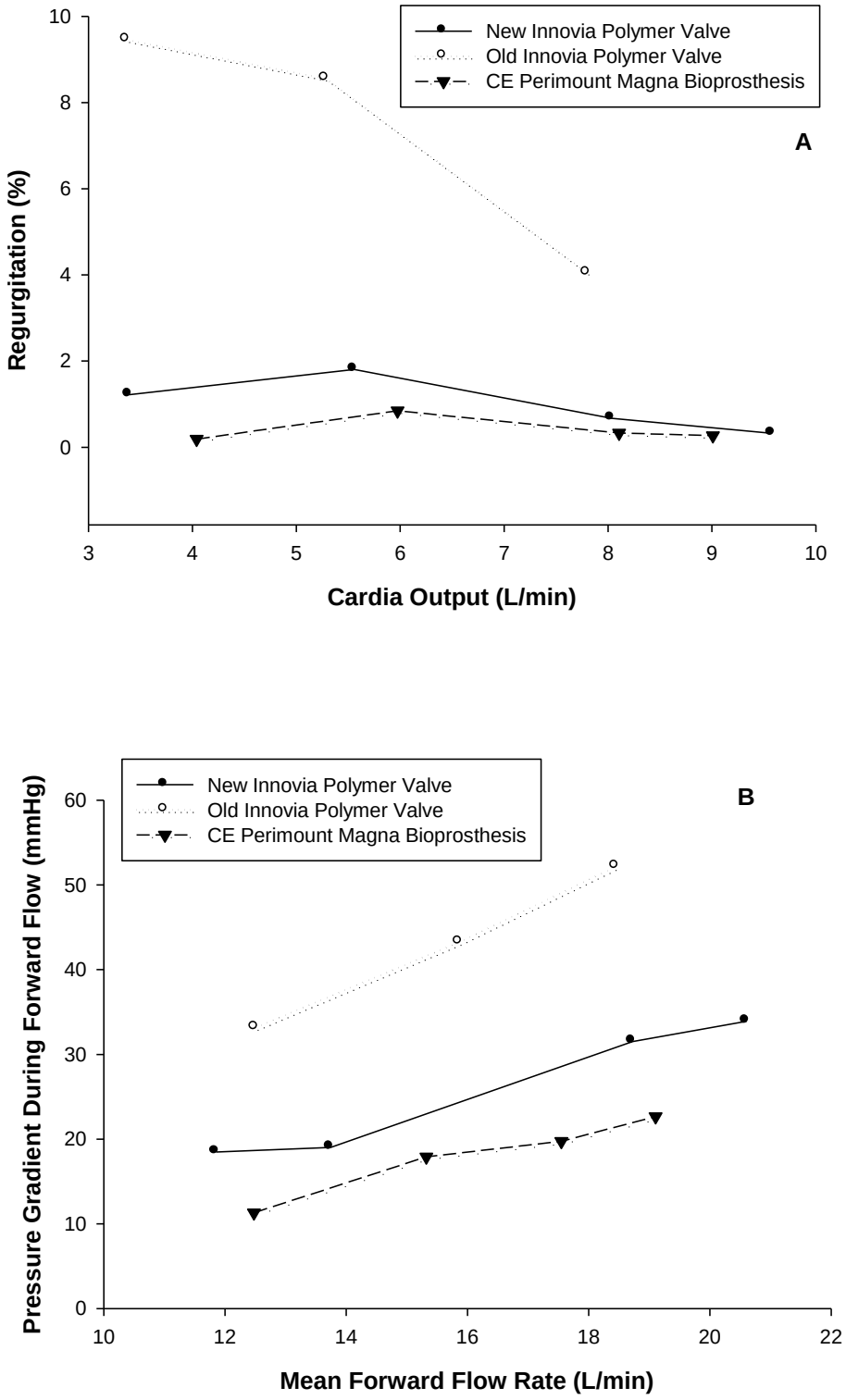


**Figure 48: Hydrodynamic results comparing polymer vs. tissue. Top (A) shows regurgitant fraction as a function of cardiac output, and bottom (B) shows pressure gradient during forward flow as a function of mean forward flow rate.**

**Discussion**

Heart valve prostheses and mechanical circulatory support devices, *e.g.* LVADs and Total Artificial Heart (TAH), have primarily been designed to prevent hemolysis. These devices have been life saving and clinically successful, but only partially address hemodynamic safety and efficacy issues. Platelet activation is implicated in post-implant thromboembolic strokes and occurs at shear stresses 10-fold lower than those required for significant hemolysis [141,152,153]. Device manufacturers mostly overlook this critical flow-induced thrombogenic evaluation during the research and development of these devices, thus mandating the use of risky anticoagulation drug therapy to mitigate the problem. Therefore, it is imperative to develop methods and tools for preclinical thrombogenic evaluation of these devices that feedback into the preclinical design process with the end goal being non-thrombogenic device design [147]. Our group has previously established the currently reported methods to compare different prosthetic heart valve designs thrombogenic potential *in vitro*, and this study represents an evolution of that ongoing effort [119,148,149].

Here we show that the cast Innovia composite valve design is 5-fold less thrombogenic ($p$=0.005) in our test system than the Edwards tissue valve, whereas previously we found no significant difference between the earlier dip coated Innovia polymer valve design and a St. Jude tissue valve [119]. Additionally, we found that both valves were significantly different from the pumping LVAD without valves *in situ* ($p$<0.05). This illustrates the effect of the presence or absence of the valves in the test system. We have previously established that the platelet activation measured is predominantly a function of flow past the valves (MHV or PHV) in the LVAD test system [119,148,149]. The purpose of the control experiments (without valves) therefore is to partly distinguish the effect of flow induced platelet activation within the LVAD chamber itself. It has been reported that flow induced stresses are much lower in the LVAD chamber than those measured due to flow past PHVs [154]. The well established flow cytometric P-selectin analysis correlated well with the PAS thrombin generation results demonstrating a 4-fold difference in PAR ($p$=0.007) [155,156]. The results suggest hemodynamics influenced by the valve design is the primary platelet activator. Therefore, these results further validate our test methods by showing the detection of significantly different PARs influenced by valve design differences, and they demonstrate the relatively low thrombogenic potential of a SIBS PHV in our test system.

We have improved our methods by utilizing freshly isolated platelets (<6 hours) at experimental counts of 20,000/μL to obtain a more realistic baseline activation level and linear response respectively. We previously used expired (>120 hours) pheresis platelet bags from the Stony Brook University Medical Center Blood Bank and experimental platelet counts of 100,000/μL [119,148]. The former method caused the baseline platelet activation to be roughly 5-fold higher than normal, which may mask activation and induce platelet-platelet interactions [157]. Furthermore, we have tested valves with identical nominal internal diameters (19 mm) in identical valve holders designed with psuedo-sinuses of Valsalva, whereas previously the Innovia polymer valve had an internal diameter of 25 mm and the St. Jude tissue valve had an internal diameter of 21 mm, although the valve holders had 25 mm diameters with adjustable internal sizing rings [119].

It was reported that the *in vivo* mean pressure gradient of the 19 mm Edwards Perimount Magna tissue valve was 11.9 mmHg +/- 4.1 and the EOA=1.58 $cm^2$ +/- 0.29, which was superior to the

standard Perimount valve in both measures [80]. Another study showed the Magna valve to be superior to the Medtronic Hancock II porcine valve in both measures [136]. Therefore, the Magna valve was a good choice as a benchmark for comparison to the prototype Innovia polymer valve.

The *in vitro* hydrodynamics of the Innovia valve approach those of the Magna valve.. The earlier Innovia valve prototype produced a mean pressure gradient during forward flow of 42.85 mmHg +/- 9.52 compared to the new design which produced 25.73 mmHg +/- 8.12. This represents a clinically significant decrease in pressure gradient according to the ACC scale by a shift from moderate to mild stenosis [3]. In comparison, the Magna valve produced a pressure gradient during forward flow of 17.91 mmHg +/- 4.81, which was clinically similar to the new Innovia design.

We have extensively utilized and validated our experimental methodology in the past. However it is important to note that the PAS assay methodology is designed with known limitations. Primarily, it uses gel filtered platelets (as previously described) [33] in lieu of whole blood, eliminating the activating potential of other serum components, *e.g.* effects of red blood cells on platelet activation by the action of adenosine diphosphate (ADP), and platelet-platelet cross-talk via the plasma von Willebrand factor (vWF) acting as a bridging factor. However, the PAS assay still retains the major contribution of activated platelets to clot formation by thrombin, namely the prothrombinase complex, and facilitates well controlled and sensitive comparative measurements of flow induced platelet activity in devices. The small volume LVAD produces near physiologic flow conditions, but cannot produce the physiologic afterload back pressure as can be produced in large volumes pulse duplicators systems which may alter the valve opening and closing dynamics. However, this reiterates the efficacy of the method for comparative measurements, as it is sensitive enough to produce significant results even if the valves do not operate under more extreme conditions. The small volume utilized in our LVAD system means that any given platelet will pass through the valves more frequently over 30 minutes than would be the case *in vivo*, which translates into an accelerated platelet response measurement system (similar to accelerated fatigue testing typically performed to test valve durability). For these combined reasons we used a slightly higher, albeit within range of normal physiology, flow rate than in our previous studies [119,148].

In future studies, we will repeat these experiments with the optimized xSIBS valves.

**Conclusion**

We have found that the latest Innovia polymer valve design is an improvement over the former design and has a significantly lower thrombogenic potential in our test system than the commercially available and FDA-approved Edwards tissue valve. This strongly indicates that the new polymer valve design is approaching the performance level of the commercially available and FDA-approved Edwards tissue valve. As this tissue valve does not require anticoagulation in most patients, it indicates that a PHV based on this new polymer valve design may not require anticoagulation as well. Further, this moves the SIBS-based polymer trileaflet valve closer to clinical applications such as traditional open-heart or transcatheter implantation and in Mechanical Circulatory Support (MCS) devices, of which the latter two may require a more durable material than animal tissue.

## DISCUSSION

Polymeric heart valves (PHV) have been under development since 1960, but to date, no PHVs have been approved for human use and commercial distribution. This has primarily been due to both the clinical success of mechanical and tissue valves and the lack of suitable polymers and designs. The recent FDA-approval of transcatheter aortic valve replacement (TAVR) for inoperable patients with severe aortic stenosis, represents the most significant change in this arena since the advent of the Carpentier-Edwards bovine pericardial valve in 1976, which have made incrementally improvements in mitigating the problem of structural valve deterioration (SVD). TAVR may be an immediate pathway to clinical viability for PHVs because of its confined use in the elderly (mean age of 83), where long term implantation is not expected. TAVR offers a solution for up to 33% of formerly inoperable CAVD patients, thus expanding the population of people whose quality of life will be improved. PHVs may be well suited for TAVR because of the potential damage to tissue valves caused by crimping and deployment. PHVs may also be well suited for applications such as in the Total Artificial Heart, which currently utilizes thrombogenic MHVs. We also have in the last decade the advent of new super-biostable polymers that may finally overcome the major obstacles of PHVs, namely *in vivo* durability and thrombosis. We are better positioned now more than ever before to realize a clinically viable PHV that will avoid SVD and anticoagulants. These are exciting times to be in this area of medical device development.

This multi-facetted project had the ambitious goal of creating a novel open-heart implantable PHV design using a new super-biostable thermoset polyolefin (xSIBS) via a combination of state-of-the-art numerical and experimental methods. We endeavored to answer two questions: (1) is xSIBS a viable polymer for PHVs, and (2) is the DTE method valid in trileaflet valves? Although we have prior experience in the design, fabrication and testing of a transcatheter PHV and delivery system, we focused on an open-heart design so as to have the broadest impact on patients if successful and to characterize an xSIBS PHV prior to moving into TAVR. This allowed us to focus mainly on the form and function of the valve, whereas in TAVR the stent becomes a major design feature.

The focal point of this project was our Device Thrombogenicity Emulation (DTE) methodology, which has the goal of reducing or eliminating anticoagulants in blood recirculating medical devices. The DTE involves numerical characterization and optimization of the device prior to prototype fabrication with the intent of reducing R&D time and costs. This virtual verification testing, using numerical tools such as FEA, FSI, and CFD, is novel in the field of blood recirculating medical device development, especially when combined with platelet activation prediction and validation, as is the case in our Thrombogenic Footprint (TF) analysis and Hemodynamic Shearing Device (HSD) experiments.

The design of the new optimized valve grew from an analysis of the failure modes of the Innovia composite PHV in the animal model and the geometry of native human aortic valve. In the original valve the failure modes were SIBS viscoelastic creep and Dacron fatigue and calcification. The native AV has a complex nonuniform thickness cross-section in the radial direction. Thus we moved to a homogeneous super-biostable polymer with hyperelastic behavior similar to tissue to eliminate the need for mechanical reinforcement such as was the case with the Dacron mesh, and a leaflet cross-section that was thickened in areas of expected high stress and thinned in areas of expected low stress. The belly of the leaflet and the

commissures bear the greatest load in diastole, where the pressure gradient across the valve can go above 80 mmHg. The coaptation surface of each leaflet can distribute the diastolic load evenly among the three leaflets as well, therefore it was maximized in the new design. The thinner regions were meant to offer improved flexibility. Once the design was created in CAD it was examined using FEA, FSI and CFD, the first half of the DTE method.

The xSIBS mechanical properties were not known *a priori*, therefore uniaxial tensile testing was performed to obtain stress vs. strain curves for input into numerical material models. This was accomplished by first fabricating sheets of xSIBS from raw material provided by Innovia via compression molding and heating (240˚C for 30 min) between two aluminum alloy plates, using teflon sheets to prevent sticking and to isolate the xSIBS from air to prevent oxidization. Cross-linking was verified by observing non-dissolution of samples in toluene. The results showed that xSIBS had much higher tensile strength than its predecessor and that it was a nonlinear hyper-elastic rubber-like material. There also appeared to be a yet unverified orthogonal anisotropic behavior, but that could have been an effect of the unperfected sheet fabrication process. The resources and time to conduct more complete mechanical testing were not available and will be part of future work. The uniaxial tensile test data was sufficient for the FEA and FSI material models.

Armed with the xSIBS tensile test data, FEA and FSI case studies were conducted using the two-parameter Mooney-Rivlin hyper-elastic material model in ADINA. Data from the literature were used for the original and tissue valve simulations. (The tissue valve has not yet been simulated using FSI.) Each FEA structural case study included identical mesh densities and loading and fixity conditions. Multiple mesh densities were run to check for the magnitude of mesh dependence mainly on the simulated motion of the valve. The stress patterns remained similar at different mesh densities, but the motion of the leaflets changed with increasing mesh density as expected, up to a point, where finer meshes only caused problems with convergence of the solution. Very coarse meshes also introduced unnatural stiffness at locations of high bending moments, such as the leaflet commissures. In comparing the original composite PHV, the tissue valve, and the xSIBS optimized valve, the stress distribution in the leaflets was clearly reduced and distributed over a broader section of the leaflet geometry. This result led us to believe that the optimized design may have improved flexibility, durability, and hemodynamics comparatively. FEA simulations were also used to obtain the open and closed valve geometries for CFD. This was achieved by alternately loading the aortic or ventricular surface of the leaflets with a normal pressure. We endeavored to utilize physiologic pressures, but it turned out that higher pressures were required in the opening phase. Pressures that were too high produced unrealistic open geometries that were discarded. All other things being equal, it was observed that the valve geometry had the largest effect on the motion of the leaflets. The closed positions were most realistic, when compared to images of real valves in action in the Vivitro LHS, and in comparison to the open positions obtained via FEA. In FSI, we observed lower velocity and stresses compared to the original PHV. However, the FSI computing capabilities for simulating thin flexible structures in fluid flow are still not ready for prime time. We have not yet been able to achieve full opening and closing in one simulation using fully coupled sharp boundary FSI. As the software improves, this will become a more useful tool in predicting valve hemodynamics and stresses.

The geometries created with FEA were used to conduct two-phase (particle and fluid) CFD studies. The studies in the three valves, tissue, original, and optimized, were conducted in separate forward flow and regurgitant flow studies, using rigid fixed valves and straight tubes. The fluid was modeled as a Newtonian blood analog and driven by velocity inlet and pressure outlet boundary conditions. In the forward flow studies, the unsteady Reynolds averaged Navier-Stokes flow model was solved with the Wilcox k-ω turbulence model and a decelerating systolic inlet velocity waveform. The Wilcox k-ω model is better suited for transitional flow, such as is found in the ascending aorta. In those cases, a boundary layer was created in the mesh. In the regurgitant flow studies unsteady laminar flow was modeled with a constant inlet velocity. 30-60,000 platelets (3 μm neutrally buoyant spheres) were seeded into the flow field in a plane upstream from the valve inlet. In all cases 350 ms of flow were simulated. The meshes in all cases were progressive with high density in the vicinity of the valve. Results showed that each valve geometry created different hemodynamics. In both forward and regurgitant flow the optimized valve produced the lowest mean platelet stress accumulation (SA) calculated with the linear model (the summation of stress x time). The statistical distribution of the SA, the probability density function (PDF), called the thrombogenic footprint (TF), indicated that the major mode of the distribution in the optimized valve resided in the lowest stress accumulation range. Analysis of the hemodynamics showed that the optimized valve had the lowest max. velocity and pressure gradient in forward flow. However, in regurgitant flow the tissue valve had the lowest velocity, but, interestingly, this did not produce the lowest SA in the commissure region of interest (ROI). Identical ROIs (spheres, r = 1 mm) at the three commissures and in the core at the free edge of the leaflets were queried in each valve to obtain the PDF. The most frequently occurring SA was used to select a representative stress loading waveform generated by a single platelet in the ROI. These four waveforms per valve were then emulated in the Hemodynamic Shearing Device (HSD) using freshly isolated human platelets. The results showed clearly that the optimized valve produced significantly lower thrombin generation in all cases. Thus the subtle changes in hemodynamics caused by the three different trileaflet valve geometries were able to be detected using the DTE and clearly showed which design was better. The DTE has turned out to be a valuable design tool. But it is limited by the results obtained from numerical studies, which can only approximate reality. One must keep this in mind when interpreting the results. Ultimately, the prototype tests will verify the numerical results and validate the optimization. But the DTE process can be repeated iteratively to move toward a fully optimized design.

Once the optimization was virtually and experimentally verified, compression mold was designed and machined for prototype fabrication. We used computer numerical controlled (CNC) machining via a collaboration with the Helmholtz Institute Applied Medical Engineering facility in Aachen, Germany. They have sophisticated 5-axis CNC machines. The mold design was created using both SolidWorks and Gambit, primarily because Gambit was able to better process Boolean operations. The optimized valve geometry was subtracted from a solid cylinder, which was then split into the various mold components. Aluminum alloy was used for ease of machining and its excellent thermal conductivity. Since xSIBS must be cross-linked thermally and is prone to oxidization during heating, the process of molding a valve was not trivial. The mold was prepared with dry-film PTFE to prevent sticking and to facilitate part release. It was filled about half full with compacted raw xSIBS (23% styrene), and then partially compressed cold. The xSIBS melts at around 200°C, so that is when full compression was completed with about 3 tons of force. The excess or flash was extruded through portholes in the

mold block. Ethanol was used to help with removal of the valve. The mold allowed reproducible prototypes to fabricated at a rate of one per day, factoring in cleaning and heating and cooling times. Ideally, we should have multiple molds for one valve geometry to minimize mold damage and speed processing time. Screw threads tend to wear out quickly in aluminum and tools easily scar the mold during the separation of mold components.

Hydrodynamic testing of the optimized valve prototypes was conducted in the Vivitro Left Heart Simulator (LHS). The test regime was developed was based upon FDA/ISO standards. Pressure and flow measurements were recorded and the output data calculated via Vivitest Software. The xSIBS optimized valve was compared to a gold standard tissue valve, the Carpentier-Edwards Perimount Magna Bioprosthesis (21 mm TAD). The data show that the optimized valve compared favorably to the THV. The pressure gradient during forward flow was slightly higher than the THV, likely because of the superior flexibility of the glutaraldehyde fixed bovine pericardium and its curved leaflet profile. The regurgitation fraction was reduced in the optimized valve compared to the THV, likely due to the larger coaptation surface area. The 23% styrene xSIBS appears to have allowed the production of a PHV with excellent hydrodynamics. Reinforcement of the optimized valve stent was not necessary to allow the valve to survive the rigorous test regime. The diastolic pressure load appeared to be distributed across the entire valve, thus preventing prolapse in lieu of a rigid stent. Reduced styrene formulations of xSIBS may produce even more flexible leaflets, but they will require metal frame reinforcement of the stent due to the decreased stiffness of the xSIBS.

The bulk platelet activation of the original Innovia composite PHV was compared to the gold-standard THV mentioned above in a Berlin pulsatile left ventricular assist device (LVAD) using freshly isolated human platelets. The LVAD volume was 200 ml with a platelet concentration of 20,000/µl. The pump was driven with a Harvard pulsatile pump to achieve a physiologic flow rate. The test was run for 30 minutes with samples taken every 10 minutes. The platelet activation rate was compared, and the data showed that the PHV had 5-fold lower PAS compared to the THV. Flow cytometry results were also in good agreement. Hydrodynamics testing showed favorable comparison of the PHV to the THV. This test will be conducted with the optimized valve and the new molded compliance tubing in future work.

Ongoing and future work will include further blood-interaction and mechanical studies of xSIBS alone, valve design refinement, valve prototype accelerated life cycle testing, and valve prototype bulk platelet activation studies

## CONCLUSIONS

This multi-faceted project produced a novel polymeric heart valve, proved the feasibility of a new hyper-elastic thermoset polyolefin (xSIBS) in PHVs, and validated the DTE method in trileaflet valves. We showed that the optimized valve design, with tapered leaflet thickness, flat leaflet profile, and increase exit orifice, produced superior hemodynamics and platelet activation compared to the original Innovia composite SIBS-Dacron design, and compared favorably to a gold-standard tissue valve. This indicates that an xSIBS based PHV may not require anticoagulants and may be more durable than previous PHVs. Therefore, this work has moved PHVs closer to clinical viability.

**APPENDIX A**

**Pulsatile Berlin LVAD Valve Holder Drawings**

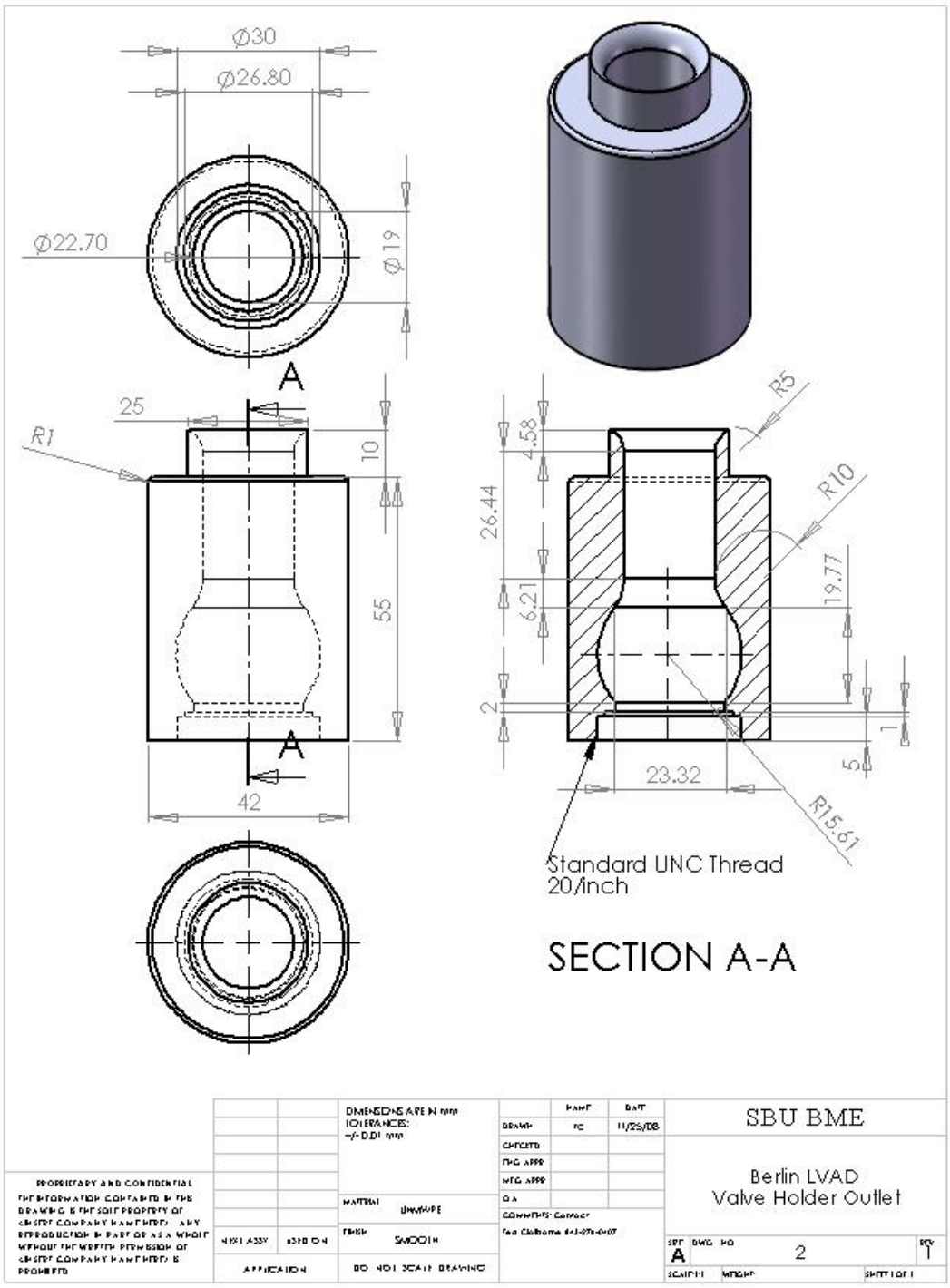


**Figure 49: Outflow valve holder for the pulsatile Berlin LVAD. The pseudo-sinus of Valsalva was created to aid valve closure and to allow space for flared valve stent posts.**

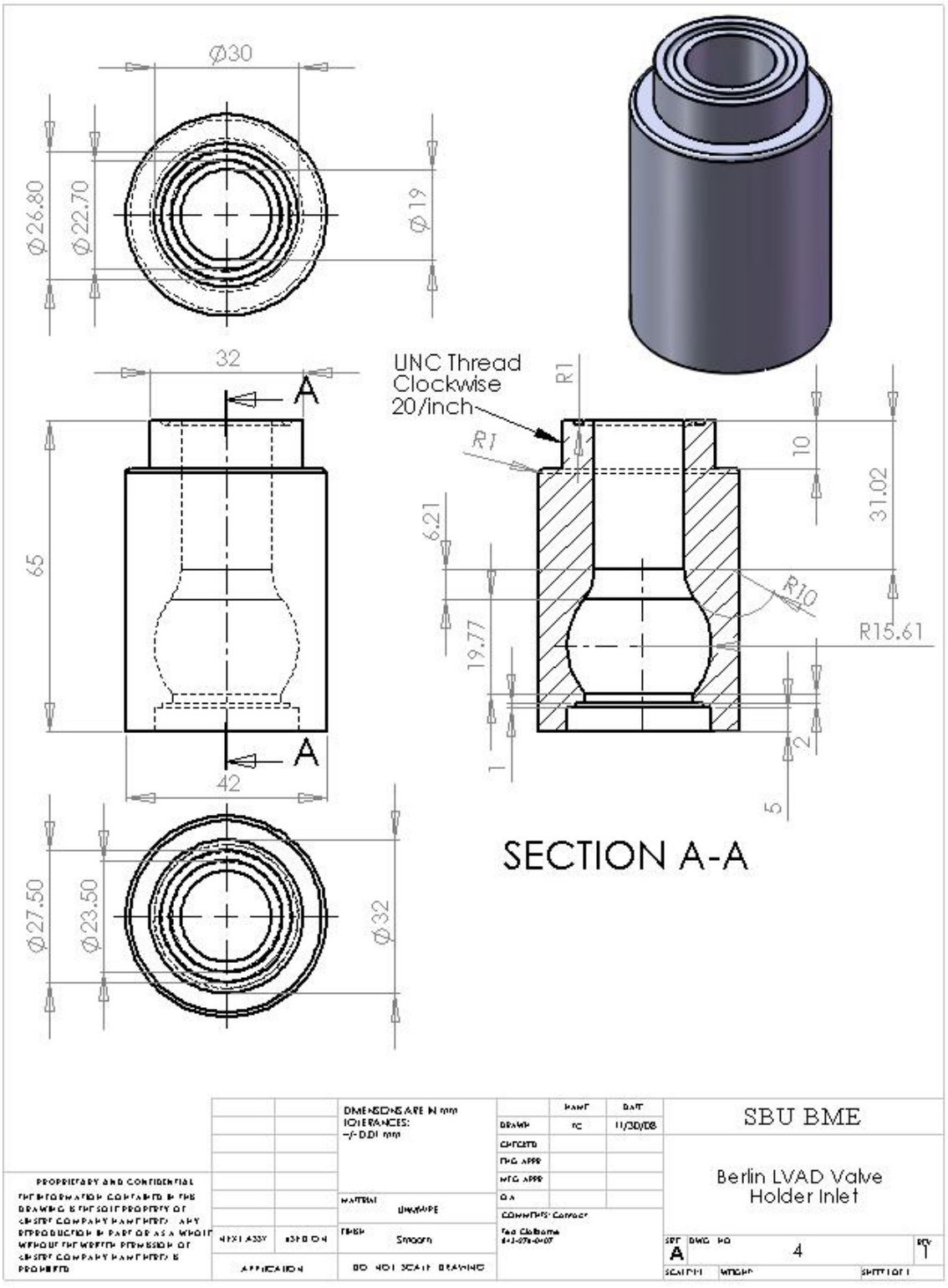


**Figure 50: Inflow valve holder for the pulsatile Berlin LVAD. The pseudo-sinus of Valsalva was created to aid valve closure and to allow space for flared valve stent posts.**

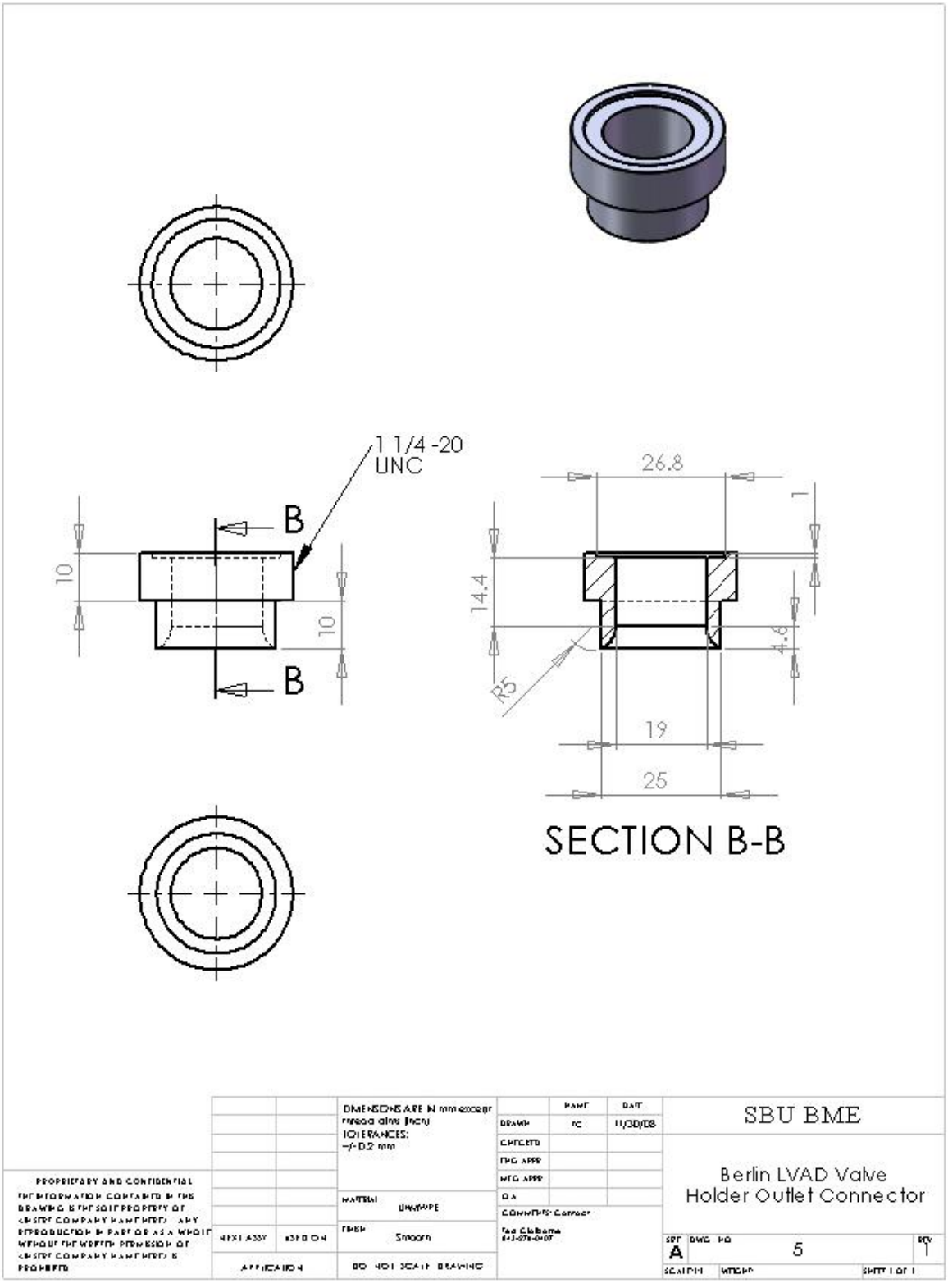


**Figure 51: Outflow valve holder connector for the pulsatile Berlin LVAD.**

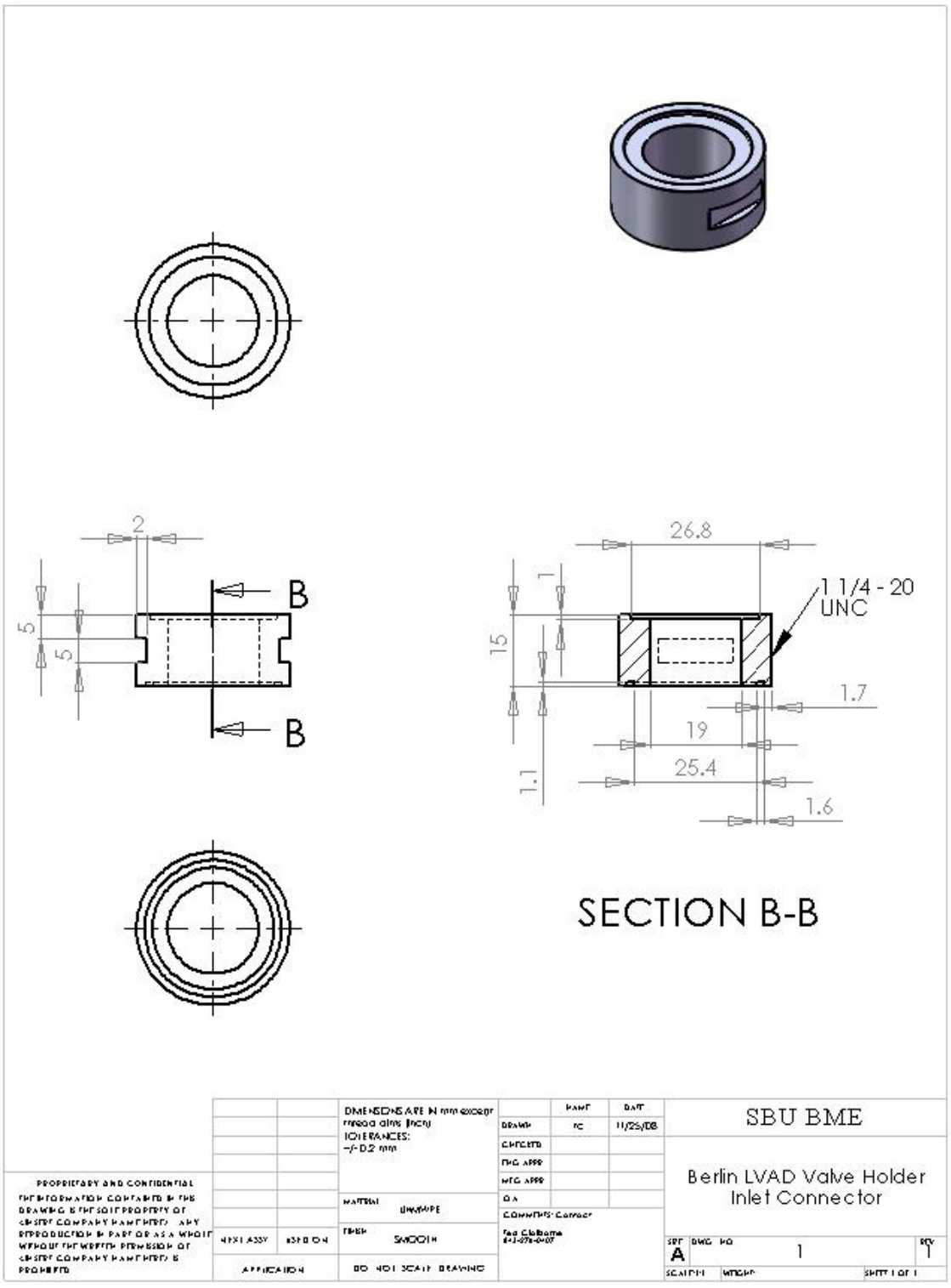


**Figure 52: Inflow valve holder connector for the pulsatile Berlin LVAD.**

**Pulsatile Berlin LVAD Compliance Tubing Mold Drawings**

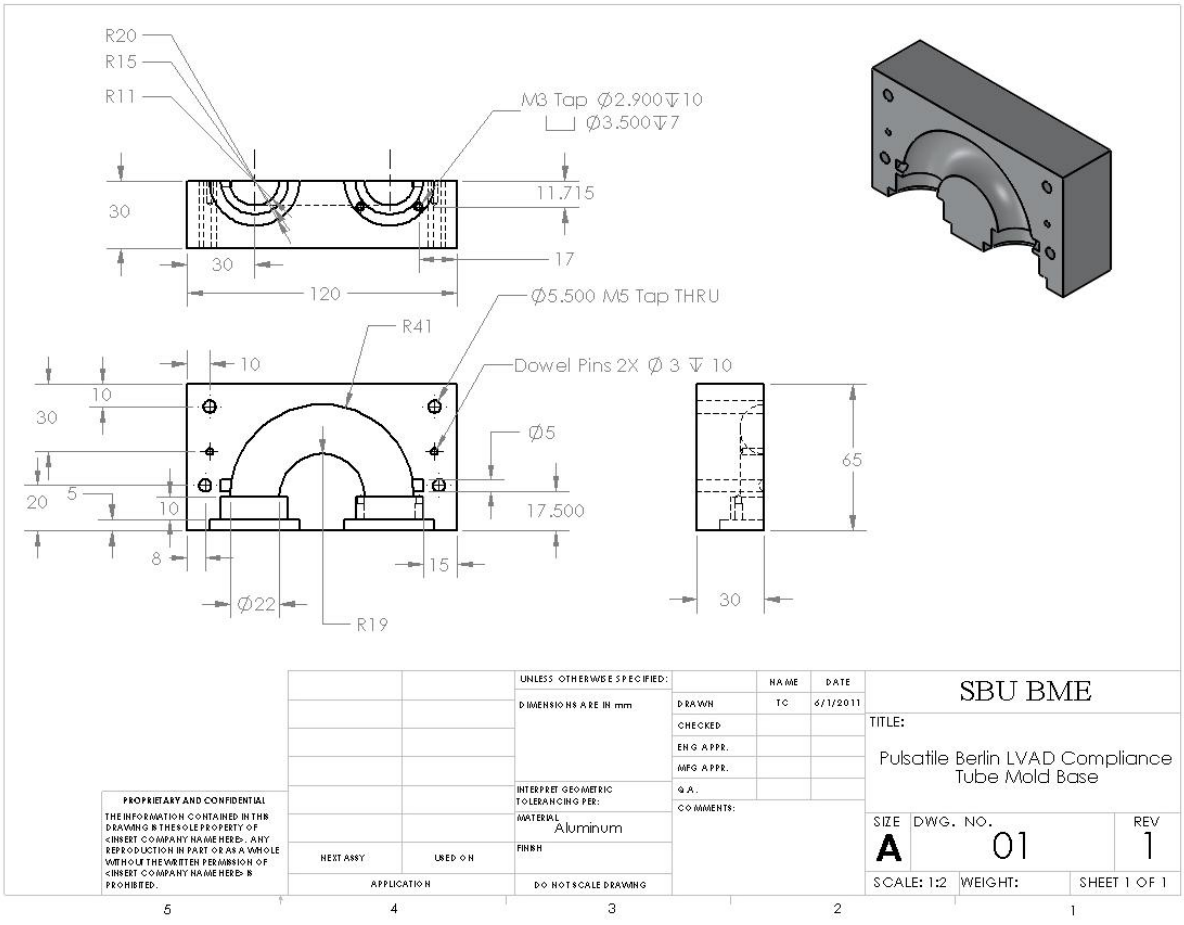


**Figure 53: Compliance tube mold base for the pulsatile Berlin LVAD.**

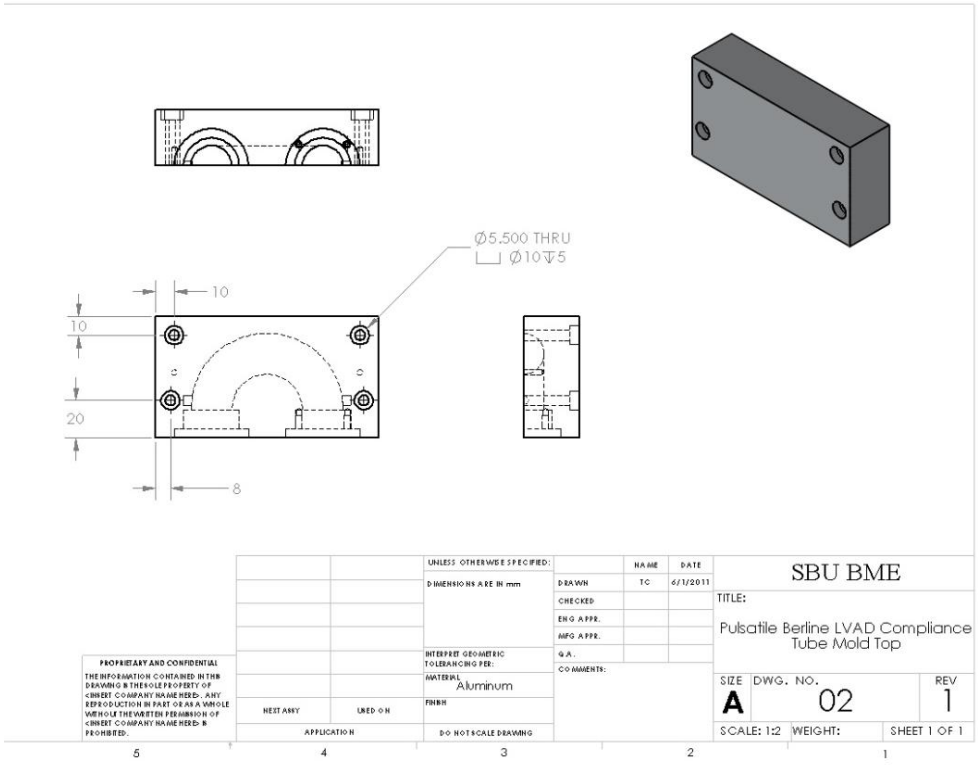


**Figure 54: Compliance tube mold top for the pulsatile Berlin LVAD.**

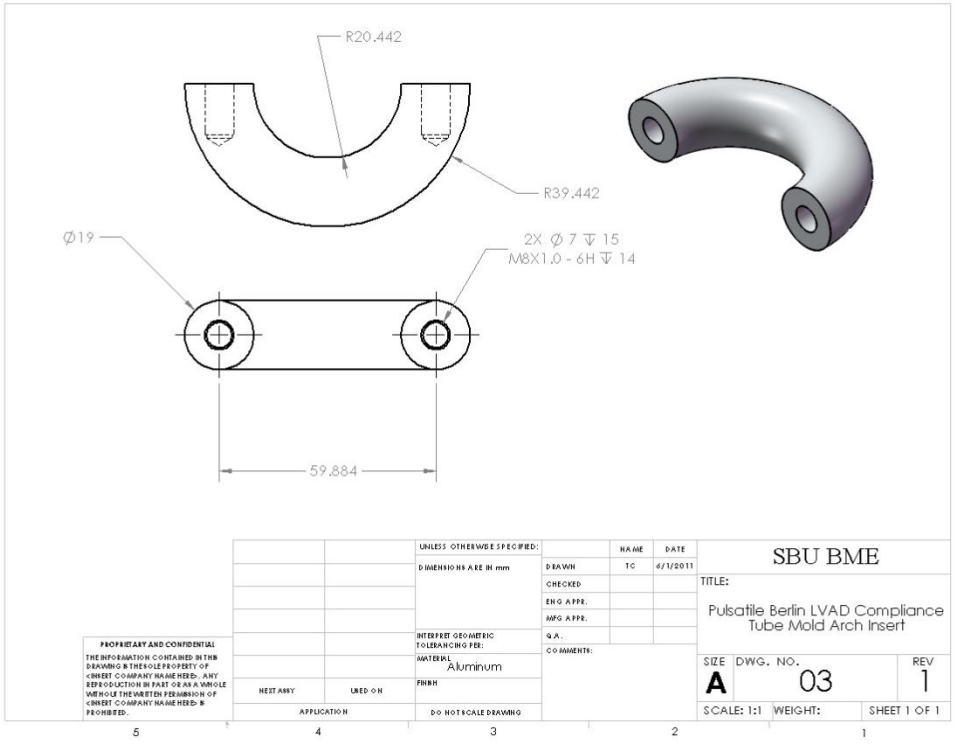


**Figure 55: Compliance tube mold arch insert for the pulsatile Berlin LVAD.**

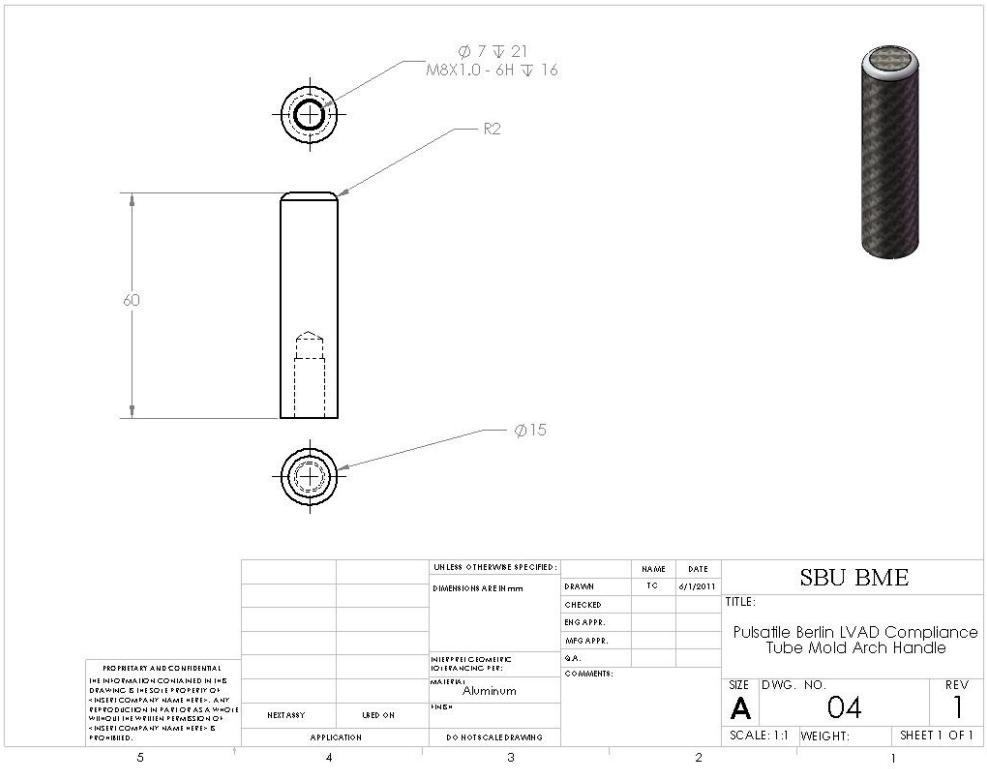


**Figure 56: Compliance tube mold arch handle for the pulsatile Berlin LVAD.**

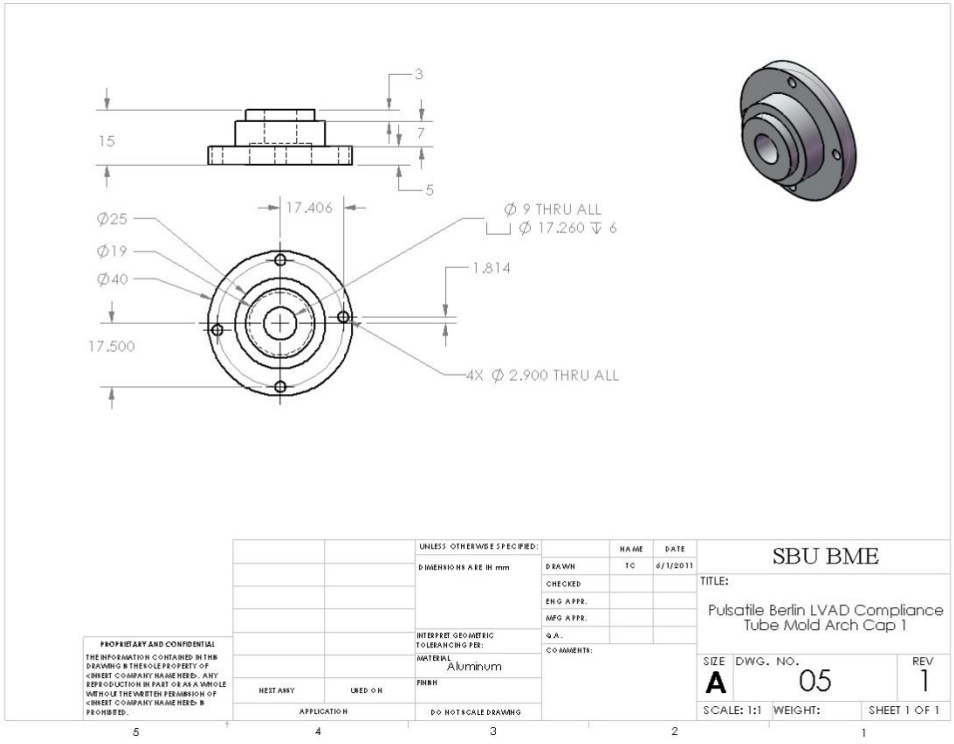


**Figure 57: Compliance tube mold arch cap 1 for the pulsatile Berlin LVAD.**

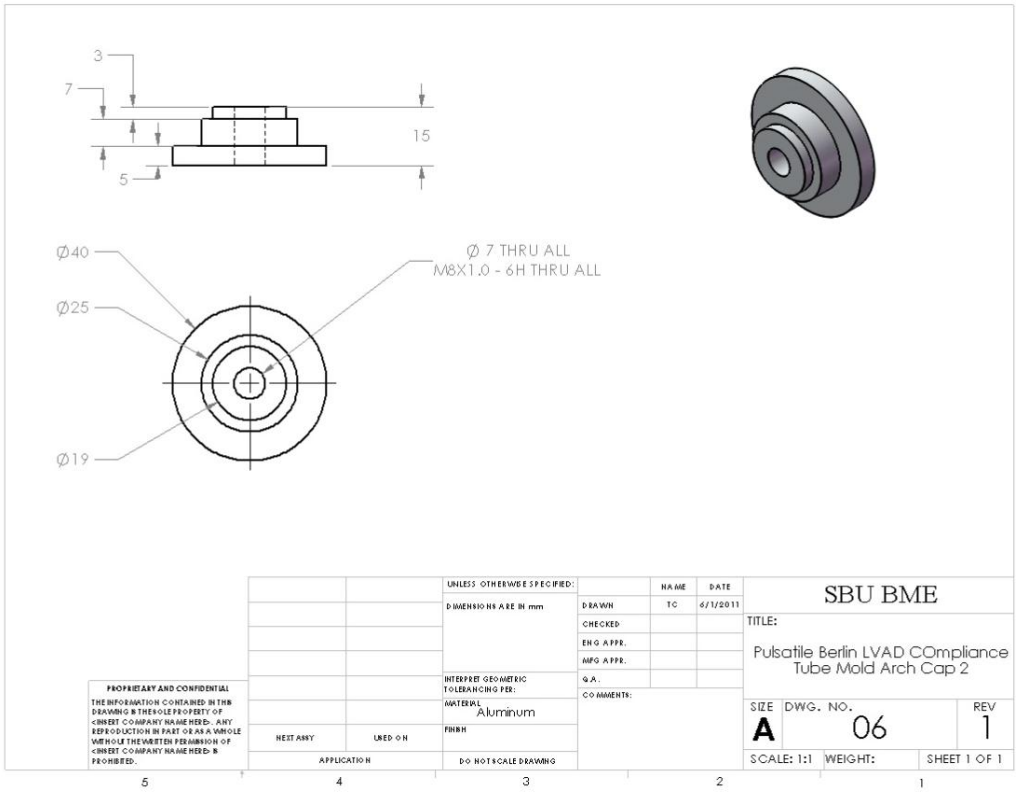


**Figure 58: Compliance tube mold arch cap 2 for the pulsatile Berlin LVAD.**

## REFERENCES


1. Rosamond W, Flegal K, Friday G, Furie K, Go A, et al. (2007) Heart disease and stroke statistics--2007 update: a report from the American Heart Association Statistics Committee and Stroke Statistics Subcommittee. Circulation 115: e69-171.
2. Rosengart TK, Feldman T, Borger MA, Vassiliades TA, Jr., Gillinov AM, et al. (2008) Percutaneous and minimally invasive valve procedures: a scientific statement from the American Heart Association Council on Cardiovascular Surgery and Anesthesia, Council on Clinical Cardiology, Functional Genomics and Translational Biology Interdisciplinary Working Group, and Quality of Care and Outcomes Research Interdisciplinary Working Group. Circulation 117: 1750-1767.
3. Bonow RO, Carabello BA, Chatterjee K, de Leon AC, Jr., Faxon DP, et al. (2008) 2008 Focused update incorporated into the ACC/AHA 2006 guidelines for the management of patients with valvular heart disease: a report of the American College of Cardiology/American Heart Association Task Force on Practice Guidelines (Writing Committee to Revise the 1998 Guidelines for the Management of Patients With Valvular Heart Disease): endorsed by the Society of Cardiovascular Anesthesiologists, Society for Cardiovascular Angiography and Interventions, and Society of Thoracic Surgeons. Circulation 118: e523-661.
4. Kulik A, Bedard P, Lam BK, Rubens FD, Hendry PJ, et al. (2006) Mechanical versus bioprosthetic valve replacement in middle-aged patients. Eur J Cardiothorac Surg 30: 485-491.
5. Reynolds MR, Magnuson EA, Wang K, Lei Y, Vilain K, et al. (2012) Cost-Effectiveness of Transcatheter Aortic Valve Replacement Compared With Standard Care Among Inoperable Patients With Severe Aortic Stenosis: Results From the Placement of Aortic Transcatheter Valves (PARTNER) Trial (Cohort B). Circulation 125: 1102-1109.
6. Ghanbari H, Viatge H, Kidane AG, Burriesci G, Tavakoli M, et al. (2009) Polymeric heart valves: new materials, emerging hopes. Trends in Biotechnology 27: 359-367.
7. Platis A, Larson DF (2009) CardioWest temporary total artificial heart. Perfusion 24: 341-346.
8. Zegdi R, Bruneval P, Blanchard D, Fabiani JN (2011) Evidence of leaflet injury during percutaneous aortic valve deployment. Eur J Cardiothorac Surg 40: 257-259.
9. de Buhr W, Pfeifer S, Slotta-Huspenina J, Wintermantel E, Lutter G, et al. (2012) Impairment of pericardial leaflet structure from balloon-expanded valved stents. J Thorac Cardiovasc Surg 143: 1417-1421.
10. Pinchuk L, Wilson GJ, Barry JJ, Schoephoerster RT, Parel JM, et al. (2008) Medical applications of poly(styrene-block-isobutylene-block-styrene) ("SIBS"). Biomaterials 29: 448-460.
11. Gallocher SL, Aguirre AF, Kasyanov V, Pinchuk L, Schoephoerster RT (2006) A novel polymer for potential use in a trileaflet heart valve. J Biomed Mater Res B Appl Biomater 79: 325-334.
12. Gallocher SL (2007) Durability assessment of polymer trileaflet heart valves. Miami: Florida International University.
13. Wang Q, McGoron AJ, Bianco R, Kato Y, Pinchuk L, et al. (2010) In-vivo assessment of a novel polymer (SIBS) trileaflet heart valve. J Heart Valve Dis 19: 499-505.
14. Claiborne TE, Girdhar G, Gallocher-Lowe S, Sheriff J, Kato YP, et al. (2011) Thrombogenic potential of Innovia polymer valves versus Carpentier-Edwards Perimount Magna aortic bioprosthetic valves. ASAIO J 57: 26-31.

15. Wang Q, McGoron AJ, Pinchuk L, Schoephoerster RT (2010) A novel small animal model for biocompatibility assessment of polymeric materials for use in prosthetic heart valves. J Biomed Mater Res A 93: 442-453.
16. Duraiswamy N, Choksi TD, Pinchuk L, Schoephoerster RT (2009) A phospholipid-modified polystyrene-polyisobutylene-polystyrene (SIBS) triblock polymer for enhanced hemocompatibility and potential use in artificial heart valves. J Biomater Appl 23: 367-379.
17. Wang Q (2008) In vivo biocompatibility evaluation of composite polymeric materials for use in a novel artificial heart valve. Miami: Florida International University.
18. Xenos M, Girdhar G, Alemu Y, Jesty J, Slepian M, et al. (2010) Device Thrombogenicity Emulator (DTE)--design optimization methodology for cardiovascular devices: a study in two bileaflet MHV designs. J Biomech 43: 2400-2409.
19. Girdhar G, Xenos M, Alemu Y, Chiu W-C, Lynch BE, et al. (2012) Device Thrombogenicity Emulation: A Novel Method for Optimizing Mechanical Circulatory Support Device Thromboresistance. PLoS One 7: e32463.
20. Kurtz CE, Otto CM (2010) Aortic stenosis: clinical aspects of diagnosis and management, with 10 illustrative case reports from a 25-year experience. Medicine (Baltimore) 89: 349-379.
21. Chandran KB, Rittgers SE, Yoganathan AP (2007) Biofluid mechanics : the human circulation. Boca Raton: CRC/Taylor & Francis. 419 p. p.
22. Hermans H, Herijgers P, Holvoet P, Verbeken E, Meuris B, et al. (2010) Statins for calcific aortic valve stenosis: into oblivion after SALTIRE and SEAS? An extensive review from bench to bedside. Curr Probl Cardiol 35: 284-306.
23. Parolari A, Loardi C, Mussoni L, Cavallotti L, Camera M, et al. (2009) Nonrheumatic calcific aortic stenosis: an overview from basic science to pharmacological prevention. Eur J Cardiothorac Surg 35: 493-504.
24. Vincentelli A, Susen S, Le Tourneau T, Six I, Fabre O, et al. (2003) Acquired von Willebrand syndrome in aortic stenosis. N Engl J Med 349: 343-349.
25. Ratner BD (2004) Biomaterials science : an introduction to materials in medicine. Amsterdam ; Boston: Elsevier Academic Press. xii, 851 p. p.
26. Bluestein D, Rambod E, Gharib M (2000) Vortex shedding as a mechanism for free emboli formation in mechanical heart valves. J Biomech Eng 122: 125-134.
27. Gailani D, Renne T (2007) Intrinsic pathway of coagulation and arterial thrombosis. Arterioscler Thromb Vasc Biol 27: 2507-2513.
28. Muller F, Renne T (2008) Novel roles for factor XII-driven plasma contact activation system. Curr Opin Hematol 15: 516-521.
29. Schousboe I (2008) Pharmacological regulation of factor XII activation may be a new target to control pathological coagulation. Biochem Pharmacol 75: 1007-1013.
30. Gailani D, Renne T (2007) The intrinsic pathway of coagulation: a target for treating thromboembolic disease? J Thromb Haemost 5: 1106-1112.
31. Baglia FA, Walsh PN (2007) Thrombin-mediated feedback activation of factor XI on the activated platelet surface is preferred over contact activation by factor XIIa or factor Xia (Retraction of vol 275, pg 20514, 2000). Journal of Biological Chemistry 282: 29067-29067.

32. Back J, Sanchez J, Elgue G, Ekdahl KN, Nilsson B (2010) Activated human platelets induce factor XIIa-mediated contact activation. Biochemical and Biophysical Research Communications 391: 11-17.
33. Jesty J, Bluestein D (1999) Acetylated prothrombin as a substrate in the measurement of the procoagulant activity of platelets: elimination of the feedback activation of platelets by thrombin. Anal Biochem 272: 64-70.
34. Sperling C, Fischer M, Maitz MF, Werner C (2009) Blood coagulation on biomaterials requires the combination of distinct activation processes. Biomaterials 30: 4447-4456.
35. Ratner BD (2007) The catastrophe revisited: blood compatibility in the 21st Century. Biomaterials 28: 5144-5147.
36. Thubrikar M (1990) The aortic valve. Boca Raton, Fla.: CRC Press. 221 p. p.
37. Food and Drug Administration.
38. International Standards Organization.
39. Hufnagel CA (1951) Plastic Cardiac Valvular Prostheses. American Journal of Medicine 11: 243-243.
40. Miller BJ, Gibbon JH, Jr., Greco VF, Smith BA, Cohn CH, et al. (1953) The production and repair of interatrial septal defects under direct vision with the assistance of an extracorporeal pump-oxygenator circuit. J Thorac Surg 26: 598-616; discussion 631-592.
41. Gott VL, Alejo DE, Cameron DE (2003) Mechanical heart valves: 50 years of evolution. Ann Thorac Surg 76: S2230-2239.
42. Ross DN (1962) Homograft replacement of the aortic valve. Lancet 2: 487.
43. Kaiser GA, Hancock WD, Lukban SB, Litwak RS (1969) Clinical use of a new design stented xenograft heart valve prosthesis. Surg Forum 20: 137-138.
44. Carpentier A (1977) From valvular xenograft to valvular bioprosthesis (1965-1977). Med Instrum 11: 98-101.
45. Carpentier A (1989) From valvular xenograft to valvular bioprosthesis: 1965-1970. Ann Thorac Surg 48: S73-74.
46. Rahimtoola SH (2010) Choice of prosthetic heart valve in adults an update. J Am Coll Cardiol 55: 2413-2426.
47. Kidane AG, Burriesci G, Cornejo P, Dooley A, Sarkar S, et al. (2009) Current developments and future prospects for heart valve replacement therapy. J Biomed Mater Res B Appl Biomater 88: 290-303.
48. Ghanbari H, Viatge H, Kidane AG, Burriesci G, Tavakoli M, et al. (2009) Polymeric heart valves: new materials, emerging hopes. Trends Biotechnol 27: 359-367.
49. Kutting M, Roggenkamp J, Urban U, Schmitz-Rode T, Steinseifer U (2011) Polyurethane heart valves: past, present and future. Expert Rev Med Devices 8: 227-233.
50. Ten Berge L (1958) A flexible cardiac valve prosthesis; preliminary report on the development of an experimental valvular prosthesis. Arch Chir Neerl 10: 26-33.
51. Elliot EC, Callaghan JC (1958) All plastic ventricle-type pump with tricuspid valves. Can J Surg 1: 308-312.
52. Braunwald NS, Cooper T, Morrow AG (1960) Complete replacement of the mitral valve. Successful clinical application of a flexible polyurethane prosthesis. J Thorac Cardiovasc Surg 40: 1-11.
53. Maisano F, La Canna G, Colombo A, Alfieri O (2011) The evolution from surgery to percutaneous mitral valve interventions: the role of the edge-to-edge technique. J Am Coll Cardiol 58: 2174-2182.

54. Bernacca GM, Mackay TG, Wheatley DJ (1996) In vitro function and durability of a polyurethane heart valve: material considerations. J Heart Valve Dis 5: 538-542.
55. Mackay TG, Wheatley DJ, Bernacca GM, Fisher AC, Hindle CS (1996) New polyurethane heart valve prosthesis: design, manufacture and evaluation. Biomaterials 17: 1857-1863.
56. Bernacca GM, Mackay TG, Gulbransen MJ, Donn AW, Wheatley DJ (1997) Polyurethane heart valve durability: effects of leaflet thickness and material. Int J Artif Organs 20: 327-331.
57. Bernacca GM, Mackay TG, Wilkinson R, Wheatley DJ (1997) Polyurethane heart valves: fatigue failure, calcification, and polyurethane structure. J Biomed Mater Res 34: 371-379.
58. Bernacca GM, Gulbransen MJ, Wilkinson R, Wheatley DJ (1998) In vitro blood compatibility of surface-modified polyurethanes. Biomaterials 19: 1151-1165.
59. Bernacca GM, Wheatley DJ (1998) Surface modification of polyurethane heart valves: effects on fatigue life and calcification. Int J Artif Organs 21: 814-819.
60. Wheatley DJ, Raco L, Bernacca GM, Sim I, Belcher PR, et al. (2000) Polyurethane: material for the next generation of heart valve prostheses? Eur J Cardiothorac Surg 17: 440-448.
61. Wheatley DJ, Bernacca GM, Tolland MM, O'Connor B, Fisher J, et al. (2001) Hydrodynamic function of a biostable polyurethane flexible heart valve after six months in sheep. Int J Artif Organs 24: 95-101.
62. Bernacca GM, O'Connor B, Williams DF, Wheatley DJ (2002) Hydrodynamic function of polyurethane prosthetic heart valves: influences of Young's modulus and leaflet thickness. Biomaterials 23: 45-50.
63. Bernacca GM, Straub I, Wheatley DJ (2002) Mechanical and morphological study of biostable polyurethane heart valve leaflets explanted from sheep. J Biomed Mater Res 61: 138-145.
64. Chandran KB, Fatemi R, Schoephoerster R, Wurzel D, Hansen G, et al. (1989) In vitro comparison of velocity profiles and turbulent shear distal to polyurethane trileaflet and pericardial prosthetic valves. Artif Organs 13: 148-154.
65. Chandran KB, Schoephoerster RT, Wurzel D, Hansen G, Yu LS, et al. (1989) Hemodynamic comparisons of polyurethane trileaflet and bioprosthetic heart valves. ASAIO Trans 35: 132-138.
66. Mori H, Hessel EA, 2nd, Nelson RJ, Anderson HN, Dillard DH, et al. (1973) Design and durability test of Silastic trileaflet aortic valve prostheses. J Thorac Cardiovasc Surg 65: 576-582.
67. Imamura E, Kaye MP (1977) Function of expanded-polytetrafluoroethylene laminated trileaflet valves in animals. Mayo Clin Proc 52: 770-775.
68. Wisman CB, Pierce WS, Donachy JH, Pae WE, Myers JL, et al. (1982) A polyurethane trileaflet cardiac valve prosthesis: in vitro and in vivo studies. Trans Am Soc Artif Intern Organs 28: 164-168.
69. Kiraly R, Yozu R, Hillegass D, Harasaki H, Murabayashi S, et al. (1982) Hexsyn trileaflet valve: application to temporary blood pumps. Artif Organs 6: 190-197.
70. Woo YR, Williams FP, Yoganathan AP (1983) Steady and pulsatile flow studies on a trileaflet heart valve prosthesis. Scand J Thorac Cardiovasc Surg 17: 227-236.
71. Woo YR, Williams FP, Yoganathan AP (1983) In-vitro fluid dynamic characteristics of the abiomed trileaflet heart valve prosthesis. J Biomech Eng 105: 338-345.

72. Hilbert SL, Ferrans VJ, Tomita Y, Eidbo EE, Jones M (1987) Evaluation of explanted polyurethane trileaflet cardiac valve prostheses. J Thorac Cardiovasc Surg 94: 419-429.
73. Nistal F, Garcia-Martinez V, Arbe E, Fernandez D, Artinano E, et al. (1990) In vivo experimental assessment of polytetrafluoroethylene trileaflet heart valve prosthesis. J Thorac Cardiovasc Surg 99: 1074-1081.
74. Corden J, David T, Fisher J (1996) The influence of open leaflet geometry on the haemodynamic flow characteristics of polyurethane trileaflet artificial heart valves. Proc Inst Mech Eng H 210: 273-287.
75. Leo HL, Simon H, Carberry J, Lee SC, Yoganathan AP (2005) A comparison of flow field structures of two tri-leaflet polymeric heart valves. Ann Biomed Eng 33: 429-443.
76. El Fray M, Altstadt V (2003) Fatigue behaviour of multiblock thermoplastic elastomers. 2. Dynamic creep of poly(aliphatic/aromatic-ester) copolymers. Polymer 44: 4643-4650.
77. El Fray M, Altstadt V (2004) Fatigue behaviour of multiblock thermoplastic elastomers. 3. Stepwise increasing strain test of poly (aliphatic/aromatic-ester) copolymers. Polymer 45: 263-273.
78. El Fray M, Altstadt V (2003) Fatigue behaviour of multiblock thermoplastic elastomers. 1. Stepwise increasing load testing of poly(aliphatic/aromatic-ester) copolymers. Polymer 44: 4635-4642.
79. El Fray M, Prowans P, Puskas JE, Altstadt V (2006) Biocompatibility and fatigue properties of polystyrene-polyisobutylene-polystyrene, an emerging thermoplastic elastomeric biomaterial. Biomacromolecules 7: 844-850.
80. Dalmau MJ, Mariagonzalez-Santos J, Lopez-Rodriguez J, Bueno M, Arribas A (2006) The Carpentier-Edwards Perimount Magna aortic xenograft: a new design with an improved hemodynamic performance. Interact Cardiovasc Thorac Surg 5: 263-267.
81. Kidane AG, Burriesci G, Cornejo P, Dooley A, Sarkar S, et al. (2009) Current Developments and Future Prospects for Heart Valve Replacement Therapy. Journal of Biomedical Materials Research Part B-Applied Biomaterials 88B: 290-303.
82. Kannan RY, Salacinski HJ, Butler PE, Seifalian AM (2005) Polyhedral oligomeric silsesquioxane nanocomposites: the next generation material for biomedical applications. Acc Chem Res 38: 879-884.
83. Kidane AG, Burriesci G, Edirisinghe M, Ghanbari H, Bonhoeffer P, et al. (2009) A novel nanocomposite polymer for development of synthetic heart valve leaflets. Acta Biomaterialia 5: 2409-2417.
84. Fishbein MC, Roberts WC, Golden A, Hufnagel CA (1975) Cardiac pathology after aortic valve replacement using Hufnagel trileaflet prostheses: a study of 20 necropsy patients. Am Heart J 89: 443-448.
85. Clark RE, Swanson WM, Kardos JL, Hagen RW, Beauchamp RA (1978) Durability of prosthetic heart valves. Ann Thorac Surg 26: 323-335.
86. Leat ME, Fisher J (1993) Comparative study of the function of the Abiomed polyurethane heart valve for use in left ventricular assist devices. J Biomed Eng 15: 516-520.
87. Robin J, Martinot S, Curtil A, Vedrinne C, Tronc F, et al. (1998) Experimental right ventricle to pulmonary artery discontinuity: outcome of polyurethane valved conduits. J Thorac Cardiovasc Surg 115: 898-903.
88. Daebritz SH, Fausten B, Hermanns B, Franke A, Schroeder J, et al. (2004) New flexible polymeric heart valve prostheses for the mitral and aortic positions. Heart Surg Forum 7: E525-532.

89. Bae JY, Chung DJ, An JH, Shin DH (1999) Effect of the structure of chain extenders on the dynamic mechanical behaviour of polyurethane. Journal of Materials Science 34: 2523-2527.
90. Leo HL, Dasi LP, Carberry J, Simon HA, Yoganathan AP (2006) Fluid dynamic assessment of three polymeric heart valves using particle image velocimetry. Ann Biomed Eng 34: 936-952.
91. Rahmani B, Tzamtzis S, Ghanbari H, Burriesci G, Seifalian AM (2012) Manufacturing and hydrodynamic assessment of a novel aortic valve made of a new nanocomposite polymer. J Biomech.
92. Hernandez R, Weksler J, Padsalgikar A, Runt J (2008) In vitro oxidation of high polydimethylsiloxane content biomedical polyurethanes: correlation with the microstructure. J Biomed Mater Res A 87: 546-556.
93. Pinchuk L (2009) Crosslinked Polyolefins For Biomedical Applicatios And Method of Making Same In: USPTO, editor. USPTO. USA.
94. Kalita H, Karak N (2012) Bio-based elastomeric hyperbranched polyurethanes for shape memory application. Iranian Polymer Journal 21: 263-271.
95. Sheng DK, Tan JJ, Liu XD, Wang PX, Yang YM (2011) Effect of organoclay with various organic modifiers on the morphological, mechanical, and gas barrier properties of thermoplastic polyurethane/organoclay nanocomposites. Journal of Materials Science 46: 6508-6517.
96. Walther T, Falk V, Mohr FW (2006) Minimally invasive surgery for valve disease. Curr Probl Cardiol 31: 399-437.
97. Andersen HR (2009) History of percutaneous aortic valve prosthesis. Herz 34: 343-346.
98. Bower JL, Christensen CM (1995) Disruptive Technologies - Catching the Wave. Harvard Business Review 73: 43-53.
99. Webb J, Cribier A (2011) Percutaneous transarterial aortic valve implantation: what do we know? Eur Heart J 32: 140-147.
100. Holmes DR, Jr., Mack MJ, Kaul S, Agnihotri A, Alexander KP, et al. (2012) 2012 ACCF/AATS/SCAI/STS expert consensus document on transcatheter aortic valve replacement: developed in collaboration with the American Heart Association, American Society of Echocardiography, European Association for Cardio-Thoracic Surgery, Heart Failure Society of America, Mended Hearts, Society of Cardiovascular Anesthesiologists, Society of Cardiovascular Computed Tomography, and Society for Cardiovascular Magnetic Resonance. Ann Thorac Surg 93: 1340-1395.
101. Davies H (1965) Catheter-Mounted Valve for Temporary Relief of Aortic Insufficiency. Lancet 1: 250-&.
102. Andersen HR, Knudsen LL, Hasenkam JM (1992) Transluminal implantation of artificial heart valves. Description of a new expandable aortic valve and initial results with implantation by catheter technique in closed chest pigs. Eur Heart J 13: 704-708.
103. Cribier A, Eltchaninoff H, Bash A, Borenstein N, Tron C, et al. (2002) Percutaneous transcatheter implantation of an aortic valve prosthesis for calcific aortic stenosis: first human case description. Circulation 106: 3006-3008.
104. Bonhoeffer P, Boudjemline Y, Saliba Z, Merckx J, Aggoun Y, et al. (2000) Percutaneous replacement of pulmonary valve in a right-ventricle to pulmonary-artery prosthetic conduit with valve dysfunction. Lancet 356: 1403-1405.

105. Azadani AN, Tseng EE (2010) Transcatheter valve-in-valve implantation for failing bioprosthetic valves. Future Cardiol 6: 811-831.
106. Gurvitch R, Cheung A, Ye J, Wood DA, Willson AB, et al. (2011) Transcatheter valve-in-valve implantation for failed surgical bioprosthetic valves. J Am Coll Cardiol 58: 2196-2209.
107. Greif M, Lange P, Mair H, Becker C, Schmitz C, et al. (2012) Transcatheter Edwards Sapien XT valve in valve implantation in degenerated aortic bioprostheses via transfemoral access. Clin Res Cardiol.
108. Elmariah S, Arzamendi D, Llanos A, Margey RJ, Inglessis I, et al. (2012) First experience with transcatheter valve-in-valve implantation for a stenotic mitral prosthesis within the United States. JACC Cardiovasc Interv 5: e13-14.
109. Hoffmann R, Mollmann H, Lotfi S (2012) Transcatheter aortic valve-in-valve implantation of a corevalve in a degenerated stenotic sapien heart valve prosthesis. Catheter Cardiovasc Interv.
110. Toggweiler S, Wood DA, Rodes-Cabau J, Kapadia S, Willson AB, et al. (2012) Transcatheter valve-in-valve implantation for failed balloon-expandable transcatheter aortic valves. JACC Cardiovasc Interv 5: 571-577.
111. Willson AB, Rodes-Cabau J, Wood DA, Leipsic J, Cheung A, et al. (2012) Transcatheter Aortic Valve Replacement With the St. Jude Medical Portico Valve: First-in-Human Experience. J Am Coll Cardiol.
112. Jarvik RK (1981) The total artificial heart. Sci Am 244: 74-80.
113. Kolff WJ (1965) An artificial heart inside the body. Sci Am 213: 39-46.
114. Goubergrits L, Leirner A, Affeld K (2003) Trileaflet valve for VAD use with purged sinus. Artif Organs 27: 586-591.
115. Roszelle BN, Deutsch S, Manning KB (2010) A parametric study of valve orientation on the flow patterns of the Penn State pulsatile pediatric ventricular assist device. ASAIO J 56: 356-363.
116. Kennedy JP (2005) From thermoplastic elastomers to designed biomaterials. Journal of Polymer Science Part a-Polymer Chemistry 43: 2951-2963.
117. Boden M, Richard R, Schwarz MC, Kangas S, Huibregtse B, et al. (2009) In vitro and in vivo evaluation of the safety and stability of the TAXUS Paclitaxel-Eluting Coronary Stent. J Mater Sci Mater Med 20: 1553-1562.
118. Arrieta EA, Aly M, Parrish R, Dubovy S, Pinchuk L, et al. (2011) Clinicopathologic correlations of poly-(styrene-b-isobutylene-b-styrene) glaucoma drainage devices of different internal diameters in rabbits. Ophthalmic Surg Lasers Imaging 42: 338-345.
119. Yin W, Gallocher S, Pinchuk L, Schoephoerster RT, Jesty J, et al. (2005) Flow-induced platelet activation in a St. Jude mechanical heart valve, a trileaflet polymeric heart valve, and a St. Jude tissue valve. Artif Organs 29: 826-831.
120. Gallocher SL (2007) Durability Assessment of Polymer Trileaflet Valves. ProQuest ETD Collection for FIU.
121. Claiborne TE, Bluestein D, Schoephoerster RT (2009) Development and evaluation of a novel artificial catheter-deliverable prosthetic heart valve and method for in vitro testing. Int J Artif Organs 32: 262-271.
122. Bathe K-J (1996) Finite element procedures. Englewood Cliffs, N.J.: Prentice Hall. xiv, 1037 p. p.

123. Alemu Y, Bluestein D (2007) Flow-induced platelet activation and damage accumulation in a mechanical heart valve: numerical studies. Artif Organs 31: 677-688.
124. Bluestein D, Einav S (1994) Transition to turbulence in pulsatile flow through heart valves--a modified stability approach. J Biomech Eng 116: 477-487.
125. Stevenson DM, Yoganathan AP (1985) Numerical simulation of steady turbulent flow through trileaflet aortic heart valves--I. Computational scheme and methodology. J Biomech 18: 899-907.
126. Stevenson DM, Yoganathan AP, Williams FP (1985) Numerical simulation of steady turbulent flow through trileaflet aortic heart valves--II. Results on five models. J Biomech 18: 909-926.
127. De Hart J, Peters GW, Schreurs PJ, Baaijens FP (2003) A three-dimensional computational analysis of fluid-structure interaction in the aortic valve. J Biomech 36: 103-112.
128. Carmody CJ, Burriesci G, Howard IC, Patterson EA (2006) An approach to the simulation of fluid-structure interaction in the aortic valve. J Biomech 39: 158-169.
129. Peskin CS, Mcqueen DM (1989) A 3-Dimensional Computational Method for Blood-Flow in the Heart .1. Immersed Elastic Fibers in a Viscous Incompressible Fluid. Journal of Computational Physics 81: 372-405.
130. Schoephoerster RT, Chandran KB (1991) Velocity and turbulence measurements past mitral valve prostheses in a model left ventricle. J Biomech 24: 549-562.
131. Donea J, Guiliani S, Halleux JP (1982) An Arbitrary Lagrangian-Eulerian Finite-Element Method for Transient Dynamic Fluid Structure Interactions. Computer Methods in Applied Mechanics and Engineering 33: 689-723.
132. Baaijens FPT (2001) A fictitious domain/mortar element method for fluid-structure interaction. International Journal for Numerical Methods in Fluids 35: 743-761.
133. Morsi YS, Yang WW, Wong CS, Das S (2007) Transient fluid-structure coupling for simulation of a trileaflet heart valve using weak coupling. J Artif Organs 10: 96-103.
134. Bathe KJ (1981) Non-Linear Finite-Element Analysis and Adina - Proceedings of the 3rd Adina Conference - Massachusetts Institute of Technology - 10-12 June 1981 - Preface. Computers & Structures 13: R5-R55.
135. Girdhar G, Xenos M, Alemu Y, Chiu WC, Lynch BE, et al. (2012) Device thrombogenicity emulation: a novel method for optimizing mechanical circulatory support device thromboresistance. PLoS One 7: e32463.
136. Borger MA, Nette AF, Maganti M, Feindel CM (2007) Carpentier-Edwards Perimount Magna valve versus Medtronic Hancock II: a matched hemodynamic comparison. Ann Thorac Surg 83: 2054-2058.
137. Tang D, Yang C, Geva T, Gaudette G, Del Nido PJ (2011) Multi-Physics MRI-Based Two-Layer Fluid-Structure Interaction Anisotropic Models of Human Right and Left Ventricles with Different Patch Materials: Cardiac Function Assessment and Mechanical Stress Analysis. Comput Struct 89: 1059-1068.
138. Alemu Y, Girdhar G, Xenos M, Sheriff J, Jesty J, et al. (2010) Design optimization of a mechanical heart valve for reducing valve thrombogenicity-A case study with ATS valve. ASAIO J 56: 389-396.
139. Dumont K, Vierendeels J, Kaminsky R, van Nooten G, Verdonck P, et al. (2007) Comparison of the hemodynamic and thrombogenic performance of two bileaflet mechanical heart valves using a CFD/FSI model. J Biomech Eng 129: 558-565.

140. Wilcox DC (1994) Simulation of Transition with a 2-Equation Turbulence Model. Aiaa Journal 32: 247-255.
141. Nobili M, Sheriff J, Morbiducci U, Redaelli A, Bluestein D (2008) Platelet activation due to hemodynamic shear stresses: damage accumulation model and comparison to in vitro measurements. ASAIO J 54: 64-72.
142. Hakki AH, Iskandrian AS, Bemis CE, Kimbiris D, Mintz GS, et al. (1981) A simplified valve formula for the calculation of stenotic cardiac valve areas. Circulation 63: 1050-1055.
143. Sirois E, Sun W (2011) Computational evaluation of platelet activation induced by a bioprosthetic heart valve. Artif Organs 35: 157-165.
144. Wang Q, Sirois E, Sun W (2012) Patient-specific modeling of biomechanical interaction in transcatheter aortic valve deployment. J Biomech.
145. Dwyer HA, Matthews PB, Azadani A, Jaussaud N, Ge L, et al. (2009) Computational fluid dynamics simulation of transcatheter aortic valve degeneration. Interact Cardiovasc Thorac Surg 9: 301-308.
146. Kereiakes DJ, Michelson AD (2006) Platelet activation and progression to complications. Rev Cardiovasc Med 7: 75-81.
147. Bluestein D, Chandran KB, Manning KB (2010) Towards non-thrombogenic performance of blood recirculating devices. Ann Biomed Eng 38: 1236-1256.
148. Yin W, Alemu Y, Affeld K, Jesty J, Bluestein D (2004) Flow-induced platelet activation in bileaflet and monoleaflet mechanical heart valves. Ann Biomed Eng 32: 1058-1066.
149. Bluestein D, Yin W, Affeld K, Jesty J (2004) Flow-induced platelet activation in mechanical heart valves. J Heart Valve Dis 13: 501-508.
150. Girdhar G, Xu S, Bluestein D, Jesty J (2008) Reduced-nicotine cigarettes increase platelet activation in smokers in vivo: a dilemma in harm reduction. Nicotine Tob Res 10: 1737-1744.
151. Gallocher S (2007) Durability assessment of polymer trileaflet heart valves [Ph.D. Thesis]. Miami: Florida International University.
152. Leverett LB, Hellums JD, Alfrey CP, Lynch EC (1972) Red blood cell damage by shear stress. Biophys J 12: 257-273.
153. Brown CH, 3rd, Lemuth RF, Hellums JD, Leverett LB, Alfrey CP (1975) Response of human platelets to sheer stress. Trans Am Soc Artif Intern Organs 21: 35-39.
154. Avrahami I, Rosenfeld M, Einav S (2006) The hemodynamics of the Berlin pulsatile VAD and the role of its MHV configuration. Ann Biomed Eng 34: 1373-1388.
155. Hagberg IA, Lyberg T (2000) Blood platelet activation evaluated by flow cytometry: optimised methods for clinical studies. Platelets 11: 137-150.
156. Rubenstein DA, Yin W (2009) Glycated albumin modulates platelet susceptibility to flow induced activation and aggregation. Platelets 20: 206-215.
157. Schulz-Heik K, Ramachandran J, Bluestein D, Jesty J (2005) The extent of platelet activation under shear depends on platelet count: differential expression of anionic phospholipid and factor Va. Pathophysiol Haemost Thromb 34: 255-262.